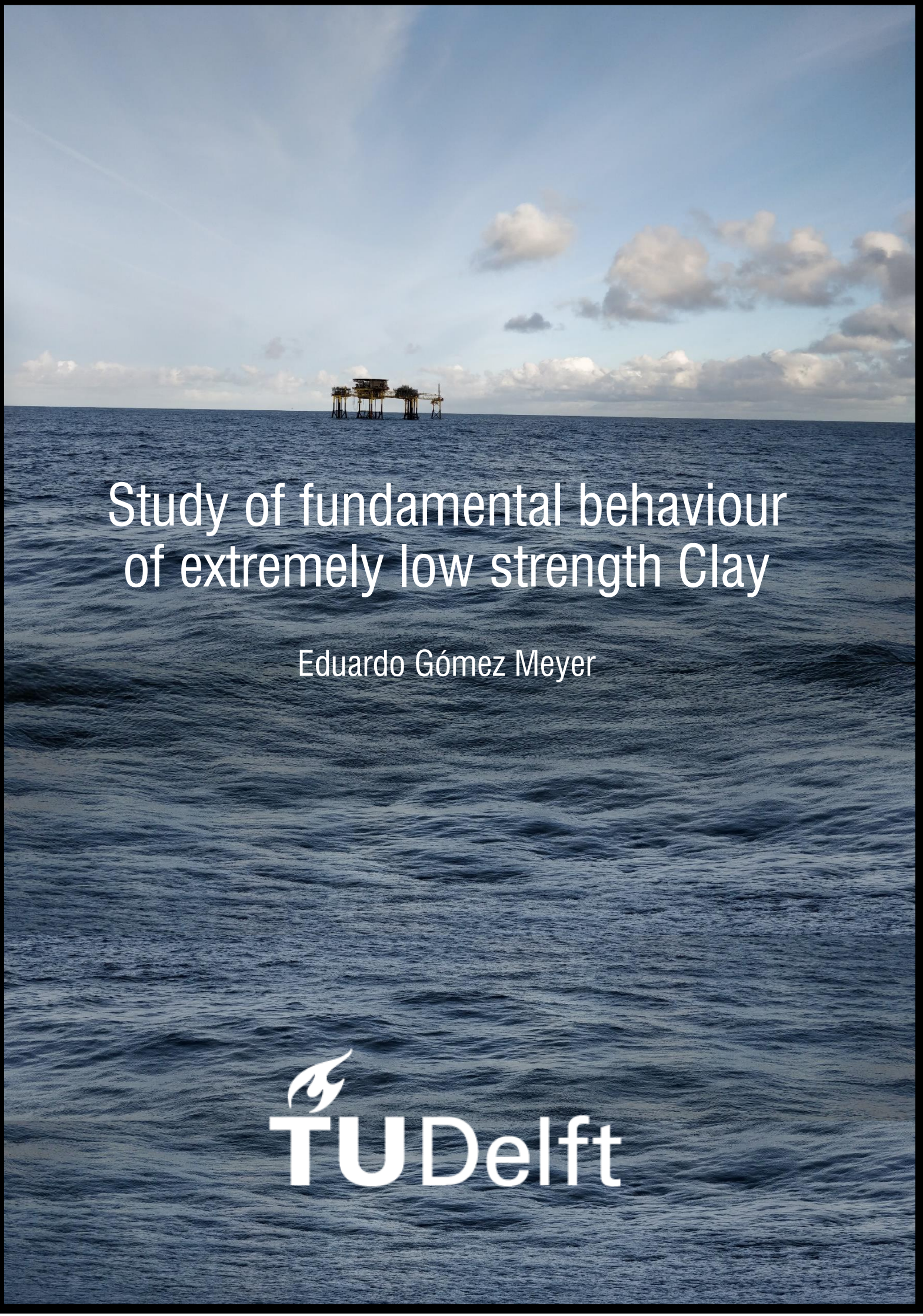

Study of fundamental behaviour of extremely low strength Clay

Eduardo Gómez Meyer

TU Delft

Study of fundamental behaviour of extremely low strength Clay

by

Eduardo Gómez Meyer

In fulfilment of the requirements for the degree of

Master of Science
in
Civil Engineering

at the Delft University of Technology,
to be defended publicly on November 22, 2018 at 15:30 PM.

Thesis committee:

Dr. A. Askarinejad (Chair)	TU Delft Geo-engineering
Ir. N. Parasie	Fugro
Ir. K. J. Reinders	TU Delft Hydraulic engineering
Prof. Dr. K. Gavin	TU Delft Geo-engineering

Department of Civil Engineering and Geosciences

Summary

Soil characterization of the upper 2 meters of the seabed is essential to optimize the design of hydrocarbon fields (mooring systems), wellheads, subsea completions, pipelines, anchors and mudmat foundations (Randolph, 2016). Additionally, it has an increasing importance for geohazard evaluation, particularly in submarine slides. In oceanic developments, where the water depth range from 200 to 3,000 meters, the geotechnical site characterization of the surficial sediments is particularly challenging, as generally extremely low to low strength, normally consolidated fine-grained deposits are encountered. Currently, different in-situ tests and sampling techniques are implemented to determine soil properties at large water depths; however, more accurate measurements are needed to improve the geotechnical designs and reduce project costs.

The preferred in situ tests when testing on extremely low strength clays are the full flow penetrometers, hence, this thesis investigates the fundamental behaviour of a full flow penetrometer by performing monotonic, cyclic and variable penetration rate tests on extremely low strength clays. The methodology followed included the design and construction of the test set-up, the determination of the system compliance, the execution of the penetration tests, the analysis and interpretation of the acquired data and the validation by comparing the results with laboratory vane shear tests.

Six (6) samples were prepared by consolidating kaolin slurry at different acceleration forces with the small TU Delft centrifuge. The intact and remoulded undrained shear strength of the samples – determined with laboratory vane shear tests - varies from 1.4 to 2.7 kPa and from 0.5 to 1.2 kPa, respectively. The full flow penetration test results have shown very good agreement when comparing the derived undrained shear strength with the ones obtained by the laboratory vane shear test. With the cyclic test data, degradation curves were derived and the ductility of the soil was analysed. During Test 1 the failure mechanism reached the surface, hence, the strength was underestimated. On the other hand, was useful as the failure mechanism, the shear bands and the width of the area of influence were observed during the execution of this test. Variable penetration rate tests were performed to analysed the rate effects on the remoulded clay. The penetration rate was systematically increased from 0.3 mm/s to 29 mm/s. An increase in resistance at low penetration rates due to partial consolidation was measured. Additionally, at high penetration rates a significant increase in resistance was measured due to viscous effects. The undrained shear strength is not a fundamental soil parameter and the assessment of the strain dependency is useful when designing structures that induce cyclic loading to the soil. Finally, the effect of confining stress was evaluated in Test 5 by performing cyclic test with varying surcharge. It was found that the measured remoulded strength and the rate effects are not influenced by the confining stress.

Keywords: Full flow penetrometer, extremely low strength clays, cyclic test, variable penetration rate test, strain softening, soil degradation, rate effects

Acknowledgments

Throughout the past months, I had the opportunity to work on a challenging project. It required some project management, some mechanical and electronic engineering, and of course, a lot of soil testing, interpretation and analyses.

First, I would like to thank my graduation committee. Their critical comments, suggestions and recommendations shaped the final product. I would like to express a special thank-you to Nico Parasie and Amin Askarinejad, my daily supervisors, for their outstanding guidance, critical observations and injection of enthusiasm and positivism.

I would like to thank FUGRO, for giving me the opportunity to execute this challenging task and for fully founding this project. Their expertise and pleasant work environment contribute to the quality of this research.

Many thanks to the technicians Kees van Beek and Han de Visser for their work done during the construction of the test set-up and the execution of the experiments.

Lastly, I would like to express my appreciation to my family for their support and confidence in me.

Table of contents

List of tables

List of figures

List of symbols and units

A_{shaft}	Cross sectional area of the shaft
A_p	Projected area of the penetrometer
A_r	Are ratio
BPT	Ball penetration test
B_q	Ratio of excess pore pressure to net bearing pressure
CPT	Cone penetration test
c_v	Consolidation coefficient
d	Diameter of the penetrometer
DAS	Data acquisition system
DMS	Manually operated box-core penetrometer
G	Soil shear modulus
FC	Fall cone
FE	Finite element analysis
f_s	limiting interface friction
I_r	Rigidity index
LV	Laboratory vane shear test
$MBPT$	Mini ball penetration test
$MTBT$	Mini T-bar penetration test
m_v	Compresibility coefficient
N_b	Ball bearing factor
N_k	Cone bearing factor
N_T	T-bar bearing factor
$N_{b,ave}$	Ball bearing factor to correlate to undrained shear strength average
$N_{b,rem}$	Remoulded ball bearing factor
$N_{b,TC}$	Ball bearing factor to correlate to undrained shear strength triaxial compression
$N_{b,vane}$	Ball bearing factor to correlate undrained shear strength vane
$N_{b,rem,fc}$	Ball bearing factor to correlate to remoulded undrained shear strength fall cone
$N_{b,rem,UU}$	Ball bearing factor to correlate to remoulded undrained shear strength undrained unconsolidated triaxial compression
$N_{b,rem,vane}$	Ball bearing factor to correlate remoulded undrained shear strength vane
q_b	Measured ball resistance
q_c	Measured cone resistance
q_{in}	Initial penetration resistance
q_{net}	Net cone penetration resistance
q_{rem}	Remoulded penetration resistance
q_t	Corrected cone resistance
s_t	Sensitivity
s_u	Undrained shear strength
$s_{u,ave}$	Undrained shear strength average
$s_{u,dist}$	Undrained shear strength disturbed
$s_{u,SS}$	Undrained shear strength simple shear
$s_{u,TC}$	Undrained shear strength triaxial compression
$s_{u,TE}$	Undrained shear strength triaxial extension
$s_{u,rem}$	Remoulded undrained shear strength

TBT	T-bar penetration test
u_2	Pore pressure at the cone shoulder
V	Normalized velocity
v	Penetration rate
VST	Vane shear test
YSR	Yield stress ratio
α	Friction ratio
μ	Strain rate parameter
γ_w	Unit weight of water
k	Permeability
σ_h	Horizontal stress
$\sigma_h{}'$	Effective horizontal stress
σ_{v0}	In situ total overburden presuure
σ_v	Vertical stress
$\sigma_v{}'$	Effective vertical stress
σ_r	Radial stress
σ_θ	Tangential stress
$\tau_{r\theta}$	Shear stress
Δ	Normalised in situ stress difference between vertical and horizontal stresses

1. INTRODUCTION

1.1 Motivation

Soil characterisation of the upper 2 meters of the seabed is essential to optimize the design of hydrocarbon fields (mooring systems), wellheads, subsea completions, pipelines, anchors and mudmat foundations (Randolph, 2016). Additionally, it has an increasing importance for geohazard evaluation, particularly in submarine slides. In oceanic developments, where the water depth range from 200 to 3,000 meters, the geotechnical site characterization of the surficial sediments is challenging, as generally extremely low to low strength, normally consolidated fine-grained deposits are encountered. Currently, different in-situ tests and sampling techniques are implemented to determine soil properties at large water depths; however, more accurate measurements are needed to improve foundation design and reduce project costs, therefore the idea of the stitch was originated.

In-situ soil testing, such as the cone penetration test (CPT), T-bar penetrometer test (TPT), and ball penetrometer test (BPT), measure a continuous profile of the resistance of the ground, which allows the interpretation of soil conditions and behaviour. The cone penetration test is the most widely used in the offshore industry (Osman & Randolph, 2015), and several design approaches and methodologies are based on its measurements. The TPT and BPT are known as full flow penetrometers, since the resistance is primarily due to flow around the probe, rather than insertion of additional volume into the ground (Einav & Randolph, 2005; Yafrate, 2008); they were first used in the late 1990s (Randolph & Gourvenec, 2011), and have the potential to determine undrained shear strength (s_u) and remoulded undrained shear strength $(s_{u,rem})$ of soft sediments more accurate than with the CPT (Yafrate & DeJong, 2007; Einav & Randolph, 2005; Nguyen & Chung, 2017; Yafrate, 2008; DNV-GL, 2017). Nevertheless, for extremely low (0-10 kPa) to very low strength (10-20 kPa) clay (British Standard Institution, 2015) there are major known challenges in adopting this approaches for strength characterization:

- The penetrometer must have sufficient resolution to measure the extremely low resistances relative to the force from the hydrostatic water pressure.
- The accuracy of the load cell decreases with increasing water depth and high temperature gradients.
- Disturbance and sinking of the seabed frame during touch-down due to its self-weight.
- Correction for pore pressure acting on the seals behind the penetrometer and subtraction of the overburden stress (Zhou & Randolph, 2011).
- Water infiltrating in the “wound” after penetration can cause additional softening during cyclic tests, which underestimates the remoulded strength of the soil (Low & Randolph, 2010; Randolph, et al., 2007; Low, et al., 2008a)

The in-situ tests are complemented with sampling and laboratory testing. Currently there are two preferred methods to sample the surficial sediments at great water depths: 1) gravity/piston cores and 2) box-cores. The gravity piston cores – including the large diameter cores – generally disturb considerably the upper meter of the sample, by inducing a large amount of shear strain. Box cores

provide a rapid method for obtaining high quality, largely undisturbed samples, that does not require a drilling system or actuate a seabed frame (White, et al., 2015). It has been suggested that box cores are the best approach for sampling the near-surface extremely low to very low strength clays (Randolph, et al., 2007; Puech, et al., 2011; Low, et al., 2008a) if the strength profile is obtained from the box-corer itself rather than extract sub-samples for further investigation and testing. In practice, the strength profile of the box corer is normally measured by miniature vane shear test. However, vane tests are time consuming to perform and only provide discrete measurements, instead of a continuous profile.

To obtain a continuous profile from the box core itself, different system and tools have been designed and tested: 1) a manually operated box-core penetrometer – the DMS, developed by the Centre of Offshore Foundation Systems (COFS), to measure profiles of s_u and $s_{u,rem}$ in box cores (Randolph, et al., 2007); and 2) the Deckscout, developed by Fugro, which is an equipment used on deck to carry out mini ball penetrometer test (MBPT) and mini T-bar test (MTBT): it has the versatility to perform monotonic and cyclic test at different penetration rates. (Fugro Engineers B.V., 2011).

The full flow penetrometers and the mini full flow penetrometers behaviour are based on the solutions and theory proposed by Einav & Randolph (2005) which neglects the presence of the shaft. Several experimental and in situ test (Nguyen & Chung, 2015; Sahdi & Gaudin, 2014; DeJong, et al., 2011; Puech, et al., 2011; Low & Randolph, 2010; Nakamura, et al., 2007; Randolph, 2004), finite element analyses (FEM) (Osman & Randolph, 2015; Randolph & Andersen, 2006; Lu, et al., 2000; Randolph, et al., 2000; Zhou & Randolph, 2007; 2009a; 2009b) and large deformation finite element analyses (LDFE) (Zhou, et al., 2013; Zhou, et al., 2016; Barbosa-Cruz & Randolph, 2005; Zhou & Randolph, 2011), have been performed to study the effect of the size of the penetrometer and its shaft, the area ratio ($A_r = A_{shaft}/A_p$), the penetration rate, the failure mechanism, and the flow mechanism. It has been found that an area ratio lower or equal to 0.1 (which is nowadays the standard), gives reliable results, making the full flow penetrometers (in-situ or in box-core) the preferred testing techniques for shallow characterization.

To even increase the reliability of the strength characterization, an idea of a new full flow penetrometer was originated at Fugro Netherlands Marine. It consists of physical measurements of a ball pulled into the soil by a rope. The idea will directly eliminate the corrections for area ratio, pore-pressure, overburden stress, temperature shock, and water infiltrating the “wound”. To study the concept, Fugro and TU Delft structure the requirements of the prototype and shaped the research goal of this master thesis: which is design and build the prototype and conduct analyses and laboratory experiments to validate the system. The prototype is limited to horizontal penetration but is planned to expand the capacities to perform cyclic test in multiple directions, making the system particularly interesting for the estimation of as-laid pipeline embedment, pipeline walking, pipeline buckling, sliding resistance of seabed foundations, rate effects, and cyclic soil response, among others.

1.2 Scope of research

The aim of this research is to design and test a new intrusive penetrometer for soil testing on soft sediments.

Specifically, this study aims to:

- Design a test set-up to investigate the soil behaviour and strength by pulling a ball through samples with varying undrained shear strength.
- Investigate the response and behaviour of the soil for monotonic and cyclic tests
- Determine intact and remoulded shear strength
- Investigate the potential of the tool to determine partial consolidation effects by performing variable penetration rate tests
- Investigate the possibility to determine strain rate dependency
- Validate the measurements by comparing with laboratory vane shear test
- Validate the potential of using the proposed testing system in the industry

1.3 Approach

An extensive literature research is conducted to point out the limitations of the exiting testing and sampling techniques on extremely low to low strength fine-grained sediments. The tool - its parts, dimensions and capacity - are designed based on the literature available for full flow penetrometers and considering the constraints in space given by the TU Delft beam centrifuge. The tool is designed, built and assembled during the thesis. The effect of the friction of the pulleys, the shaft resistance of the rope and the effect of the tension on the rope are evaluated experimentally to determine the correction factors of the measured resistance to obtain the net resistance. Finally, monotonic, cyclic and variable penetration rate test are performed on 5 samples consolidated at different g-force levels, followed by data processing, interpretation and derivation of geotechnical parameters. Complementary test such as miniature laboratory vane shear test and fall cone are performed on each sample to validate the stitch results.

1.3.1 Report structure

The literature study is presented in Chapter 2 and it elaborates on the existing sampling and testing techniques used to determine the geotechnical parameters of soft sediments. Special attention is given to the full flow penetrometers since its theory was used as baseline for the design of the prototype.

Chapter 3 presents the design of the test set-up. It starts with the description of the tool and the capabilities of the system, followed by a detailed description of the approach for the selection of each component (e.g. dimensions of the test box, strength of the rope, dimension of the ball penetrometer, resolution and capacity of the load cells, etc.)

Next, the testing program, the factual data and the main observations of each tests are presented in Chapter 4. It elaborates on the sample preparation and the test calibration, including the determination of the system compliance and the shaft resistance of the rope. Subsequently, the factual data of the stitch test and the laboratory test are shown in Section 4.3.

Chapter 5 describes the data processing, analyses and interpretation of the monotonic, cyclic and variable penetration rate tests.

Future developments of the prototype, future research and engineering applications are discussed in Chapter 6. Finally the conclusions of the research are presented in Chapter 7.

2. LITERATURE REVIEW

The current in situ test and sampling techniques have difficulties to accurately measure undrained shear strength of extremely low to very low strength fine grained surficial seabed sediments. The advantages and limitations of these techniques will be briefly discussed in this chapter.

2.1 Undrained shear strength (s_u)

The main objective of this thesis is to develop a new tool which is accurate, efficient and versatile; and able to measure undrained shear strength, intact and remoulded, directly from a box core. One of the questions is, what undrained shear strength will it measure? As the behaviour of the soil and its response is dependent on the direction of the loading, soil anisotropy, strain rate and stress history, is not possible to have a single value of undrained shear strength (Boggess & Robertson, 2011), as s_u is not a fundamental soil parameter (Low, et al., 2010). Additionally, the undrained shear strength also depends on the quality of the sample subjected to shearing (Low, et al., 2010). Four values of undrained shear strength are normally determined for the different engineering applications, and can be determined with in situ and laboratory test:

- $s_{u,TC}$: Triaxial compression undrained shear strength
- $s_{u,TE}$: Triaxial extension strength
- $s_{u,ave}$ or $s_{u,SS}$: average of triaxial compression, simple shear and triaxial extension. Simple shear direction of loading is often close the $s_{u,ave}$– which is defined as $s_{u,ave} = 1/3(s_{u,TC} + s_{u,SS} + s_{u,TE})$
- $s_{u,rem}$: remoulded shear strength

Generally, ($s_{u,TC} > s_{u,SS} > s_{u,TE}$), with a larger difference for low plasticity soils (Boggess & Robertson, 2011).

The CPT, BPT, and TPT, measure a single value of soil resistance, which can be correlated to $s_{u,TC}$, $s_{u,ave}$ and $s_{u,TE}$, by assigning different bearing factors (N_k). Usually, the bearing factor is calibrated with laboratory test results, and generally the penetration resistances of the CPT and full flow penetrometers reflect equally well, the different values of undrained shear strength (Low, et al., 2010). Nevertheless, performing laboratory test on intact specimens with extremely low to very low strengths is generally non-viable, as the manipulation of the samples will disturb them considerably and will give non-reliable results. Therefore, it is often preferred to use in situ test measurements to determine the intact undrained shear strength of soft sediments.

2.1.1 Remoulded undrained shear strength ($s_{u,rem}$) & sensitivity (S_t)

The remoulded undrained shear strength ($s_{u,rem}$), is the residual strength of a fine-grained soil. This is an important parameter when dealing with structures that apply a cyclic loading to the soil. In a marine environment, most of the structures induce cyclic loading to its foundation, caused by for example wind, current and wave induced forces.

This parameter can be determined by performing cyclic test with the full flow penetrometers, the DSS, laboratory vane test or cyclic triaxial. Generally, the soil is considered remoulded when further softening within each cycle is essentially negligible (Randolph, et al., 2007), which is generally after 10 cycles – in highly sensitive clays degradation occurs more quickly. With the remoulded resistance and the initial resistance is also possible to determine the sensitivity of the soil. For over consolidated clay (OC) the sensitivity is typically between 1.2 and 1.8 and for normally consolidated clay (NC) between 2 and 4 (Fugro Netherlands Marine - Internal document, 2017). Numerical analyses (Andersen, 2006; Zhou & Randolph, 2009b), suggested that the resistance sensitivity (q_{in}/q_{rem}) – Initial resistance over the remoulded resistance - will always be less than the shear strength sensitivity $(s_u/s_{u,rem})$ (Lunne, et al., 2011). There are three correlations that are usually implemented to determine the shear strength sensitivity from full flow penetration tests:

- The first one was developed by Yafrate, et al. (2009) based on the data obtained from 16 samples and four sites. The equation is derived based on the remoulded ratio. It is important to note that the regression is based on a large range of sensitivities, but with limited data sensitivity values $(S_t > 10)$

$$S_t = \left(\frac{q_{in}}{q_{rem}}\right)^{1.4} \quad 2.1$$

- Yafrate, et al. (2009) suggested that is also possible to estimate the soil sensitivity from the extraction ratio (q_{in}/q_{ext}), as the initial strain softening is interrelated to the soil sensitivity.

$$S_t = \left(\frac{q_{in}}{q_{ext}}\right)^{3.7} \quad 2.2$$

- A more theoretical approach, is the one proposed by Einav & Randolph (2005), where they suggested that the sensitivity (S_t) is the inverse of the fully remoulded strength ratio (δ_{rem})

$$S_t = 1/\delta_{rem} \quad 2.3$$

$$\delta_{rem(i+1)} = \left[\delta_{rem(i)} + \left(1 + \delta_{rem(i)}\right)e^{-1.5\xi_P/\xi_{95}}\right]\Delta_{rem} \quad 2.4$$

  Where, $\delta_{rem(i)} = 1/\alpha$; $\alpha =$ friction ratio; $\xi_P =$ average cumulative strain; $\xi_{95} =$ cumulative shear strain required to cause 95% reduction. These parameters can be derived from cyclic test using full flow penetrometers (see 2.3.2.4 for detailed explanation).

For extremely low to very low strength clays is also possible to determine the strength sensitivity with the laboratory vane shear test; ISO 19901-8 distinguishes multiple methods for deriving its value.

2.2 Sampling techniques

There are several sampling techniques and in situ tests used to derive parameters of soft surficial sediments, and most of them are summarised by Peuchen & Westgate (2018) in Table 1. The table was constructed to provide guidance for the execution of a site investigation for surface-laid pipelines; it shows how often the tool is used, the geotechnical parameters that can be derived and the soil applicability.

The free fall piston corer and gravity corer are used commonly more often than the piston sampler because a larger continuous sample can be acquired - the recovery depends on the core diameter, soil strength and the corer weight, but generally, ranges from 3 to 25 meters. Despite improvements of this technology, it is difficult to obtain undisturbed samples of the upper meter of soft sediments (Randolph, et al., 2007; Low, et al., 2008a). The box corer and the piston sampler are preferred for sampling the shallow extremely low to very low strength clays.

Table 1 - comparison of site investigation tools for design of surface-laid subsea pipelines (Peuchen & Westgate, 2018)

			Applicability							
			EL Clay		Layered Clay and Sand		VL to M Clay		>M Clay	
Tool	Use	Geotechnical Parameter	SP	GP	SP	GP	SP	GP	SP	GP
Marine geophysical investigation										
Seafloor and sub-seafloor mapping	****		+/–	–	+/–	–	+/–	–	+/–	–
In-situ testing										
Cone penetration test (CPT)	****	s_u ($s_{u,r}$, γ')	+	++	+	+	++	++	+	+
T-bar/ ball penetration test (TPT/BPT)	**	s_u	+/–	++	+/–	+/–	+/–	++	–	–
Cyclic T-bar/ ball penetration test (TPT, BPT)	*	$s_{u,r}$	+/–	++	+/–	+/–	+/–	++	–	–
Piezocone pore pressure dissipation test	*	c_v (s_u)	++	++	++	+	++	++	+	+/–
Piezoprobe/ piezo-ball pore pressure dissipation test	*	c_v (s_u)	–	++	+/–	+/–	+/–	++	–	–
In-situ vane shear test	*	s_u, $s_{u,r}$	–	++	–	–	–	++	–	–
Free fall penetration test—CPT penetrometer	*	s_u	+	+	+/–	+/–	++	++	+/–	+/–
Free fall penetration test—accelerometers	*	s_u	–	–	+/–	+/–	+	+	+/–	+/–
Pipeline section test—self-weight	*	s_u	+/–	++	–	–	+/–	+/–	–	–
Pipeline section test—SMARTPIPE®	*	s_u, $s_{u,r}$, c_v	+/–	++	–	+/–	+/–	++	–	–
Sampling (+ laboratory testing)										
Piston sampler—SMARTSURF® incl. CPT or (miniature) TPT/ BPT	*	s_u, $s_{u,r}$, $s_{u,res}/\sigma'_{v0}$, δ_{res}, γ', c_v	++	+	+	+	++	++	+/–	+/–
Box corer + MTPT/ MBPT	***	s_u, $s_{u,r}$, $s_{u,res}/\sigma'_{v0}$, δ_{res}, γ', c_v	++	+	+/–	+	+/–	++	–	–
Free fall piston corer/ gravity corer	***	s_u, $s_{u,r}$, $s_{u,res}/\sigma'_{v0}$, δ_{res}, γ', c_v	–	–	+/–	+/–	+	+	–	–
Vibrocorer	**	s_u, $s_{u,r}$, $s_{u,res}/\sigma'_{v0}$, δ_{res}, γ', c_v	–	–	–	–	+/–	+/–	+/–	+/–
Rotary core sampler	*	s_u, $s_{u,res}/\sigma'_{v0}$, δ_{res}, γ'	–	–	–	–	–	–	+	+
Laboratory testing										
Laboratory miniature vane test (MV)	****	s_u, $s_{u,r}$	–	+	–	+	–	++	–	–
Low stress interface shear box test	**	$s_{u,res}/\sigma'_{v0}$, δ_{res}, c_v	–	++	–	+	–	++	–	+
Incremental oedometer or CRS test	**	c_v	–	+	–	+	–	++	–	+/–

SP = stratigraphic profiling; GP = geotechnical parameter values; EL = extremely low strength (s_u 10 kPa); VL = very low strength (10 kPa s_u 20 kPa); M = medium strength (40 kPa s_u 75 kPa); Parameters between brackets have possible applicability; they are not considered for the GP applicability rating; ++ = high applicability; + = medium applicability; +/– = possible applicability; – = no applicability; * = less than 0.1% of tool deployments; ** = between 0.1% and 1%; *** = between 1% and 10%; **** = more than 10%.

The piston sampler is usually mounted on a seabed frame like the SMARTSURF® developed by Fugro. The SMARTSURF® is equipped with three independent push-in devices: 1) conventional CPT, 2) mini T-bar or mini ball penetrometer and 3) 100 mm-diameter piston sampler, and it has been rated by Peuchen & Westgate (2018) as a technique with high applicability for extremely low strength clays, although its used in less than 0.1% of tool deployments for pipeline site investigations.

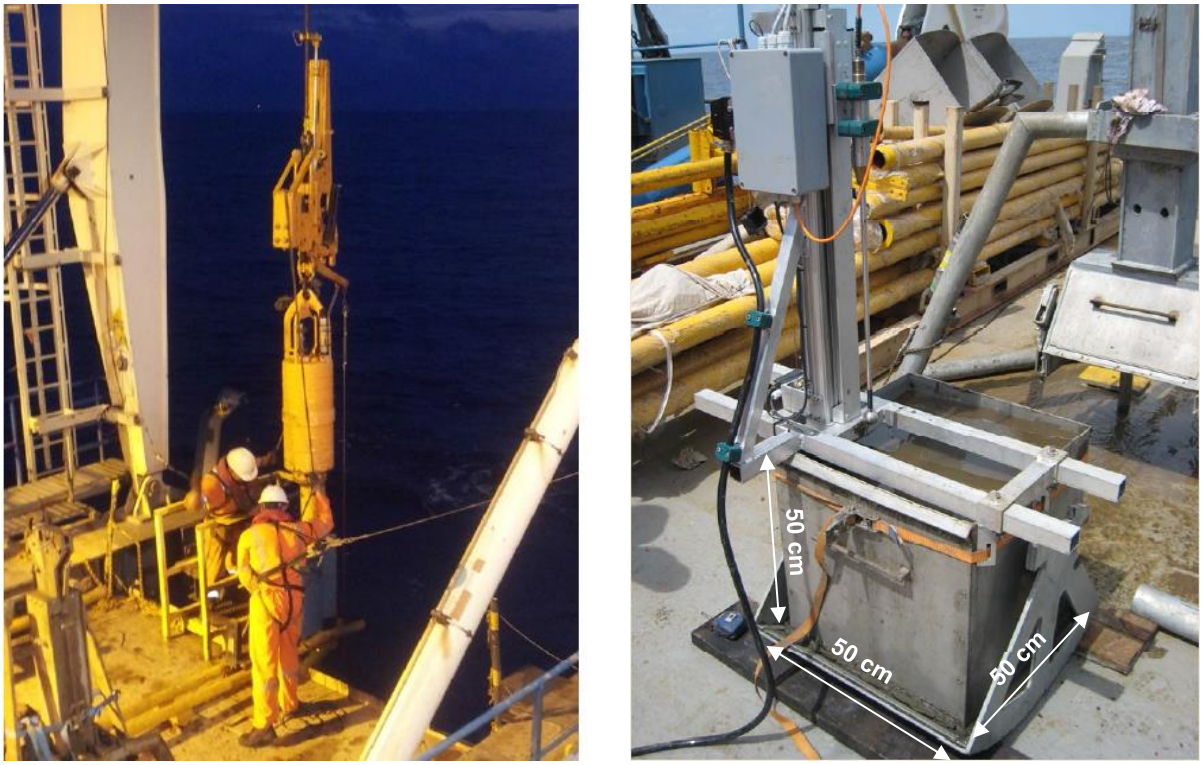

Figure 2.1 – Left: large diameter piston corer being deployed; and right: set-up for miniature ball penetrometer test on a box core (Fugro)

A box corer offers a better approach to obtain undisturbed samples of the upper meter compared with the piston corer (Low, et al., 2008a; Randolph, et al., 2007; Puech, et al., 2011). The block samples are retained by steel boxes - maximum height of 600 mm - pushed into the ground, and then a scissor blade closes the base of the box after penetration is completed, followed by retrieving the box to the vessel. The stress conditions are inevitably changed upon extraction of the sample, which can lead to swelling, loss of saturation and formation of voids due to gas scape (Peuchen & Westgate, 2018). Therefore, the best approach to minimize this effect is to determine the strength profile from the box core itself immediately after sample recovery, by preforming miniature shear vane test and mini-penetrometer tests (see Figure 2.1). Randolph, et al. (2007) and Puech, et al. (2011) compared the undrained shear strength obtained from miniature vane tests in a box core and a gravity piston core recovered from the Gulf of Mexico, and concluded that the box core appears to be more accurate at very shallow depths (Figure 2.2).

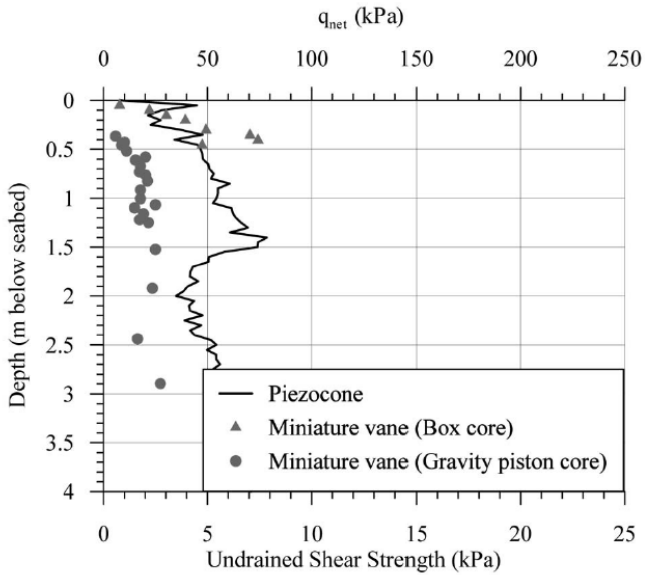

Figure 2.2 - Example of undrained shear strength profile obtained by miniature vane tests in box core and gravity piston core (Randolph, et al., 2007)**.** q_{net}: net penetration resistance (measured resistance corrected for pore water pressure, overburden stress and area ratio).

2.3 In situ tests methods and laboratory test methods

This chapter will focus on explaining the concept, advantages and limitations of the cone penetration test (CPT) and the full flow penetrometers. Special attention is given to the full flow penetrometer as its theory is used for the design of the test set-up. Additionally, the laboratory tests to be used on the test program will be explained in this section.

2.3.1 Cone penetration test

The CPT is used more than any other in-situ tool and sampling technique, and is the preferred alternative for pipeline design due to the combination of data quality versus cost of data acquisition (Peuchen & Westgate, 2018). The CPT involve the continuous measurement of penetration depth, cone resistance, sleeve friction, and, optionally, pore pressure and inclination. These measurements permit interpretation of ground conditions. However, the CPT does not give a direct measurement of s_u; instead, it measures the ground resistance exerted on the tip, when is being pushed at a constant rate. The measured cone resistance needs to be corrected for pore pressure and overburden pressure effects. Once the corrected cone resistance is obtained, it is divided by the empirical cone factor (N_k), to deduce the undrained shear strength. Wrong estimations of pore pressure and overburden stress, may lead to large inaccuracies in the derived undrained shear strength, predominantly for very soft deposits (Chung, 2005). In general, all theories result in a relationship (equation **2.5**) between corrected cone resistance q_t and s_u of the form:

$$s_u = \frac{q_t - \sigma_v}{N_k} \qquad 2.5$$

In very soft clays, the accuracy of q_t can be sometimes uncertain, therefore s_u can be estimated from the excess pore pressure using the following equation proposed by Boggess & Robertson (2011):

$$s_u = \frac{\Delta u}{N_{\Delta u}} \; where, \; N_{\Delta u} = B_q N_k \qquad 2.6$$

The accuracy of the CPT decreases with increasing water depth and when testing on extremely low strength clays due to the following issues:

- Reduced sensitivity of the loadcell in measuring the small increment from the soil resistance compared with the high ambient pressure (Lunne, et al., 2011; Weemees, et al., 2006; Stainer & White, 2015).

- Uncertainty in corrections of the area effect and overburden stress to the cone resistance (Lunne, et al., 2011).

- For the selection of the N_k values the limited embedment of a penetrometer is often ignored, underestimating the undrained shear strength in the upper 20 cm, possibly up to 30% (Peuchen & Westgate, 2018).

- Temperature change on the cone causes straining of the steel and strain gauges, increasing the uncertainty of the measurements. Note that the difference in temperature can be from 35°C (e.g. west Africa) to 4°C, which can be the temperature of water at great depths.

- Soil disturbance, pore pressure build-up and consolidation of the near surface sediments encounter at seafloor due to the use of a reaction equipment – sea bed frame (Fugro Netherlands Marine - Internal document, 2018).

Compared with the CPT, the full flow penetrometers offer a better approach for testing on extremely low to very low strength clays as they have a larger projected area which increases the resolution and reduces the uncertainties caused by unequal overburden stress, pore pressure and area effect (Chung, 2005; Low & Randolph, 2010; DeJong, et al., 2011).

2.3.2 Full-flow penetrometers

The TPT and BPT are known as full flow penetrometers, as the soil can flow fully around the probe (ignoring the cone shaft) (Einav & Randolph, 2005). The TPT was first developed to improve the accuracy of strength profiling, and was first implemented in 1996 (Randolph, et al., 1998). The BPT was developed later in 2003 with a more suitable geometry for deployment down a borehole (Peuchen, et al., 2005). The requirements and recommendations for offshore TPT and BPT are standardised in ISO 19901-8 (2014), EN (2015) and NORSOK (2004). ISO 19901-8 describes these penetrometers as "particularly suitable for characterizing very soft to soft clays and clayey silts with undrained shear strength <50 kPa". The standard TPT consist of a cylinder of 40 mm-diameter and 250 mm length connected to a shaft of 35.7 mm-diameter (same as the standard piezocone), which gives a projected area of 100 cm^2; a load cell is installed in the connection between the cylinder and the shaft. Similarly, the BPT consist of a ball of 113 mm-diameter, which gives a projected area of 100 cm^2, 10 times higher than the CPT; the larger projected area provides a larger force increment measurement compared with the CPT, which is an increase of resolution (Yafrate, 2008). These techniques not only can determine a continuous profile of intact undrained shear strength, but also measure the remoulded strength, $s_{u,rem}$, by carrying out cyclic tests, until fully remoulded conditions are achieved. Compared with the time

consuming, discrete measurements obtained from FVT the full flow penetrometer provides a more efficient approach to determine the strength of the sample (Yafrate, 2008).

Compared with the CPT, these penetrometers require a lower correction for overburden and pore pressure, providing a more accurate s_u and $s_{u,rem}$ measurements in soft sediments (Yafrate & DeJong, 2007; Einav & Randolph, 2005; Nguyen & Chung, 2017). It has been reported that the uncertainty value for q_t is about $\pm 3\ kPa$ during penetration (Peuchen & Terwindt, 2016) and slightly higher uncertainty applies for the extraction or cyclic phases (Peuchen & Westgate, 2018). The total adjustment has been reported to be less than 10% of the adjustments required for the piezo probe, reducing uncertainty in the net penetration resistance (Yafrate, 2008). Another advantage is that the resistance is less affected by secondary soil characteristics such as rigidity index (defined as $I_r = G/s_u$, where G is the shear modulus) and in situ stress ratio because the resistance is primarily due to flow around the probe, rather than insertion of additional volume (of cone shaft) into the ground (Einav & Randolph, 2005).

Similar to the CPT, the full flow penetrometers resistance can correlate to s_u by assigning the bearing factors N_b (BPT) and N_T (TPT), with the difference that the values are supported by the exact plasticity solution for the limiting pressure acting on a cylinder or sphere moving through an isotropic cohesive soil (Randolph & Houlsby, 1984; Randolph, et al., 2000; Einav & Randolph, 2005). The theoretical solution, which neglects the presence of the cone shaft, suggests a range of bearing factors for the TBT (N_T) between 9.1 (smooth) and 11.9 (rough). For the BPT the bearing factor (N_b) range from 11.0 (smooth) to 15.5 (rough). The measured resistance of the ideal situation (see Figure 2.4) does not need a correction for overburden stress, since the ambient stress, σ_{v0}, cancels out above and below the penetrometer (Randolph, et al., 2007).

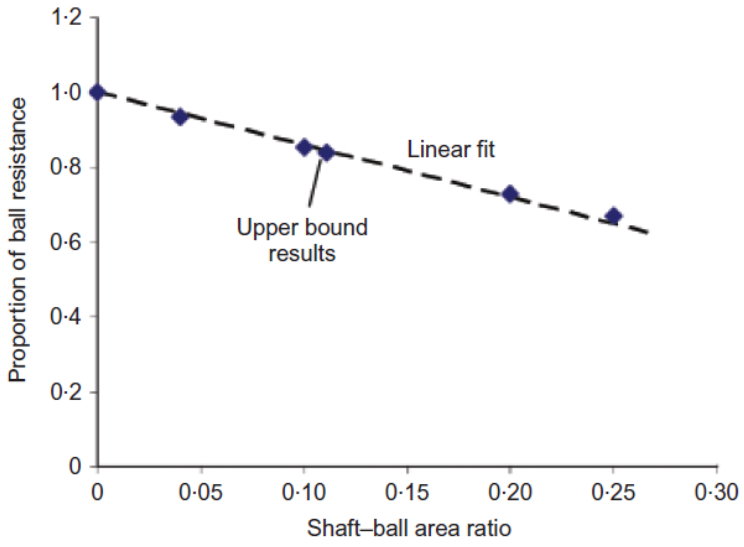

Figure 2.3 - Normalized resistance for BPT as function of A_r (Zhou & Randolph, 2011)

As the full flow penetrometers do have a shaft, typically of an area equal to 10% of the projected area of the penetrometer (A_p), several finite element (FE) modelling (Andersen, 2006; Randolph & Andersen, 2006) and large deformation final element modelling (Randolph & Zhou, 2006; Barbosa-Cruz & Randolph, 2005; Zhou & Randolph, 2007; Zhou & Randolph, 2009b) studied the response of the soil to assess the effect of the presence of the shaft, the influence of sensitivity, the effect of strain rate and

softening behaviour. Zhou & Randolph (2011) found that as the relative size of the shaft increases, the width of the failure mechanism reduces, and therefore the penetration resistance reduces (Figure 2.3).

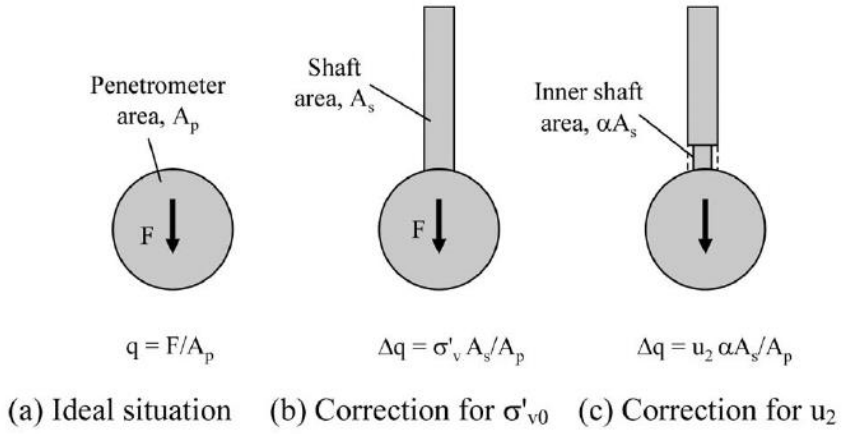

Figure 2.4 - Logic for correction of penetration resistance for full-flow penetrometers (Randolph, et al., 2007)

Figure 2.5 was develop based on several studies to show the influence of the friction ratio (α) and the area ratio (A_r) on the bearing factor (N_b). The bearing factor decreases with increasing area ratio ($A_r = A_{shaft}/A_p$), where A_{shaft} is the cross-section area of the shaft, and A_p is the projected area of the penetrometer. Based on centrifuge results made by Chung & Randolph (2004) and the field results presented by Weemees, et al. (2006) - which showed no effect on the penetration resistance for length to diameter ratios within a range of 4 to 10 - Lunne, et al. (2011) suggested a criterion to maintain the area ratio below 15%.

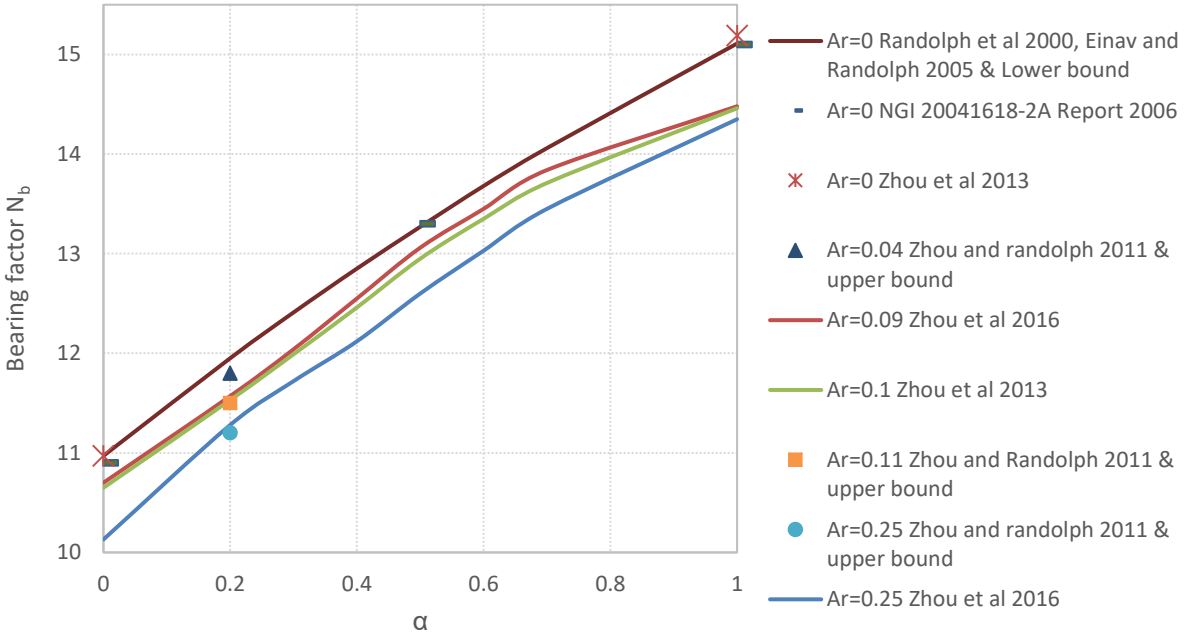

Figure 2.5 - Bearing factor vs friction ratio (α) for different values of area ratio (A_r)

Like the CPT, the measured resistance of the full flow penetrometers is corrected against the in-situ total overburden stress (σ_{v0}) missing due to the presence of the shaft, the pore pressure (u_0) acting on the o-ring and area ratio (A_r), as follows:

$$q_{net(b)} = q_b - [\sigma_{v0} - (1 - a_{cone})u_0]A_r \quad 2.7$$

Where, $q_{net(b)}$ is the net ball penetration resistance and a_{cone} is the cone area ratio. The smaller the area ratio (A_r) the smaller the influence of σ_{v0} and u_0.

With $q_{net(b)}$ and N_b, is possible to determine the undrained shear strength ($s_u = q_{net(b)}/N_b$). In practice the bearing factor is calibrated empirically based on the results of complementary laboratory tests, and is often presented as a range (low and high estimate).

Full flow penetrometers can be used to measure $s_{u,rem}$, by carrying out cyclic tests, until fully remoulded conditions are achieved. Due to its advantages over the CPT and the ability to measure $s_{u,rem}$, the full flow penetrometers have become the standard tool to investigate the strength properties of the surficial sediments for deep water developments (White & Randolph, 2007; Randolph & Gourvenec, 2011).

2.3.2.1 Mini full flow penetrometers

The miniature full flow penetrometers were developed to measure a continuous profile of undrained shear strength on a sample which is typically confined by its sampler (e.g. box core or sample liner). There are currently two versions of this technology: 1) the Deckscout and 2) manually operated box-core penetrometer (DMS). They are ideal for the determination of the strength of extremely low to low strength fine grained soils, where sub sampling is not recommended due to high disturbance, and in situ test fail to log accurately the strength at near-surface depths (see sections 2.3.1 and 2.3.2). Currently the best approach to determine strength profile of soft surficial sediments, is to perform MBPT or MTPT directly on a box core (Low & Randolph, 2010; Fugro Engineers B.V., 2011).

2.3.2.1.1 Deckscout

The Deckscout is developed by Fugro, and it is a device that can be placed on top of a box core to perform monotonic and cyclic MBPT and MTPT. The MBPT consists of ball diameter of 33.9 mm, connected to a shaft with 11.3 mm-diameter and an area ratio of 0.11. The MTPT consists of a bar with 12 mm-diameter, and 75 mm long connected with a shaft with 11,3 mm-diameter. It has a maximum stroke of 540 mm, and the penetration can be achieved with a speed ranging from 0 to 20 mm/s. The capacity of the system is limited to a maximum measurable soil strength of 33 kPa. Cyclic tests are typically performed with 15 to 20 cycles. The logging frequency for penetration and extraction is 4 Hz.

Currently the Deckscout is one of the best tools to determine a continuous profile, in situ, of undrained shear strength of extremely low strength fine-grained sediments. It is also suitable to determine a degradation curve and remoulded undrained shear strength. It is important to note that a small area ratio produce highly consistent degrading curve at all depths (Yafrate & DeJong, 2007; Nguyen & Chung, 2015).

Figure 2.6 - Fugro's Deckscout mounted on a box core

2.3.2.1.2 The DMS

The centre for offshore foundation systems (COFS), in collaboration with TDI brooks international, developed a manually operated box-core penetrometer called the DMS. It can be used to measure profiles of intact and remoulded strength directly in the box-cores. The penetration rate is displayed and the operator must keep it as constant as possible; this induces human error that may influence the results. A T-bar – 8 mm in diameter by 42 mm in length and a 21 mm -diameter ball penetrometer can be installed. The resolution of tip resistances and displacement are less than 1 kPa and 0.1 mm respectively (Low, et al., 2008a). The set-up of the system is shown in Figure 2.7.

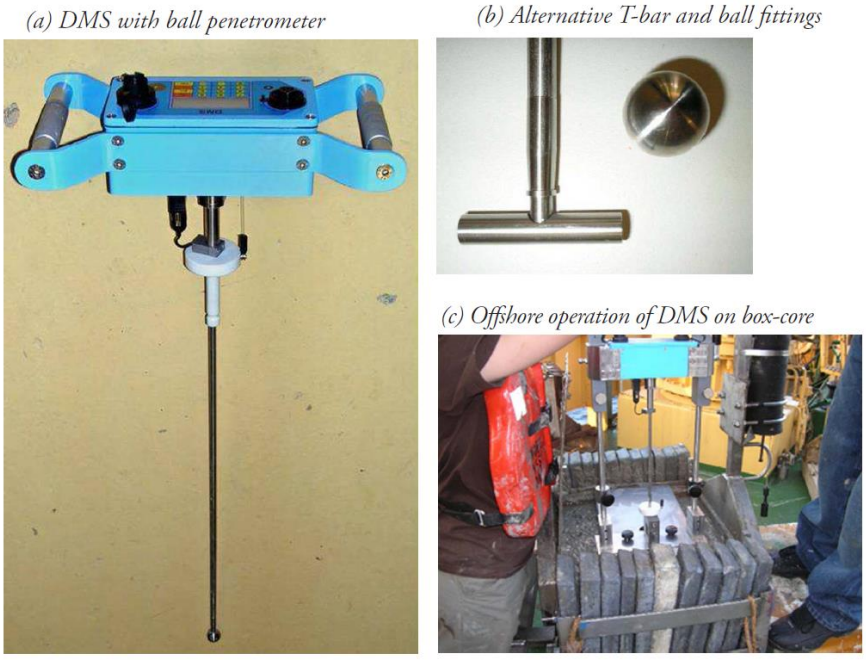

Figure 2.7 - Manually operated box-core penetrometer - the DMS (Randolph, et al., 2007)

While testing the DMS concept (Low & Randolph, 2010), free water on the sample surface was allowed, to simulate the box-core sample and to prevent drying of the surface soil. However, it was found that the water infiltrated the wound after penetration causing additional softening during cyclic tests, which underestimated the remoulded strength of the sample. The miniature ball penetrometer test was the most severely affected by water entrainment (see Figure 2.8). Once they noticed the effect of the water on top, they removed the water and added a layer of wax to prevent loss of moisture.

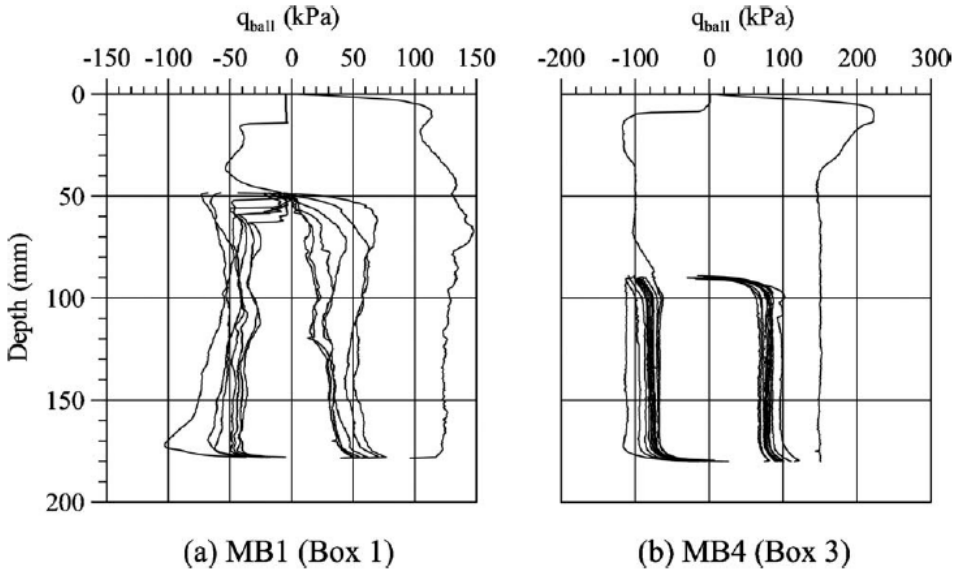

Figure 2.8 - Effect of water entrainment on measured resistances (Low & Randolph, 2010)

2.3.2.2 Failure mechanism around a BPT

Einav & Randolph (2005) proposed the upper bound-based strain path method (UBSPM), to provide a theoretical sound to study the penetration resistance, failure mechanism, evolution of shear bands, sensitivity, rate dependency and strain softening behaviour of full flow penetrometers (with no shaft). Several FE and LDFE analyses followed the proposed theory, to validate the failure mechanism, the width of remoulded zone, the width of the disturbed zone, the effect of penetration rate, the effect of area ratio and anisotropy (Randolph, et al., 2000; Randolph, 2004; Randolph & Andersen, 2006; Yafrate & DeJong, 2005; Andersen, 2006; DeJong, et al., 2010; Zhou & Randolph, 2009a). The penetrometer shape and area ratio are the most relevant factors affecting soil flow during penetration (Yafrate, 2008).

The general kinematic failure mechanism around an advancing ball penetrometer is shown in Figure 2.9 (a quarter of a ball due to symmetry). Essentially a wedge of non-deforming soil (see points UFA in Figure 2.9) is attached in front of the ball and it moves with the same velocity as the penetrometer. The size of the wedge depends on the interface friction. For a smooth surface – friction ratio equal to 0 ($\alpha = 0$) - all the soil will flow around the ball, and for a rough surface ($\alpha = 1$) the wedge of soil advancing will be maximum. The streamlines of the flowing soil will follow an involute curve, unwrapping about an inner spherical evolute whose radius is some fraction λ of the radius of the ball. In general, the failure mechanism suggests a compressive behaviour near the base of the advancing penetrometer, shearing at middle of the shear band, and extension at the top (Yafrate, 2008).

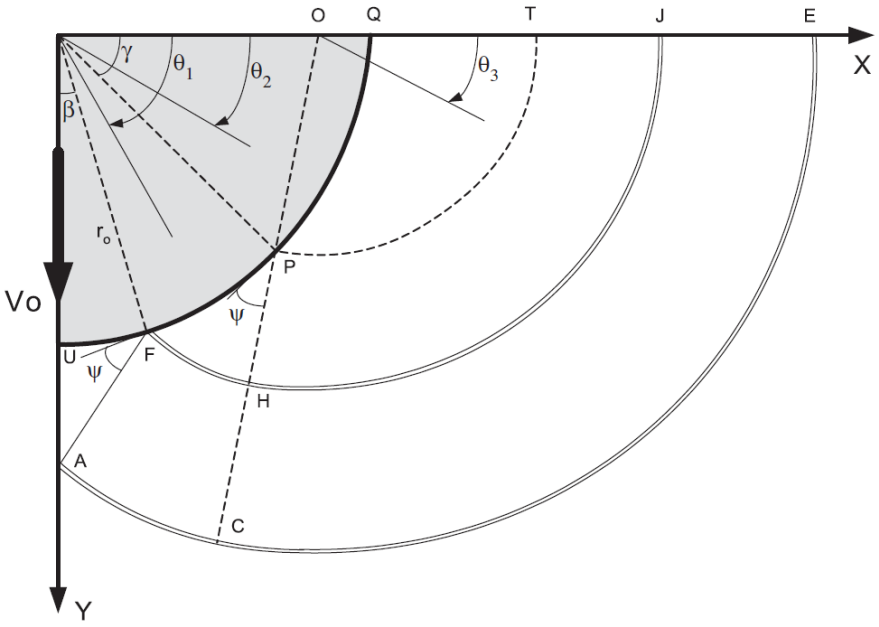

Figure 2.9 - Upper bound mechanism for both cylinder and sphere (Einav & Randolph, 2005)

Where:

β: angle determining the extend of a leading wedge (or cone) of undeforming material;

ψ: angle between lines orthogonal to the velocity characteristics and the penetrometer surface;

γ: angle marking a transition from an evolute mechanism to a rotational one;

r_0: penetrometer radius;

UFA: moves with the same velocity as the penetrometer;

PTQ: contains internal shearing due to the hoop strains and velocities that decreased inversely with radius from the axis of symmetry;

$ACHF$: to the left of line OC describes a fan shear zone where the current center for the fan moves gradually around an evolute circle with radius $r_0 \cos\psi$;

FHP: is a wedge of diffusely shearing material;

OC: All the velocities characteristics in the zones to the right of line OC are circular about point O;

$PHJT$: consists of a series of concentric cylindrical shells, center around O, rotating relatively to each other with the angular velocity decreasing with increasing radius;

$HCEJ$: is a fan shear zone moving about center O.

During initial penetration, some softening occurs, therefore the resistance is lower than the ideal intact or non-softened value (Zhou & Randolph, 2009b). Andersen (2006) identified that the strength may typically be reduced during the first penetration to the average between s_u and $s_{u,rem}$. The shear zone during the initial penetration will be more concentrated towards the penetrometer (Andersen, 2006), this zone will be called the disturbed zone. The width of the disturbed zone increases with increasing penetrometer roughness (Einav & Randolph, 2005)

The mechanism width can be expressed as:

$$\frac{w}{2r_0} = \sin\frac{(\beta)}{\cos(\beta+\psi)} + \left(\frac{\pi}{2} - \beta - \gamma\right)\cos\psi + \frac{\cos\psi + \sin\psi}{\cos(\gamma-\psi)} \qquad 2.8$$

Figure 2.10 was reconstructed with the values of γ obtained by Einav & Randolph (2005) for a lower bound (Von Mises model) and upper bound (Tresca model) assuming $\psi = \gamma$, $\beta = 0$. The width of the failure mechanism (W) increases with increasing friction ratio (α), to a maximum width of approximately 2.5 times the diameter.

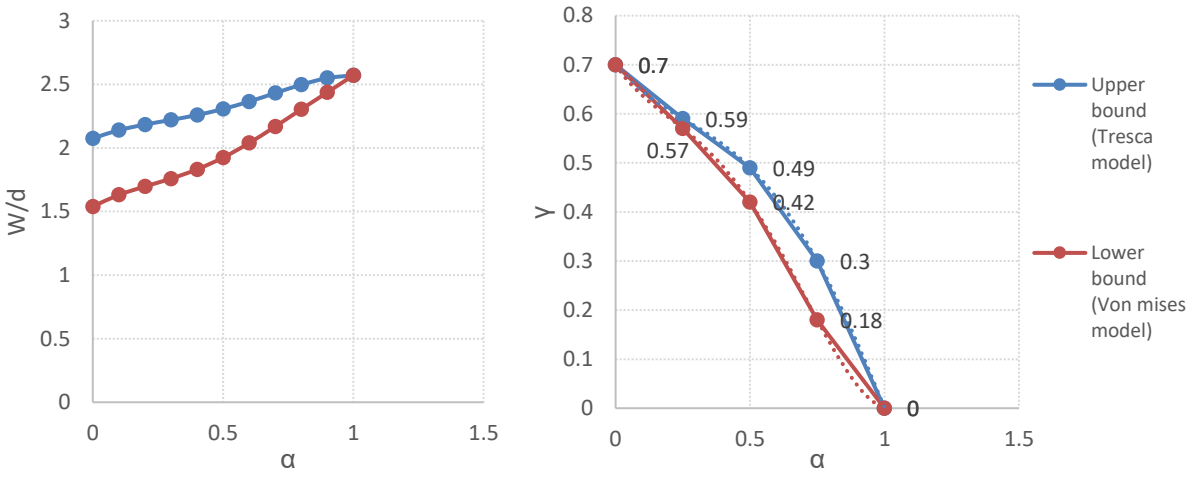

Figure 2.10 – Left: width of the failure mechanism normalized with the diameter of the penetrometer (W/d) vs friction ratio (α) with $\psi = \gamma$, $\beta = 0$. Right: γ vs α obtained from (Einav & Randolph, 2005)

During cyclic loading, the shear strength will be gradually reduced, and the failure zone may become concentrated towards the penetrometer (Andersen, 2006). When the clay has reached the residual state, it is expected to have three regions: 1) an inner zone with $s_{u,rem}$, 2) a disturbed zone of $s_{u,dist}$, and 3) the intact clay with s_u.

Randolph & Zhou (2006) and Zhou & Randolph (2007; 2009b) performed numerical analysis for cyclic tests. They varied the rate parameter μ between 0.05 and 0.2, the ductility parameter ξ_{95} between 10 and 25, and the sensitivity S_t between 2.5 and 10 (thus δ_{rem} and α are between 0.4 and 0.1). Figure 2.11 shows how the width/diameter ratio changes with the number of cycles, where it can be identified that the width of the failure mechanism, will not be, theoretically, larger than 2.5 times the diameter, and the width of the remoulded zone is consistently lower than the width of the initial penetration. In general, the authors agreed that the width of the failure mechanism decrease rapidly, due to softening of the material close to the penetrometer. With further cycling, the remoulded area expands until it reaches a constant value.

This is important for the selection of the dimensions of the penetrometer and the size of the sample, as the vertical and horizontal domain must be large enough to prevent influence of the walls of the sampler in the behaviour and resistance of the soil.

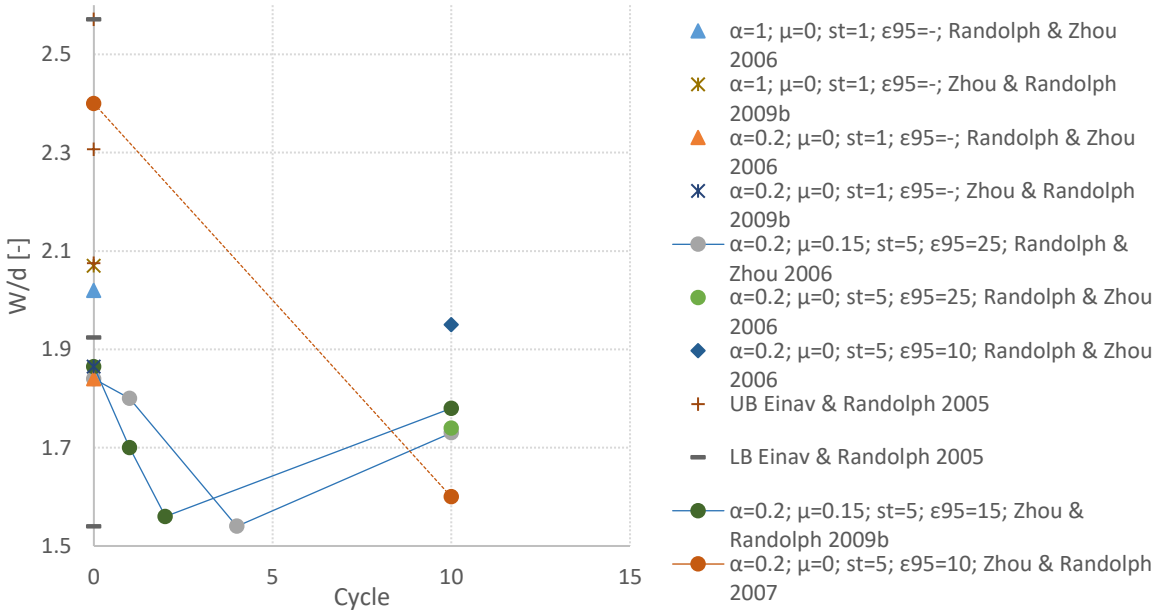

Figure 2.11 – change of the width of the failure mechanism over the diameter of the penetrometer (W/d) with increasing cycles

2.3.2.3 Strain rate dependency

The undrained shear strength of the soil can have a strain rate dependency. A fast penetration rate increases penetration resistance (Chung, et al., 2006; Low, et al., 2008b; Yafrate & DeJong, 2007; Zhou & Randolph, 2009a; Nguyen & Chung, 2015), due to the viscous influence of the strain rates (Colreavy, et al., 2016). The decrease of the penetration rate to a certain limit will cause partial pore pressure dissipation wand subsequent increases the soil strength and the penetration resistance (Randolph, 2004; Nguyen & Chung, 2015). The strain rate dependency of soil strength is an important issue, as it can lead to wrong interpretation of the test data and is also important for the selection of the undrained shear strength, as it can vary for different design applications (Lunne, et al., 2011).

To determine this parameter, Colreavy et al. (2016) performed several tests with a 60mm-diameter ball, and concluded that testing with the standard penetration rate of 20 mm/s is over two orders of magnitude higher than the minimum penetration velocity required for undrained conditions, leading to an overestimation of s_u by 40%. For the recommended size of the BPT (113mm) a penetration rate of 20 mm/s is suggested (Lunne, et al., 2011). If the size of the penetrometer varied from the standard dimensions, the penetration rate should be around 0.2-0.3 diameters per second (DeJong, et al., 2010; Lunne, et al., 2011).

The strain rate dependency can be assessed by varying the penetration rate during a penetration test (CPT, TPT OT BPT) (Chung, et al., 2006; Low, et al., 2008b). There Is evidence that the rate dependency of penetration resistance is similar for intact and remoulded soil conditions (Low, et al., 2008b). This allows the rate dependency parameter μ, to be estimated by varying the penetration rate during the final stages of a cyclic test, once softening is largely complete.

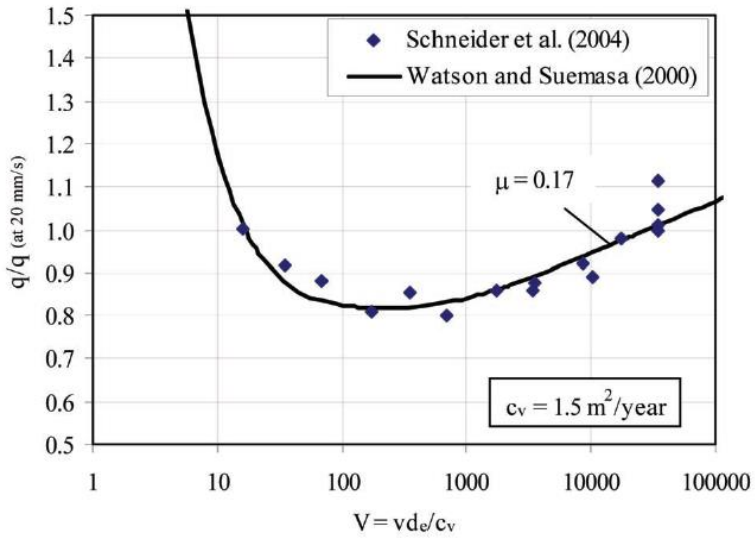

Figure 2.12 - Example of field twitch T-bar test results (Randolph, et al., 2007). Vertical axis: normalized resistance (reference resistance at 20 mm/s. Horizontal axis: Normalized velocity, where v is the penetration rate d is the diameter of the penetrometer and c_v the consolidation coefficient

Procedures, such as the twitch test (see Figure 2.12), where the penetration rate is systematically changed during penetration, allow also the assessment of the rate dependency (Randolph, et al., 2007). Alternatively, the variable-rate vane shear test can be used, as suggested by Peuchen & Mayne (2007). Either way the strain parameter can be evaluated by fitting the data of the variable rate penetration test to a semi-logarithmic or hyperbolic sine strain rate law as follows:

- Semi-logarithmic rate coefficient (Low, et al., 2008b):

$$\frac{q}{q_{ref}} = 1 + \mu \log\left(\frac{v}{v_{ref}}\right) \qquad 2.9$$

  Where, μ is the strain rate parameter, v is the penetration rate and v_{ref} is the reference penetration rate. However, this method does not consider viscous rate effects at high penetration rate and the transition to zero viscous effect at low rates (Low, et al., 2008b). Consequently, the hyperbolic sine rate law was introduced;

- Hyperbolic sine rate law (Low, et al., 2008b):

$$\frac{q}{q_{ref}} = \left(a + \frac{b}{1 + cV^n}\right)\left\{\frac{1 + \{[\mu/\ln(10)]\}[\sinh^{-1}(v/v_0)]}{1 + \{[\mu/\ln(10)]\}\left[\sinh^{-1}\left(v_{ref}/v_0\right)\right]}\right\} \qquad 2.10$$

  Where a, b, c and n are the backbone curve parameters, V is the normalised penetration rate and v_0 is the penetration rate at which the viscous rate effect starts to decay towards zero.

  The backbone curve parameters have been calibrated based on data from CPT and TPT test performed at various penetration rates in a centrifuge facility (Watson, et al., 2000; House, et al., 2001; Randolph & Hope, 2004). The normalised penetration rate V is taken as vd/c_v (Chung, et al., 2006) where d is diameter and c_v is the consolidaiton coefficient. Therefore, by fitting the hyperbolic sine curve to the laboratory data, three parameteras can be estimated: $\boldsymbol{\mu, c_v}$ **and** $\boldsymbol{v_0}$.

2.3.2.4 Strain softening & degradation curves

The degradation curve and the residual or remoulded strength of a fine-grained material are essential parameters for designers. This can be accomplished with full-flow penetrometers, which offers a rapid, cost-effective alternative to accurately assess in situ these parameters (Yafrate, et al., 2009). The penetrometer is cycled over a desired depth interval, degrading the soil by creating a turbulent large strain shearing and fabric de-structuration within the influence zone (Yafrate, et al., 2009).

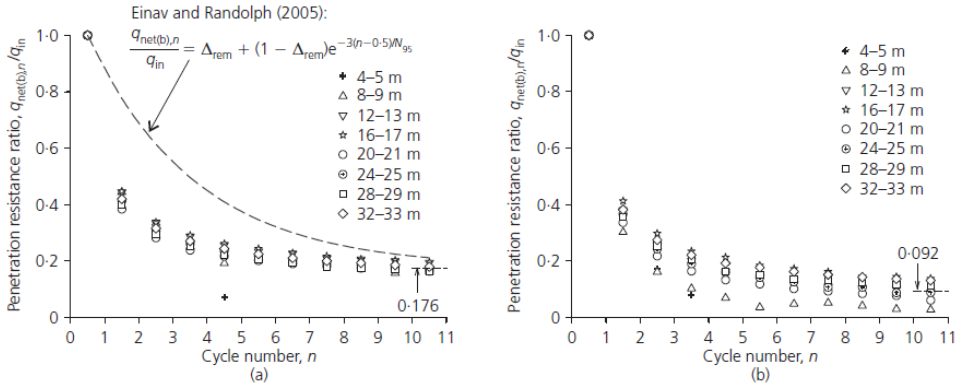

Figure 2.13 Degradation behaviour expressed by normalised resistance plotted against cycle numbers (Nguyen & Chung, 2015)

The degradation curve is usually presented as the ratio of the penetration of each cycle (q_i) to the initial penetration (q_{in}) versus the number of cycles. Some results obtained by Nguyen & Chung (2015) are shown in Figure 2.13, where they studied the degradation for penetrometer with different area ratios. They found that balls with small values of A_r, produce highly consistent degrading curves at all depths.

The degradation curve can be analytically derived following the theory proposed by Einav & Randolph (2005) by considering the theoretical average shear strain per passage of the penetrometer (ξ_P) and measuring (a) the number of cycles N95 to achieve 95% of the degradation (Deg_{95}) and (b) the remoulded penetrometer resistance normalized by the initial penetration resistance Δ_{rem}. The penetration resistance of each subsequent cycle can be expressed as:

$$\Delta(n) = \Delta_{rem} + (1 - \Delta_{rem})e^{-3(n-0.5)/N_{95}} \quad 2.11$$

This equation is generally plotted with the test results as shown in Figure 2.13.

Using the calculated value of ξ_P from the UBSPM, ξ_{95} may then be deduced from:

$$\xi_{95} = 2\xi_P N_{95} \quad 2.12$$

Table 2 - Calculated strain values with the UBSPM (Einav & Randolph, 2005)

α	ξ_p
0	2.41
0.25	2
0.5	1.71
0.75	1.45
1	1.35

The fully remoulded strength ratio δ_{rem} is taken as equal to the friction ratio (α) or as the inverse of the sensitivity $(1/S_T)$ for the first iteration (i). Then $\delta_{rem,i+1}$ is back-calculated using equation **2.13** until it reaches a constant value.

$$\delta_{rem,i+1} = \left[\delta_{rem,i} + (1 - \delta_{rem,i})e^{-1.5\xi_P/\xi_{95}}\right]\Delta_{rem} \quad 2.13$$

2.3.2.5 Interpretation of full flow penetrometer tests

To get to the net penetration resistance of the full flow penetrometers one can start by looking at the equation used for the measured cone resistance (CPT). The measured resistance is corrected for the pore pressure generated in the shoulder where the o-ring is installed, as follows:

$$q_t = q_c + (1 - a)u_2 \quad 2.14$$

Where,

q_c: measured cone resistance
a: cone area ratio
u_2: pore pressure at the cone shoulder

The net cone penetration resistance (q_{net}) is corrected for overburden pressure:

$$q_{net} = [q_c + (1 - a)u_2] - \sigma_{v0} = q_t - \sigma_{v0} \quad 2.15$$

σ_{v0}: In-situ total overburden pressure at the cone tip

For the BPT the total ball resistance ($q_{t(b)}$) is similar as q_t, but the area ratio factor reduces the pore pressure correction:

$$q_{t(b)} = q_b + \left[(1 - a)u_{2(b)}\right]A_r \quad 2.16$$

Where,

q_b: measured ball resistance (similar to q_c)
A_r: ratio of the cross-sectional area of the shaft to the projected area of the ball (Shaft-ball area ratio $A_r = A_{shaft}/A_{ball}$

The net ball penetration resistance ($q_{net(b)}$) is corrected for overburden stress, which is also reduced by the area ratio:

$$q_{net(b)} = q_b - \left[\sigma_v - (1 - a)u_{2(b)}\right]A_r = q_{t(b)} - \sigma_v A_r \quad 2.17$$

Where,

σ_v: Total overburden stress at the ball level
$u_{2(b)}$: Pore pressure at the connection between the ball and the shaft

As determining σ_v and $u_{2(b)}$ correctly is difficult, $q_{t(b)}$ and $q_{net(b)}$ may be calculated using the in-situ total overburden stress (σ_{v0}) and the static equilibrium water pressure (u_0) as follows:

$$q_{t(b)} = q_b + [(1-a)u_0]A_r \quad 2.18$$

$$q_{net(b)} = q_b - [\sigma_{v0} - (1-a)u_0]A_r \quad 2.19$$

Note that the correction for pore pressure and overburden stress for the full flow penetrometer is lower than the one applied for CPT interpretation. For the case of the standard area ratio of 0.1, the correction is reduced 90%.

For a penetrometer with a negligible area ratio, which has not been invented by the date of this research, the measure resistance does not need to be corrected from either the pore pressure or in-situ vertical stress. In such hypothetic case the equation **2.19** can be approximate to:

$$q_{net(b)} = q_b = N_b s_u \quad 2.20$$

Where N_b is the bearing factor and s_u the undrained shear strength.

The remoulded undrained shear strength is:

$$s_{u,rem} = \frac{q_{rem}}{N_{b,rem}} \quad 2.21$$

The bearing factor N_b is defined as function of the friction ratio ($\alpha = f_s/s_u$) where f_s is the limiting interface friction (Einav & Randolph, 2005; Lu, et al., 2000), area ratio (Zhou, et al., 2016; Zhou & Randolph, 2011; Zhou, et al., 2013) soil sensitivity and viscous rate effect (Peuchen, et al., 2005; Lu, et al., 2000). Randolph & Houlsby (1984), Randolph, et al. (2000), Randolph (2004), Einav & Randolph (2005) and Yafrate & DeJong (2006) conducted analytical solutions to determine N_b for the ideal situation of a ball with no shaft, suggesting a range between 11.0 and 15.3 for smooth and rough ball penetrometers, respectively (see Figure 2.5). Compared with the CPT, the bearing factors for full flow penetrometer are better in relating penetration resistance to shear strength, since they are derived from a more robust theoretical basis, where a well-defined failure mechanism exists (Randolph, et al., 2000; Randolph & Houlsby, 1984; Einav & Randolph, 2005). Nevertheless, these factors can fall outside the theoretical ranges due to the soil sensitivity and the viscous effects (Peuchen, et al., 2005).

In general bearing factors for soils of high sensitivity are lower than those with moderate sensitivity (Low, et al., 2010). (Yafrate & DeJong , 2006) found that $N_{b,vane}$ for soils with sensitivity up to 90 could be as low as 7. Due to its variability (Low, et al., 2010) derived statistics of the N factor based on several locations (Table 3). Yafrate, et al. (2009) used the results of field vane shear test of 16 sites to determine the sensitivity (S_t), and correlate it with the results of several penetration resistance factors. He proposed the following equation:

$$S_t = \left(\frac{q_{in}}{q_{rem}}\right)^{1.4} \quad 2.22$$

q_{in}: Initial penetration
q_{rem}: remoulded penetration resistance
q_{rem}: is the average of penetration and extraction resistance of the last cycle

It is possible to estimate S_t from the ratio between the initial penetration (q_{in}) and the extraction penetration (q_{ext}):

$$S_t = \left(\frac{q_{in}}{q_{ext}}\right)^{3.7} \quad 2.23$$

The relationship proposed by Yafrate, et al. (2009) to determine the remoulded strength factor $N_{b,rem}$ is function of sensitivity as follows:

$$N_{b,rem} = 13.2 + \frac{7.5}{1 + \left(\frac{S_t}{8}\right)^{-3}} \quad 2.24$$

$$N_b = 13.2 - \frac{7.5}{1 + \left(\frac{q_{in}/q_{ext}}{1.8}\right)^{-20}} \quad 2.25$$

DeJong, et al. (2011) considered experimental data from 6 different sites, and the theoretical N factors for soils with $S_t = 1$, proposed the following equations:

$$N_b = 13.2 - \frac{7.5}{1 + \left(\frac{S_t}{10}\right)^{-3}} \quad 2.26$$

$$N_b = 13.2 - \frac{7.5}{1 + \left(\frac{q_{in}/q_{ext}}{1.9}\right)^{-20}} \quad 2.27$$

Table 3 - Statistics of N_b (Low, et al., 2010)

	No. Data	Range	Range	Mean	Std dev	COV
$N_{b,rem,UU}$	10	13.51	30.26	19.55	5.56	0.28
$N_{b,rem,fc}$	11	13.36	16.95	15.23	0.97	0.06
$N_{b,rem,vane}$	11	11.32	17.05	14.18	1.56	0.11
$N_{b,su,TC}$	14	8.22	10.66	9.44	1.72	0.18
$N_{b,su,ave}$	19	10.8	11.53	11.17	0.51	0.05
$N_{b,su,vane}$	24	12	12.38	12.19	0.27	0.02

An approximate expression for first penetration through the soil, considering strain rate and strain softening was proposed by Einav & Randolph (2005) as follows:

$$N_b = (1 + 4.8\mu)\left(\delta_{rem} + (1 - \delta_{rem})e^{-1.5\xi_p/\xi_{95}}\right)N_{b-ideal} \quad 2.28$$

Where $N_{b-ideal} = 11.41$ is the value derived for an ideal rigid-plastic material, μ is the strain rate parameter, ξ_p is the theoretical average shear strain, ξ_{95} is the cumulative shear strain required to cause 95% reduction and δ_{rem} is the fully remoulded strength ratio. Einav & Randolph (2005) suggested that the interface friction ratio should be taken as $\alpha = \frac{1}{S_t} = \delta_{rem}$.

Gradual softening of the soil as it passes through the mechanism is modelled by factoring the shear strength by a damage factor (Randolph, et al., 2005), δ, expressed as:

$$\delta(\xi) = \frac{s_{u,rem}}{s_u} = \delta_{rem} + (1 - \delta_{rem})e^{-3\xi/\xi_{95}} \quad 2.29$$

2.3.3 Temperature effects

A known issue of penetration tests, either CPT or full flow penetrometers is the apparent cone resistance registered when the penetrometer is exposed to differential thermal conditions; this is due to straining of the load cell, its strain gauges and its adhesives (Peuchen & Terwindt, 2014). The change is proportional to the temperature change, and it could be induced by change in ambient temperature (e.g. by lowering the CPT from deck at 35°C to the seabed where temperature can be as low as 4°C (Low, et al., 2008a)), or by self-heating of a probe as a result from frictional heat during penetration and thermal flux through rods.

A high temperature gradient has also an effect when testing in offshore box-cores with mini full flow penetrometers, as the gradient arises from and atmospheric pressure of ~30°C and a seabed temperature of ~4°C (Low, et al., 2008a). This can lead to a large zero drift of the embedded load cell (Randolph, et al., 2007; Low, et al., 2008a). To reduce the effect of temperature gradient, the probes are sometimes, in practice, stored in cooling boxes to reduce the temperature of the steel before testing. Another common practice is to arrest the penetrometer at a certain depth below the sample until the load cell reading stabilizes before the start of the test (Low, et al., 2008a; Yafrate, 2008).

An alternative approach to overcome the zero-drift issue caused by the temperature gradient would be to measure the resistance externally by installing the load cell way up in the shaft. On the other hand, this would lead to uncertainty regarding the correction for shaft friction and would also increase the risk of bending of distortion of the readings to the bending moments (Low, et al., 2008a).

2.3.4 Vane shear test

The vane shear test (VST), is an in-situ test used to determine s_u and $s_{u,rem}$, It has been used extensively since late 1940s (Chung, 2005). Its use, procedures, calibrations and calculations are standardised by ASTM International (2015), NORSOK (2004) and ISO (2014). The vane consists of four rectangular blades, with known thickness, set at right angles. The dimension of the blades can be changed depending on the strength of the soil; three different sizes, with a height to width ratio of two and the height ranging between 80 mm and 130 mm are used (NORSOK, 2004). The primary advantage of this test is that it gives a direct measurement of intact undrained shear strength (s_u), remoulded undrained shear strength $(s_{u,rem})$, and therefore the sensitivity of the soil. For the calculation of s_u and $s_{u,rem}$, the

peak torque, the post-peak torque, and the size of the blade is needed, and its interpretation is given by:

$$T = \frac{\pi d^3}{6}\left(1 + \frac{3h}{d}\right)s_u \qquad 2.30$$

However, there are known effects of other factors that are not easy to assess and integrate, to obtain a more accurate result (Peuchen & Mayne, 2007; Low, et al., 2008a; Chung, 2005); these are:

- Disturbance during insertion of the vane;
- Waiting time after insertion;
- Rate of rotation of the vane (strain rate effects);
- Geometry of the failure surface;
- Progressive failure;
- Aspect ratio (length/diameter) of the vane due to anisotropy of strength on the horizontal shear plane versus that on the vertical shear plane.;
- Errors caused by soil-rod and internal friction.

Despite these known errors, the VST provides a convenient measurement that can be compared with in situ penetration tests, as well as triaxial and simple shear tests (Peuchen & Mayne, 2007). Nonetheless, it only provides a discrete measurement of the strength of the soil instead of a continuous profile.

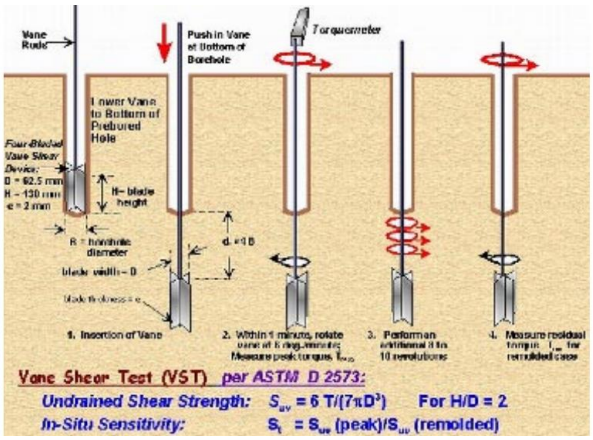

Figure 2.14 - Procedures for field vane testing during boring advancement (Peuchen & Mayne, 2007)

2.3.5 Laboratory miniature vane shear test

This test is the miniature version of the in-situ vane shear test, and is classified as a strength index test (CEN 2007). It consists of inserting a four-bladed vane in an intact tube sample, or remoulded specimen, and rotate the blade at a constant rate until failure. It records the peak torque and the post-peak torque, therefore is possible to calculate s_u, $s_{u,rem}$ and sensitivity. It has the same effects and errors explained in section 2.3.1. The testing procedures, application, calibration, and calculations are standardised by ASTM D4648 (2016), NORSOK (2004) and BS 1377-7 (1990).This laboratory test is usually performed at the laboratory facilities of the vessels or on deck. If testing on a box core, is recommended to do the test on the box core itself instead of performing it on a sub-sample (Randolph, et al., 2007; Puech, et al., 2011).

2.3.6 Fall Cone

The fall cone is a rapid index testing for determining s_u and $s_{u,rem}$. The test consists of letting a standard cone of specific dimensions and mass, fall over on the sample and penetrate it under its self-weight. The depth of penetration is measured and is correlated to undrained shear strength. The cone size and weight can be selected to suit the expected undrained shear strength. Its application, calibration and calculations are standardised by ISO/TS 17892-6 (2004) and ISO 19901-8:2014 (2014). Due to the nature of this test (free fall of a cone) it is not performed offshore, as the waves, heave and general movement of the vessel will affect the readings. The test is used onshore as an index test and to determine consistency parameters.

3. DESIGN OF TEST SET-UP AND ITS CAPABILITIES

As explained in section 1.1, the motivation of this innovative tool is to tackle some of the issues that the standard in situ tests, and its miniature versions have when testing on extremely low strength fine-grained material. The design focuses on reducing as much as possible the shaft area to eliminate the corrections for pore water pressure and overburden stress. Additionally, it should prevent temperature shocks on the strain gauges, by installing the sensors to not be in contact with the sample. This versatile design allows to study the soil behaviour for monotonic, cyclic and variable penetration rate tests. Parameters like intact undrained shear strength, remoulded undrained shear strength, degradation curve, strain rate parameter and consolidation coefficient can be estimated.

3.1 Requirements

Prior the start of the thesis, a meeting was held between the three parties (TU Delft, Fugro and student) to define the requirements of the prototype to be designed. It was requested that the set-up will have the following characteristics:

- The ball will not have any internal instrumentation for measurements
- The size of the ball can range from 30 to 50 mm. The optimum diameter of the object must be determined
- The set-up will be design to guarantee a constant pulling rate (displacement controlled) when testing, if possible the design should also allow for load controlled testing
- The pulling velocity can range between 0.5 and 20 mm/s. The minimum and maximum rate to be determined prior construction of the tool. Velocity must be high enough to ensure undrained conditions. Monotonic and cyclic test must be performed
- Possibility of testing with a force-controlled rate, by using a high-speed feedback loop.
- Pulling will be done only in the horizontal direction
- Kaolin clay will be use as artificial sample
- Design of the load cell and its capacity; depends on selected ball size
- Dimension of the sample case is 50x50x60 cm to simulate the dimensions of the box corer. If consolidation time is too long, the small centrifuge can be used. The centrifuge sample has dimensions 15 (W) x 35 (L) x 20 (H) cm
- Pulling wire material and diameter: to be defined (e.g. steel wire, fishing rope)

3.2 Test set-up

The prototype was designed to perform horizontal monotonic, cyclic and variable-penetration tests (Figure 3.1). It consists of a stiff frame **(1)** with a linear actuator **(2)**, that pushes an aluminium trolley **(3)**, connected to a draw-wire and two S-type loadcells **(4)**, the load cells are perfectly aligned with the pulleys **(5)** and the box **(6)**. A rope **(7)** is connected to the strain gauges and the ball **(8)**, and it is pre-tensioned to reduce the vertical displacement and rotation of the penetrometer when testing.

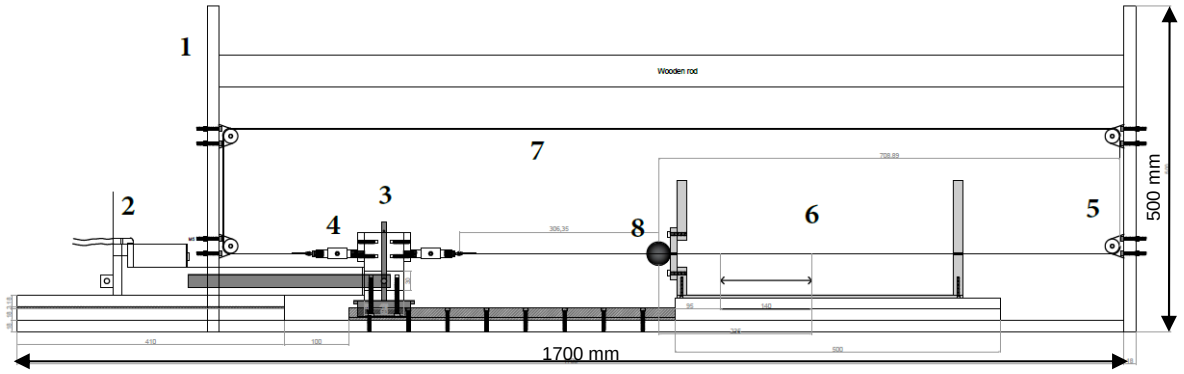

Figure 3.1 - Test set-up

The actuator will pull the ball through the soil at a constant penetration rate which is measured by the encoder and controlled by the motor controller. The load increments of the penetration and extraction cycles are measured by the load cells and the displacement is measured by a draw-wire connected to the trolley. The load cell installed at the left of the trolley measures the penetration resistance and the one at the right the extraction resistance.

A 1.2 mm-diameter rope with high elasticity modulus and low creep is selected. The rope is pre-tensioned to a specified value to limit the vertical displacement of the ball due to its own weight and to limit the rotation due to the undrained shear strength gradient (see details in chapter 3.6). The balls are made of aluminium or polyoxymethylene (POM) and have a diameter of 30 mm or 35 mm, giving an area ratio of 0.0016 or 0.0012, respectively. The area ratio, compared with the one of a standard for full flow penetrometer is negligible

The ball penetrometer does not have any instrumentation: the load cells and the displacement sensor are installed outside the penetrometer, and they will not be in contact with the sample. Hence, there will not be any temperature shock on the strain gauges due to the difference between the ambient temperature and the temperature of the sample.

The summary of the system and its capabilities is shown in Table 4.

Table 4 - Stitch set-up characteristics

Outer dimensions of the box	[mm]	180x190x440 (HxWxL)
Inner dimensions of the box	[mm]	175x170x410 (HxWxL)
Artificial sample		Kaolin clay
Ball diameter	[mm]	30 and 35
Cyclic range	[mm]	4D
Minimum constant tension	[N]	100
Resolution of tip resistance	[kPa]	1
Measurable soil resistance	[kPa]	>1
Measurable shear strength	[kPa]	>0.1

Motor		DC-Linear-Electric-DSZY4
Maximum force	[N]	500
Maximum stroke	[mm]	300
Penetration speed	[mm/s]	0.2 - 29
Load cell		S-type AS4H
Output sensitivity	mV/V	3.0+/-0.008
Load cell accuracy	[N]	+/- 0.013
Load cell capacity	[kg]	100
Safe load cell overload	[kg]	150
Ultimate load cell overload	[kg]	300
Rope		LIROS PPSL 191
Diameter of the rope	[mm]	1.2
Rope breaking load	[N]	2000
Strain at braking load	[%]	3

3.3 Test box

The strong aluminium box was designed to sustain the high pressure when consolidating the sample in the centrifuge and to be used for the experimental test which is performed at ambient pressure. The box has outer dimensions of 180x190x440 mm (H, W, L), and inner dimensions of 175x170x410 mm (H, W, L). It is certainly smaller than the standard box core (500x500x500 mm), since the size is limited by the centrifuge. It contains a 2 mm-diameter opening at the back, and a 40 mm-diameter opening at the front. The opening at the front is closed with two aluminium plates and a rubber sheet in between, to prevent leakage when consolidating the sample. The sample will be large enough to perform the penetration test without disturbing a section of the sample, which is essential to perform laboratory tests at the same depth of the stitch test for comparison.

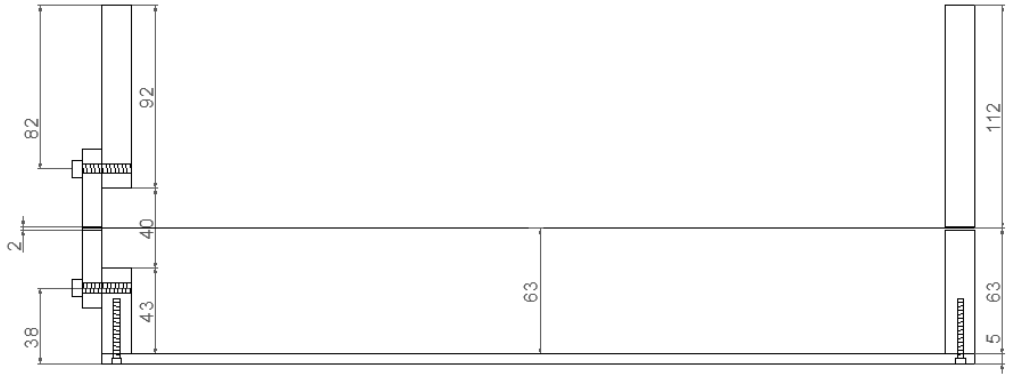

Figure 3.2 - Test box (dimensions in mm)

3.4 Ball penetrometer

The ball size was selected based on the dimensions of the test box. As explained in section 2.3.2.2, the width of the failure mechanism is function of the penetrometer roughness. The initial disturbance width can range from 1.8 to 2.6 times the penetrometer radius. If the failure mechanism reaches the surface

of the box (walls or bottom) the interface will contribute to the measured resistance, giving unreliable results. To prevent an increase in the measured resistance due to the interface between the soil and the box, a maximum width of 3 times the radius was selected as boundary condition for the maximum ball size (see Figure 3.3). Therefore, a maximum ball-diameter of 40 mm can be used based on the dimensions of the test box.

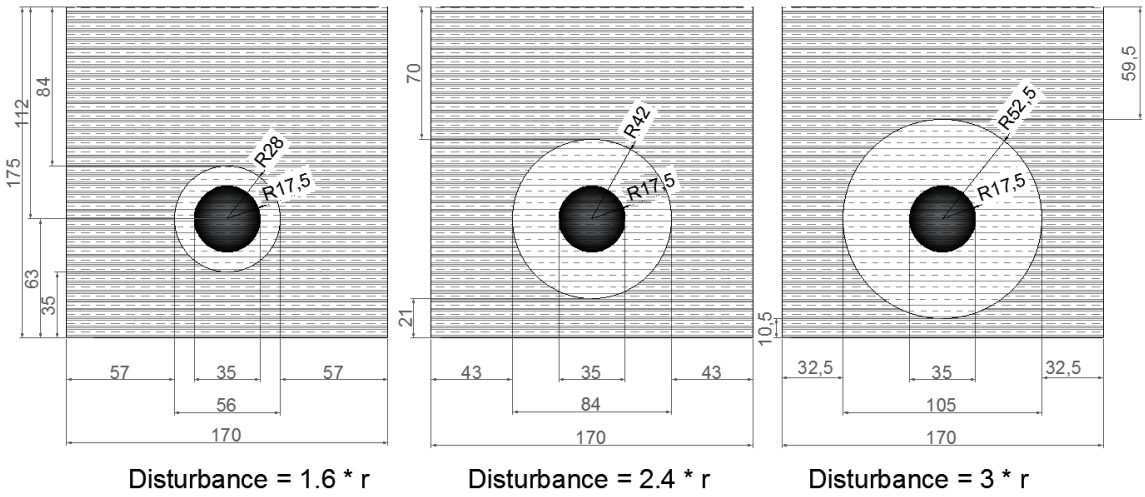

Figure 3.3 - Expected soil disturbance of the ball penetrometer, based on Figure 2.11. Left: steady state. Centre: Initial disturbance. Right: Design scenario for the selection of the ball diameter and the penetration depth.

The balls have a diameter of 35 mm or 30 mm and are made of aluminium (Al-2024) or polyoxymethylene (POM). The roughness of the ball has an influence on soil response as it has been reported that the soil resistance increases approximately linearly with friction ratio (α) (Lu, et al., 2000). This is reflected in the selection of the bearing factor N_b, which considers, among others, the penetrometer roughness. For this research the approximation of $\alpha = \frac{1}{st} = \delta_{rem}$ is used (see 2.3.2.5).

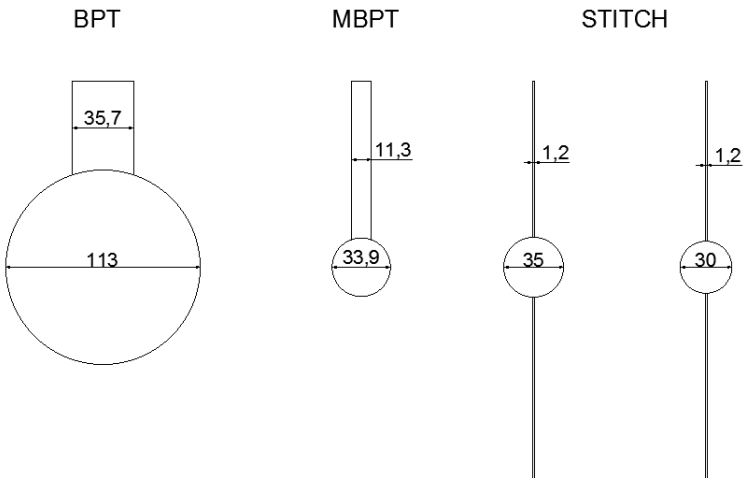

Figure 3.4 - Geometry of the BPT, MBPT and the stitch (dimensions in mm)

The ball size will have an influence on the selection of the capacities of the motor, the load cells and the rope. One of the main advantages of the full flow penetrometers compared with the CPT is the increase

of resolution due to a bigger projected area. The bigger the ball, the larger the external force it must apply to displace the penetrometer. The external force is calculated by multiplying the soil resistance (q_b) by the projected area of the penetrometer (A_p):

$$F = q_b * A_p \quad 3.1$$

The soil resistance is then chosen based on the minimum and maximum undrained shear strength that is aimed to be measured. The bearing factor is expected to be close to the ideal value of the theory of a penetrometer with no shaft, which is around 12, nonetheless, uncertainties and other factors like sensitivity, might influence this value, and it will be assessed in the experimental stage. Therefore, a lower estimate of $N_b = 8$ and a high estimate of $N_b = 16$, and a best estimate of $N_b = 12$ were selected to calculate the soil resistance for selection of the motor and the loadcell capacities. This gives, for a maximum of 20 kPa of undrained shear strength, a resistance of 320 kPa. Equation **3.1** is plotted in Figure 3.5.

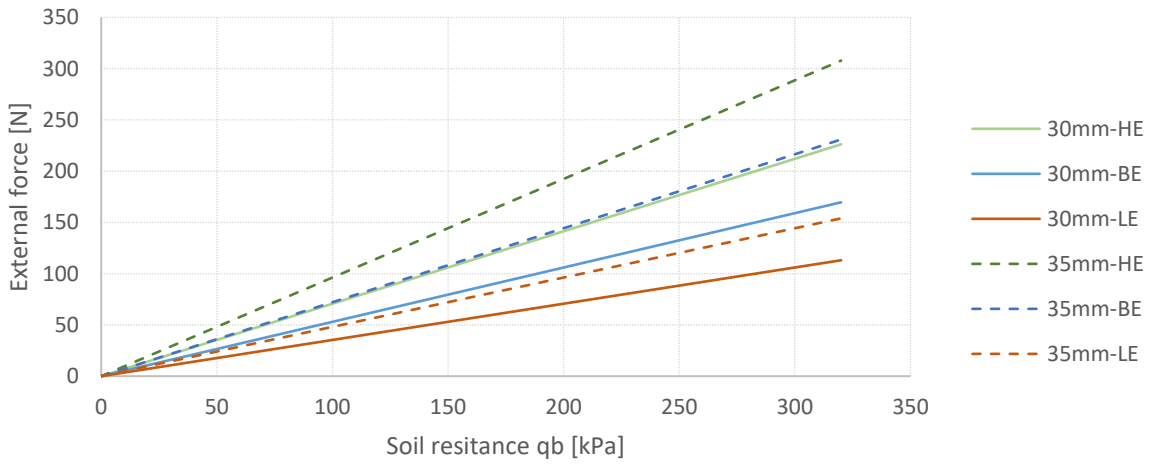

Figure 3.5 - External force versus soil resistance for a 30mm and 35mm ball penetrometers

3.5 Motor

The motor was selected based on three main characteristics: workable load, stroke and rate. As shown in Figure 3.5, it is required an external force of 320 N to mobilise the penetrometer in the scenario of a sample with 20 kPa of s_u (assuming a very conservative value of $N_b = 16$). The motor will also have to push the aluminium trolley that sits on a rail, therefore, a higher value for the maximum force must be selected. The stroke was selected to be enough to penetrate the sample 6 times the diameter of the ball (210 mm), because cyclic test will be performed from 2D to 6D. The actuation rate of the motor was selected to have sufficient range to perform a variable penetration rate test.

A linear motor (DC-Linear-Electric-DSZY4) with a maximum axial load of 500 N, a stroke of 300 mm and an actuation rate between 0.2 and 29 mm/s was selected.

3.6 Pulling rope

The rope is a crucial element for the test. It was desired to have a rope, wire or chain, with the smallest possible diameter, but with a high elastic modulus and low creep. The elongation of the rope when testing, will create uncertainties in the measurements. To select the appropriate material, first the range

of tension induced on the rope was estimated. This is given by the tension required to maintain the ball horizontally and on the desired path when testing - which I will refer to as “minimum constant tension” - plus the expected soil resistance. The second is taken from Figure 3.5 as 320 N.

The minimum constant tension is estimated by doing a static analysis of the ball penetrometer. The tension on the rope is function of the vertical deflection, the weight of the ball, and the length of the rope Figure 3.7 shows the relationship between the tension in the rope and the vertical displacement of the penetrometer for the three available balls.

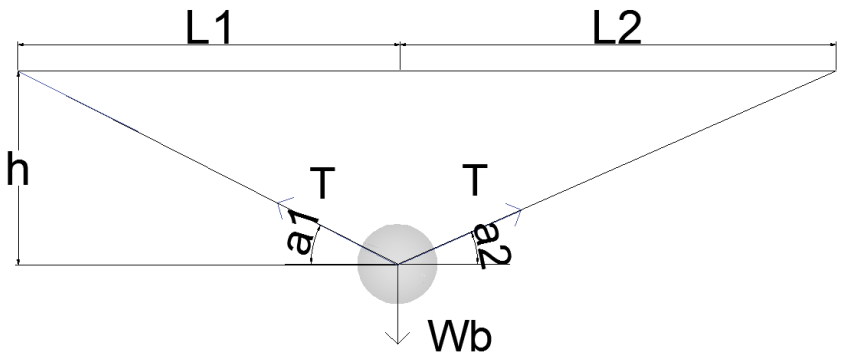

Figure 3.6 - sketch of the forces applied on the rope

$$\sum Fy = 0 = T \sin \alpha_2 + T \sin \alpha_1 - W_b \quad 3.2$$

$$T = \frac{W_b}{\sin \alpha_2 + \sin \alpha_1} \quad 3.3$$

$$\alpha_1 = \tan^{-1}\left(\frac{h}{L1}\right) \quad 3.4$$

$$\alpha_2 = \tan^{-1}\left(\frac{h}{L2}\right) \quad 3.5$$

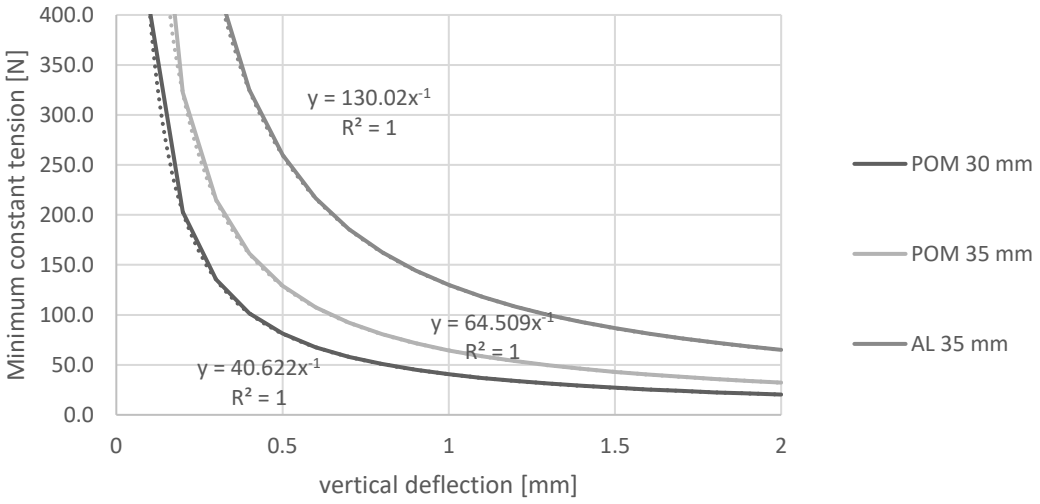

Figure 3.7 - Minimum constant tension vs deflection of the penetrometer (ignoring buoyancy)

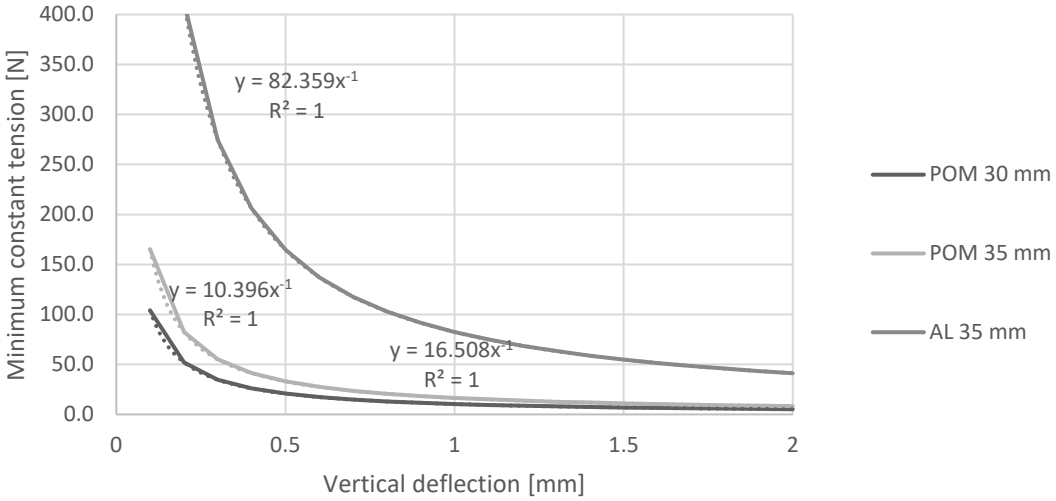

Figure 3.8 - Tension vs deflection of the penetrometer (with buoyancy)

The ball will tend to rotate as it advances horizontally due to the shear strength gradient and the vertical and horizontal stresses, and its particularly relevant for the first penetration, when the soil is in its intact state. With further remoulding, the strength difference decreases, and therefore, the rotation of the ball will tend to zero with increasing number of cycles. Compared with a vertical penetration, the stresses and strength around the penetrometer are asymmetrical, with asymmetry increasing with increasing s_u gradient. As it will be reported later in chapter 0, the undrained shear strength gradient depends on the G-force at which the sample is consolidated, ranging from 4 kPa/m to 30 kPa/m.

Analytical assessment of the rotation of the ball is challenging, as the failure mechanism, combined with the resistance of the rope (shaft resistance and flow resistance) complicate the system and difficult the assessment. To have a rough estimation of the rotation of the ball, a simplified approach was proposed, with the following assumptions:

- The undrained shear strength is selected as the average value of the influence zone of the penetrometer.
- The soil resistance is applied directly at the top and bottom of the penetrometer. The true failure mechanism involves a combination of compression, extension and DSS on a shear band, and is expected to induce a lower moment on the ball than this simplified approach in which the soil resistance is applied at the quadrants of the penetrometer (see Figure 3.9).

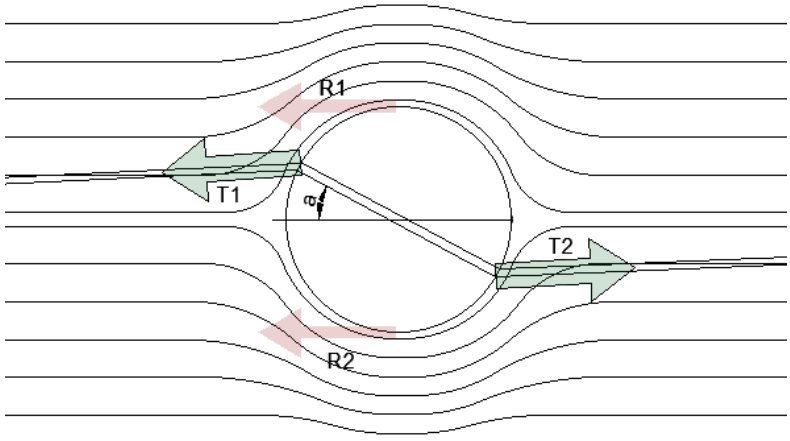

Figure 3.9 - assumed equilibrium around the penetrometer in steady state conditions

By analysing the system on a steady state conditions, the angle of rotation when the moment around the penetrometer reaches equilibrium, was calculated as function of the minimum constant tension and presented in Figure 3.10. with a higher s_u gradient, a higher tension is required to limit the rotation of the ball. To select a suitable rope for this application, it was assumed that a maximum of 400 N will be applied on the rope to reduce the rotation of the ball; this value, summed with the tension induced by the high estimate of maximum soil resistance (320 N), suggests that the rope will be subjected to a maximum service load of 720 N.

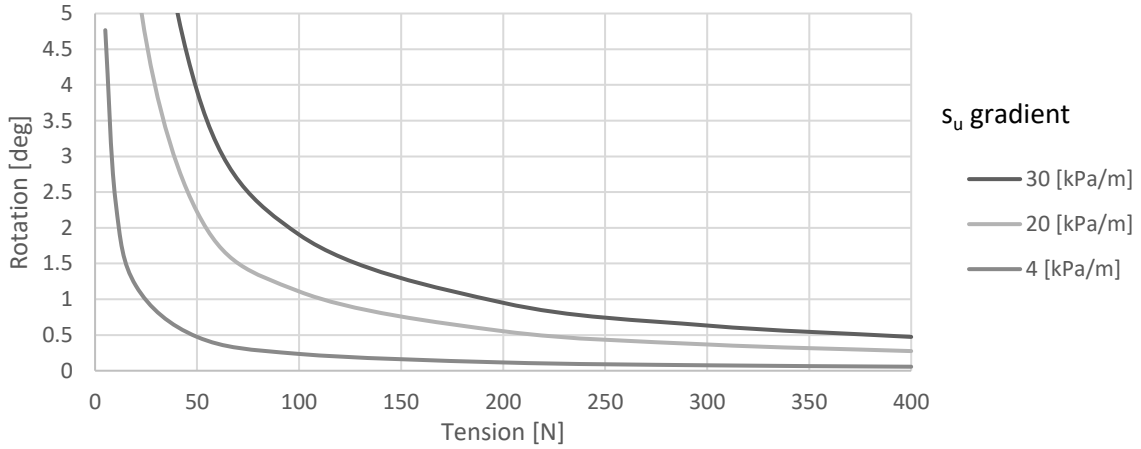

Figure 3.10 - Rotation of the ball as function of the minimum constant tension

The rope selected for this application (Liros PPSL191) consist of a core of Dyneema® cover with polyester. It has a breaking load of 1900N - more than twice the calculated maximum service load. It has a diameter of 1.2 mm, which gives an area ratio of 0.0016 for the 30mm-ball and 0.0012 for the 35mm-ball. Compared with the BPT or MBPT the area ratio is negligible (see Figure 3.4), which eliminates the correction for overburden stress and pore pressure. The force-strain relationship of the rope was constructed with the information provided by the supplier, and its shown in Figure 3.11

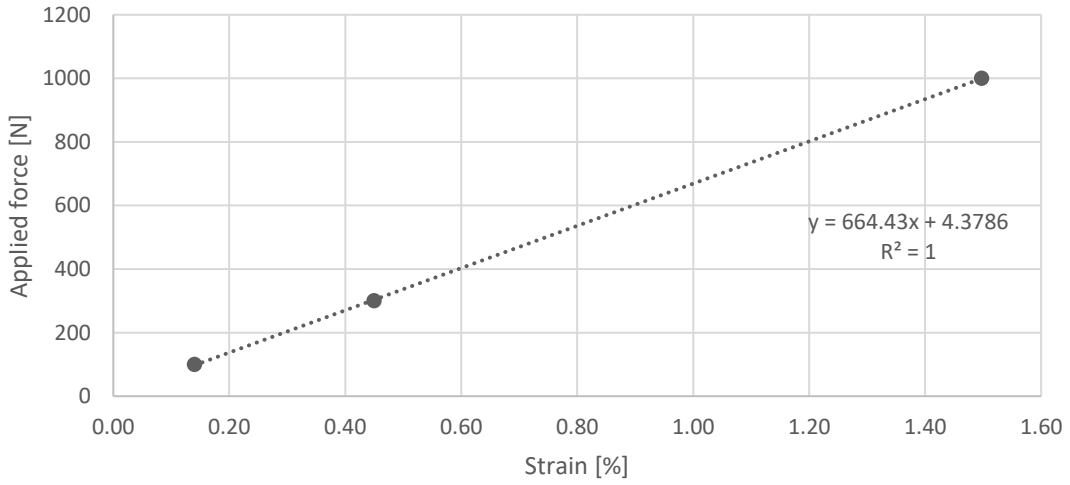

Figure 3.11 - Rope force-strain relationship

To assess the incremental load induced by the rotation of the ball, the elongation was calculated and correlated to force. Given a defined rotation, the rope will deform a certain value. It is important to note that the rope sections have different length (see Figure 3.12). The longer the rope, the more it will

elongate by a given tension. Section 2 is around 8 times longer than section 1, which means that for a given rotation the tension in section 2 will be lower than in section 1 (see Figure 3.14). If excessive rotation happens, due to the different rope lengths, the rotation will not be symmetric, but it will involve also vertical displacement of the ball with respect to its idealised trajectory. For this assessment, the ball will be considered to rotate perfectly and symmetrically around its centre of gravity (see Figure 3.13). Now, for a given rotation (α), the elongation of the rope is calculated as follows:

$$L_i' = \sqrt{(r\sin\alpha)^2 + \left(L_i + r(1+\cos\alpha)\right)^2}$$

Where L_i' is length of the rope for a given α rotation, L_i is the initial length of the rope,i refers to the section (1 or 2), and r is the radius of the penetrometer. Given the elongation, the strain is calculated, and with the force-strain relationship, the force required to cause the strain is calculated and presented in Figure 3.14. An excessive rotation of 20 degrees will cause increase in tension of around 2N in the shortest rope (section 1). This value would be recorded by the loadcell, and assuming $N_b = 12$ and $A_p = 962\ mm^2$, it can be misinterpreted as a soil resistance of around 0.2 kPa, which is a significant value for the extremely low strength samples that are aimed to be measured. If the rotation is limited to 5 degrees (which is still a high value), the induced tension on section 1 would be around 0.15 N, which correlates to 0.013 kPa of s_u, a value that becomes acceptable for the application. As it can be seen in Figure 3.10, the rotation is highly limited by the minimum constant tension, and if the tension is higher than 50 N, the rotation, in any case, will be less than 5 degrees. This rotation will induce an additional tension on the rope, which will be recorded by the loadcell, but as mention before, its magnitude is not relevant and it can be neglected.

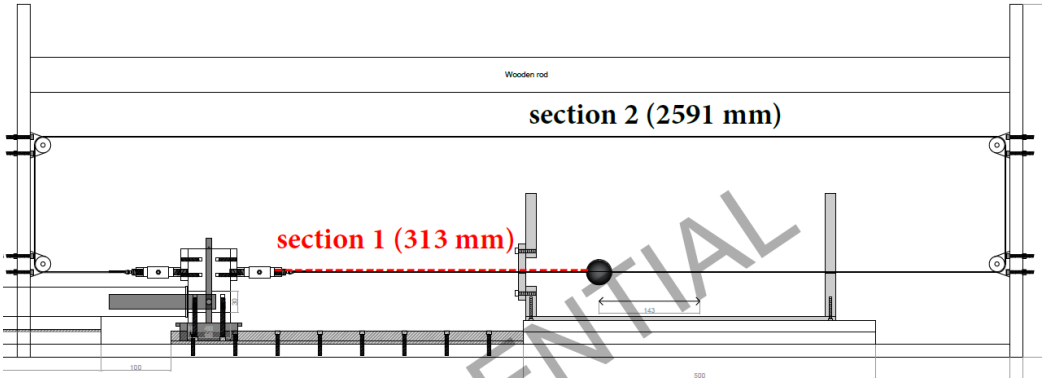

Figure 3.12 - Length of the rope for rotation assessment

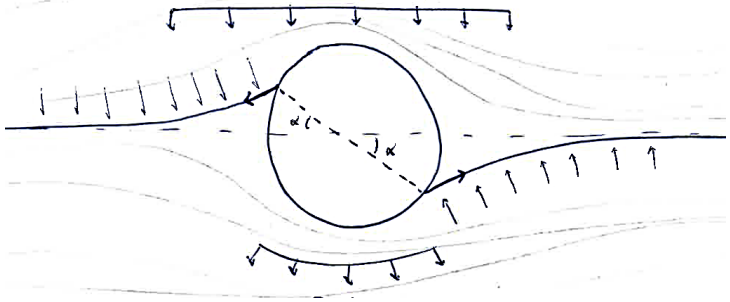

Figure 3.13 - Equilibrium around the ball penetrometer in steady state conditions

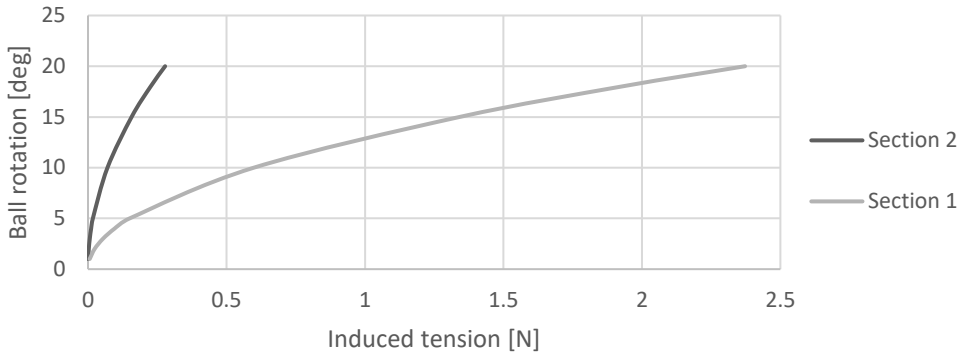

Figure 3.14 – Rotation of the ball vs induced tension on the rope

3.7 Load cells

The load cell will be subjected to a constant tension, which its maximum value was calculated in section 3.6, to be 400 N. A maximum soil resistance of 320 kPa was determined in section 3.4. This will sum to a maximum load of 720 N applied to the load cells. Additionally, it is aimed to capture small load increments; 0.1 kPa of s_u is roughly interpreted as 1 N increment in the load cell. The strain gauge load cells are normally limited to work on a minimum stable increment of 1/10000 of the load capacity.

As the load cell is installed outside the sample, in the aluminium trolley, the issues related to temperature and bending identified in the standard full flow penetrometers does not apply to this system.

Two nickel plated alloy steel IP67 S-type load cells (AS4H) with 1 kN of capacity, 1.5 kN of safe overload and 3 kN of ultimate overload, were selected (see Figure 3.15). The load cell accuracy is +/- 0.013N which falls in the desired resolution.

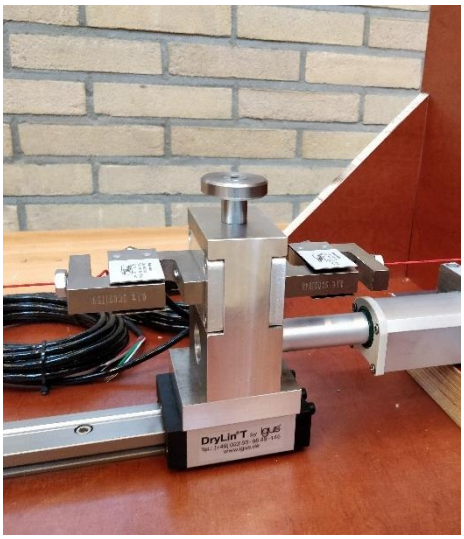

Figure 3.15 - S-type load cells (AS4H) mounted on the trolley

3.8 Pulleys

The rope will be installed in a system of 4 pulleys. The interaction between the rope and the pulleys will generate friction and vibrations, which will be capture by the load cells. Initially four commercial pulleys with plastic ball bearings were installed. It was identified that the pulleys had an eccentricity which caused an oscillatory behaviour when pulling in a single direction, generating load increments where the peak to peak differences were up to 12N, which is an enormous value. Therefore, better pulleys

were purchased to reduce the noise generated by the interaction between the pulleys and the rope. The selected pulleys have a safe lifting capacity of 130kg or 1270 N. The system compliance will be further assessed in Section 4.2.

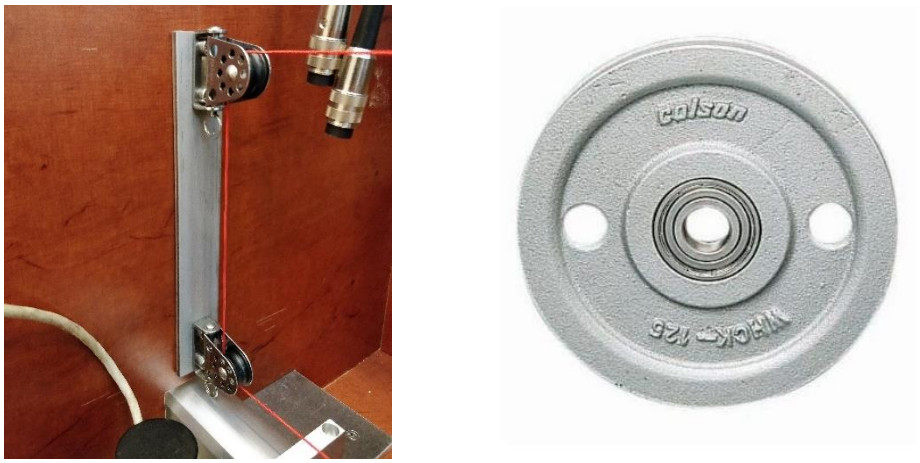

Figure 3.16- left: commercial pulleys with plastic ball bearings. Right: final pulleys with steel ball bearings

3.9 Control unit

The data acquisition system consists of a micro controller and a macro controller, which converts the impulses and signals from the load cells, encoder and draw-wire to physical measurements. A maximum measurement interval of 10 mm (2 Hz for a penetration at 20 mm/s) is recommended in the literature (DeJong, et al., 2010; Lunne, et al., 2011). The stitch is capable to record data with a frequency equal or lower than 10 Hz. Strain-controlled monotonic, cyclic and variable penetration rate tests can be performed. For the cyclic and variable penetration rate test, the user must change a text file specifying the target position and speed for each cycle. A standard PC/laptop can be used for controlling the motor and log the data. The software Mp3 © TU Delft is used to input the data, visualize the measurements in real-time and store the output results.

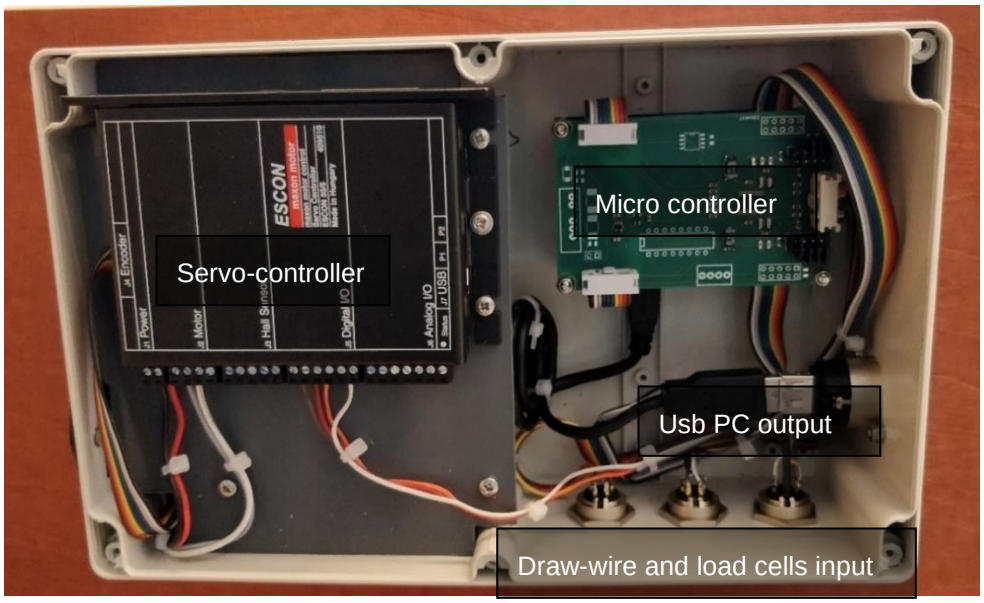

Figure 3.17 - Stitch control unit

3.10 Installation

The installation of the rope will disturb the sample and reduce its strength prior testing by any mean. The alternative of the insertion of the rope with a needle was studied. The length of the box is 440 mm, and has two holes for the insertion of the rope of 2 mm-diameter. The rope has a diameter of 1.2 mm. The needle diameter need to be as small as possible to reduce the induced disturbance during rope installation. A 1.5 mm steel needle will buckle by its own weight, and it will be particularly challenging to penetrate the soil and reach a 2-mm hole at the other side of the box. It was consequently decided that for this research the rope will be installed in the box prior pouring the slurry and consolidating it in the box. This alternative might have less influence on the sample than inserting with a needle. On the other hand, having these alternative can lead to leakage during consolidation, unbalancing the loads and damaging the equipment. Therefore, special attention must be given to the seals and installation technique.

The installation process is best resumed in the following 6 steps (also see Figure 3.18):

1. First the seals and testing rope are placed and pre-tensioned, then the slurry of kaolin clay is poured in the testing box. The sample is reconsolidated in the centrifuge.

2. Once consolidation is finished, the testing box is placed in the test frame, and the rope is connected to de load cells.

3. The rope is then tensioned until the defined value is reached.

4. The aluminium plates and the rubber at the front of the box are removed to allow the intrusion of the penetrometer.

5. The motor is actuated to introduce the penetrometer in the sample.

6. Once the ball has penetrated at least one diameter, the aluminium plates are screwed back again to prevent leakage, and thereafter the test can start.

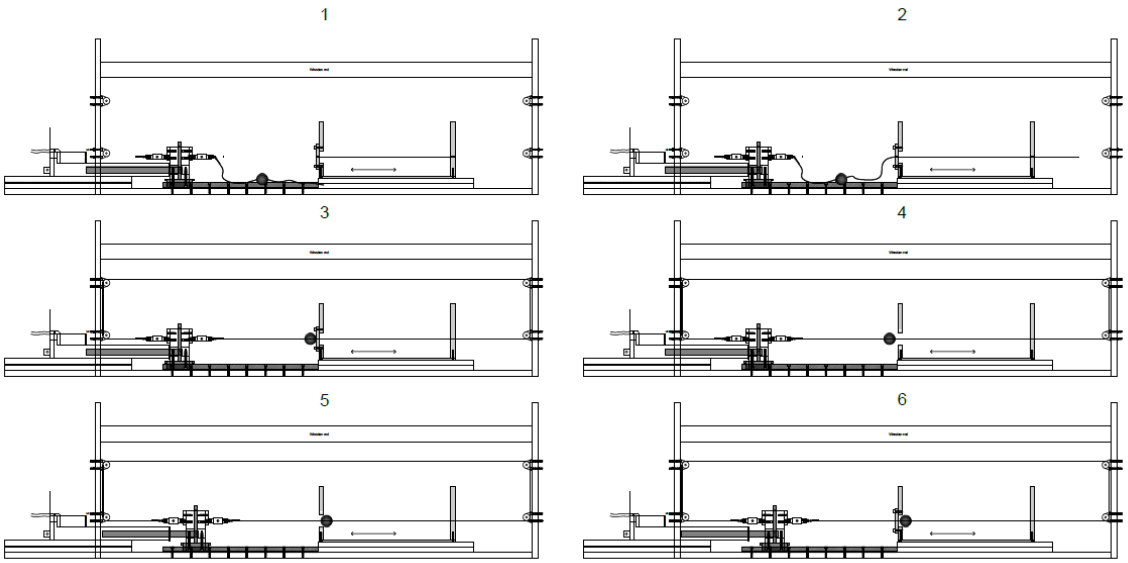

Figure 3.18 - Installation process

3.11 Overburden stress

As discussed in section 2.3.2 the correction for overburden stress for the full flow penetrometers is lower compared with the CPT. The correction decreases with decreasing area ratio. Zhou & Randolph (2011) conducted LDFE analysis and presented the effect of overburden stress, assuming an effective unit weight of $\gamma' = 7\ kN/m^3$(see Figure 3.19). All the curves converged on a normalized resistance of 12.4 for a ball with no shaft, which confirms that for a shaft-ball area ratio of zero, the overburden stress has no effect when testing vertically.

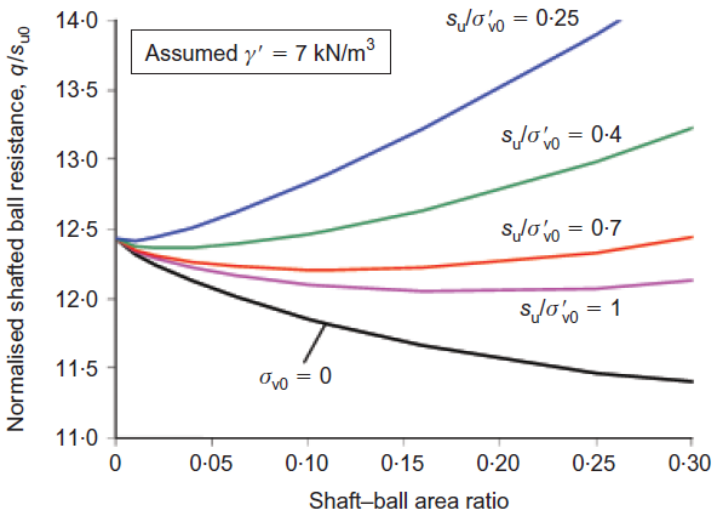

Fig. 7. Effect of overburden stress on normalised penetration resistance

Figure 3.19 - Effect of overburden stress on normalised vertical penetration (Zhou & Randolph, 2011)

When testing horizontally, the overburden stress underneath the ball can be as large as twice the overburden stress above the ball for the current test set up. The ratio becomes larger for the area of influence, where the initial disturbance could be 2.4 times the diameter of the ball. This can lead to a non-symmetric flow of the soil around the probe (see Figure 3.21), as the soil on top is in a lower stress state than the soil on the bottom. The theory and FE analyses that have been performed are for a ball penetrating vertically a media, therefore the particles at both sides of the ball are in the same vertical and horizontal stress. Figure 3.20 shows the stresses in polar coordinates of an infinitesimal particle of soil at distance r from the centre of the probe. The radial (σ_r), tangential (σ_θ), and shear ($\tau_{r\theta}$) stresses, for a vertical penetration are the same at a given depth, which means that the flow is symmetrical around the penetrometer; for a horizontal penetration (advancing in the x axis) the stresses in the failure mechanism differ at given penetration (x), for the reason that the stresses and strength changes with depth, therefore the failure mechanism is expected to be asymmetrical, being wider at the top of the ball and narrower at the bottom.

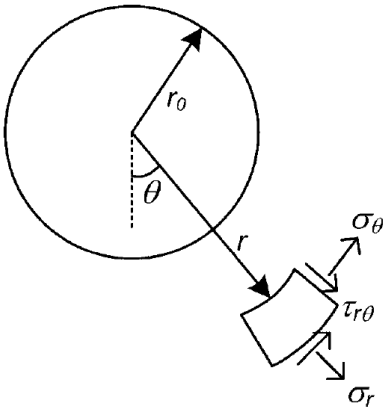

Figure 3.20 - Stress in polar coordinates (Klar & Osman, 2008)

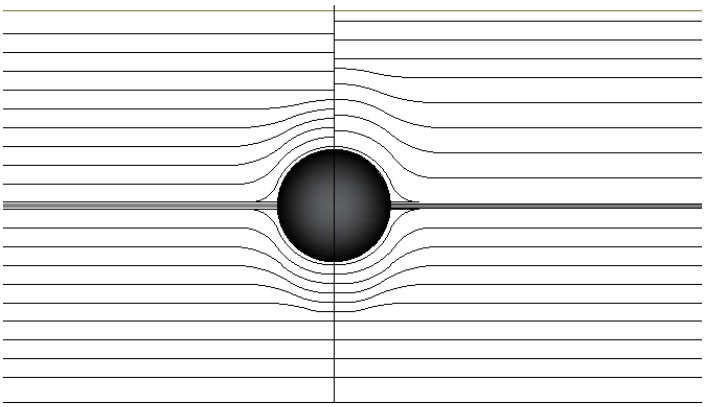

Figure 3.21 - left: symmetrical streamlines. Right: non-symmetrical streamlines

4. STITCH TESTS

In this Chapter the strength characterization of the kaolin clay, the determination of the system compliance and the observations during the execution of each stitch test are discussed. A total of eight samples were prepared. Two samples were used for the characterization of the strength of the kaolin clay by laboratory vane shear tests and fall cone tests. Six samples were prepared for the stitch tests to study the behaviour and soil resistance with varying undrained shear strength. The first four stitch test were performed with the 35 mm-diameter polyoxymethylene (POM) ball. The stitch Test 4 was performed with 1.4 kPa of surcharge to increase the confining stress. Stitch Tests 5 and 6 were performed with the 30 mm-diameter POM ball. 2 series of tests were performed in sample 5; first, monotonic, cyclic and variable penetration rate tests were performed without surcharge. The second series of Test 5 were performed on the remoulded clay to investigate the influence of overburden stress by conducting cyclic test with varying surcharge.

4.1 Samples for strength characterization

The kaolin clay slurry is constantly prepared at the TU Delft facilities by mixing dry kaolin powder with water under vacuum in a barrel mixer. From the bottom of the mixer the water-kaolin mixture is pumped to a glass container where the clay particles slowly segregate; forming an extremely soft slurry with high water content (above 100%). A second glass tank contains “old slurry” which has been consolidated by its own weight and has a water content lower than 70%. The samples for the strength characterization and the stitch tests were prepared by mixing clay from both tanks to reach a water content between 60 and 80%.

The small centrifuge has an arm length of 475 mm (to the bottom of the sample) and the box used for the strength characterization is 140 mm height. The first sample was consolidated from slurry with 67% water content and then spun at 420 RPM for 24 hours. The second sample was prepared with a water content of 80% and then spun at 320 RPM for 24 hours. The distrubition of the centrifuge acceleration through the sample is shown in Figure 4.1.

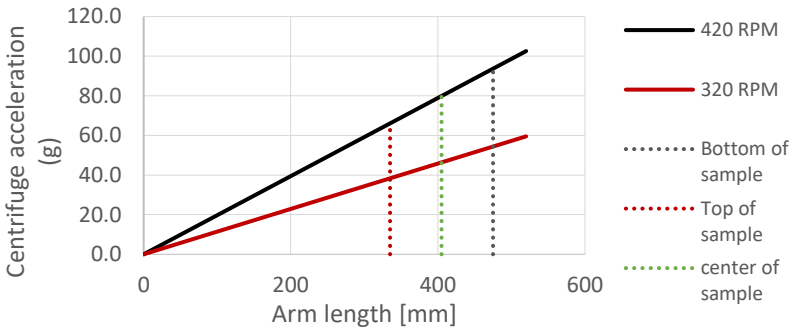

Figure 4.1 – Centrifuge acceleration (g) as function of arm length for different angular velocities

Several laboratory vane shear tests were performed at different depths of the consolidated samples. The sample surface was thereafter scraped away to perform fall cone tests at different depths and locations. A non-linear trend in the s_u profile was identified (Figure 4.2). The pore water pressure, effective stress and void ratio changes non-linearly with depth due to the change of the acceleration acting on the sample when its being consolidated. The variability of the fall cone results, increases with increasing depth due to the disturbance caused by the removal of the soil. A curve was fitted to the

results by assigning a s_u/σ_v' ratio of 0.062 for the first sample and 0.07 for the second. The vertical effective stress in the centrifuge is defined as $\sigma'_{centrifuge} = \rho * (Ng) * d$; where ρ is the density of the material, Ng is the acceleration in the centrifuge which is function of the arm length, and d is depth.

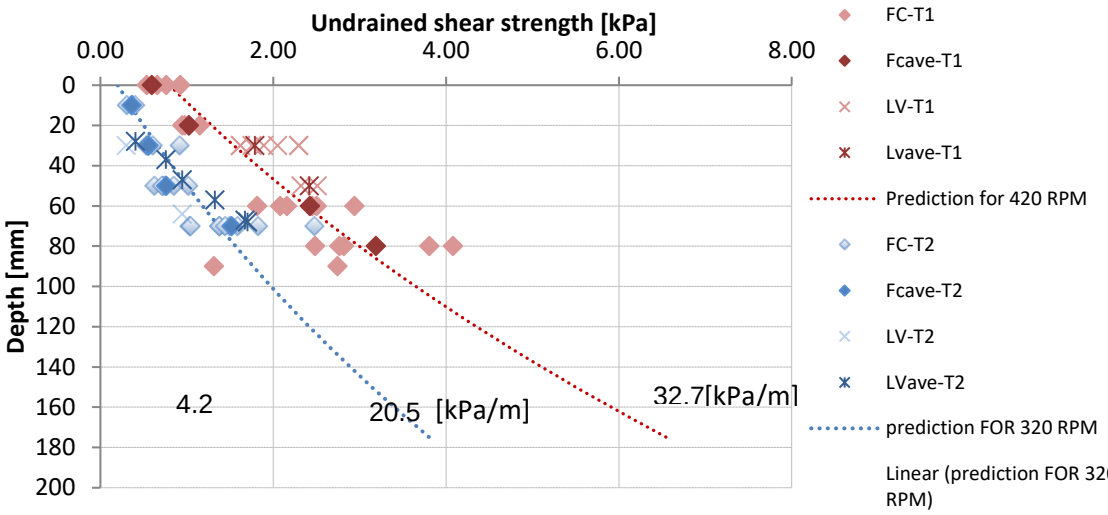

Figure 4.2 - Undrained shear strength profile from laboratory vane (LV) and fall cone (FC) tests (intact samples)

As the stitch test will be performed at ambient pressure, the consolidated sample will have a high s_u gradient compared with the gradient that characterize marine deposits at great depths (typically 2 kPa/m). The average of undrained shear strength at the area of influence of the ball penetrometer is around 4.0, and 2.2 kPa and the gradient of undrained shear strength is approximately 32.7 and 20.5 kPa/m for 420, and 320 RPM, respectively. As the test will be performed horizontally, the high gradient might have an influence on the failure mechanism, soil resistance and interpretation. The higher the centrifuge acceleration the larger the s_u gradient and therefore, the larger the difference in soil strength between the top and bottom of the penetrometer. The difference in soil resistance might cause rotation and uplift of the ball, which is restricted by the pulling rope. Nonetheless, rotation and uplift will generate an additional tension on the rope which might lead to wrong interpretations; this is most likely to happen during the monotonic test, when the strength of the sample is intact.

The undrained shear strength and unit weight profiles were used to calculate the overconsolidated ratio and to estimate a relationship between the pre-consolidation stress and s_u. The classical relationship (equation **4.1**) of $(s_u/\sigma_v')_{nc}$ with OCR proposed by Ladd et al. (1977), suggests that $(s_u/\sigma_v')_{nc}$ varies between 0.25 and 0.3 for $OCR = 1$. Taking OCR as the average acceleration factor (N) though the soil profile (45 for the first test and 77 for the second), $(s_u/\sigma_v')_{nc}$ is around 0.17 for Test 1 and 0.16 for test 2. The resulting OCR profile is shown in Figure 4.3. The pre-consolidation stress was calculated by multiplying the unit weight profile with the acceleration (g) profile and it is plotted as function of undrained shear strength (Figure 4.3).

$$\frac{s_u}{\sigma_v'} = \left(\frac{s_u}{\sigma_v'}\right)_{nc} OCR^{0.8} \qquad 4.1$$

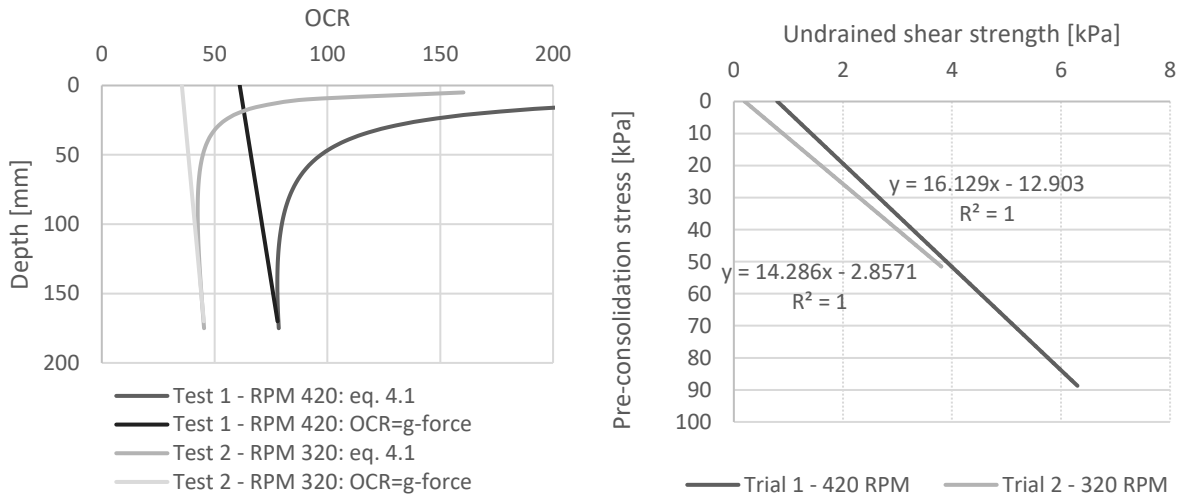

Figure 4.3 – Left: OCR versus depth for the trial samples. Right: Undrained shear strength as function of pre-consolidation stress

4.2 System compliance

The additional tension induced by the interaction of the pulleys and the rope (hereby called system compliance) is assessed experimentally, by pulling the rope while measuring the load increments. Several tests are performed to assess the system compliance dependency with penetration rate and tension. For the ideal situation of having a perfectly shaped and frictionless pulley, the load increments when pulling the rope will be zero.

Initially, four 20 mm-diameter pulleys with plastic ball bearings were installed. Due to the combination of the plastic ball bearings and the eccentricity of the pulleys, a sinusoidal trend of the load was measured for all the test performed a different tensions and penetration rates. Four tests with initial tension ranging from 22N to 143N were performed.

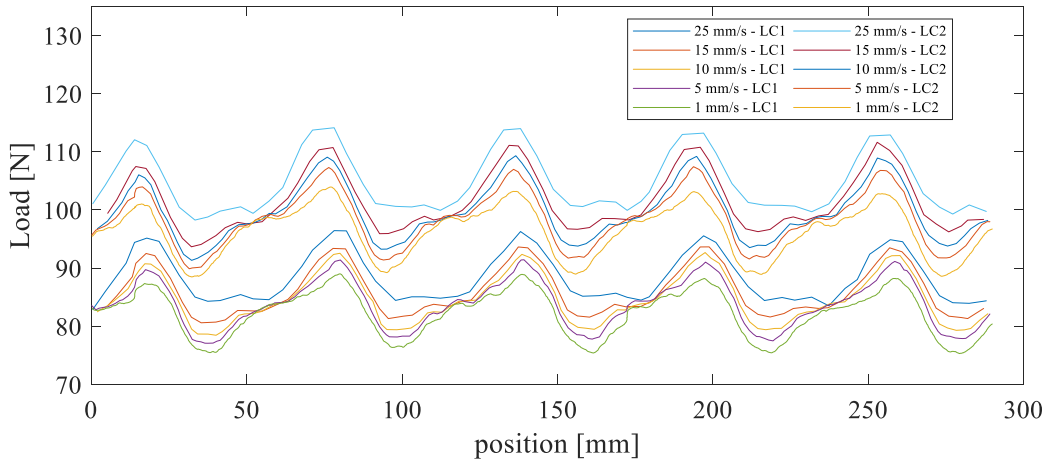

Figure 4.4 - Friction of the pulleys with plastic ball bearings at different pulling rates. Initial tension: 90N

For each of the data sets the maximum, minimum and average value were determined for both load cells and plotted as error bars in Figure 4.5. The average measurement increases with increasing speed, and the increment is higher with increasing tension. The quality of the ball bearings affects the motion of the wheels, which is seen in the data as an increase and decrease in the measured value. The difference in the average values between the two load cells increases with increasing tension. The largest difference between the two loadcells was for the test with 143 N pulled at 25 mm/s, reaching a value of 33.45 N. With the results of the 4 tests it was decided to change the pulleys.

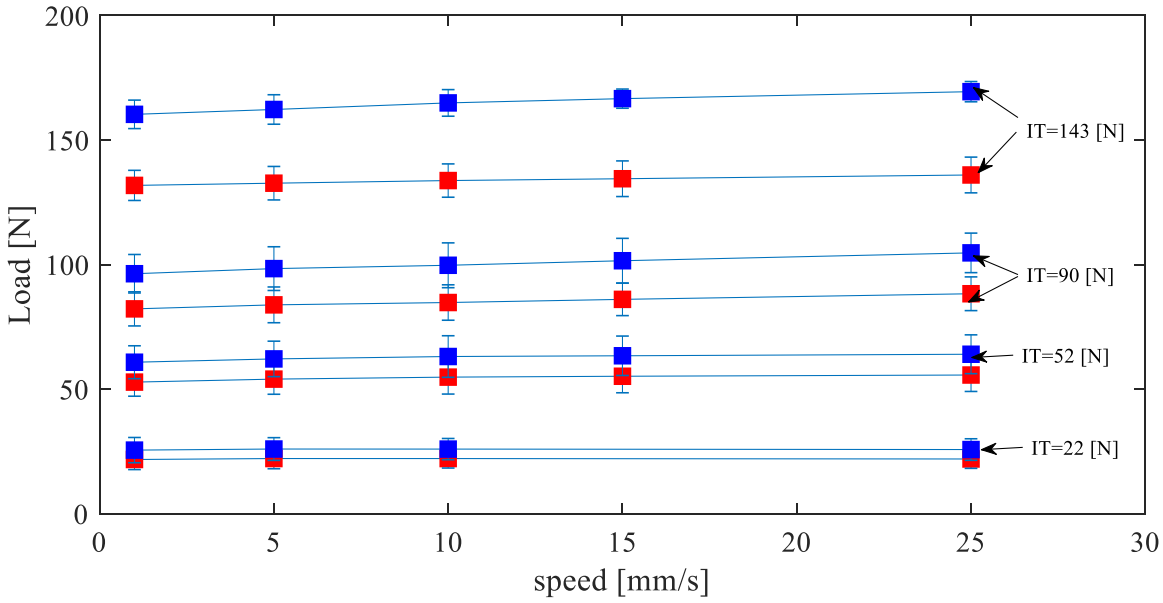

Figure 4.5 - Error bars of load measurements for variable tension and penetration rate. In read the readings from load cell 1 and in blue the readings from load cell 2. IT states for initial tension.

The new pulleys (Figure 3.16) consist of a 60mm-diameter cast iron disc with steel ball bearings. Several cyclic and variable penetration rate tests were performed at varying tension. The difference between the measured loads of the two loadcells (LC1-LC2) are plotted against position in Figure 4.6 and as expected, the difference increases with increasing tension. Compared with the previous pulleys, the variability of LC1-LC2 was reduced significantly ($LC1 - LC2_{plastic\ pulleys\ at\ 143\ N\ of\ tension} = 33.45\ N\ and\ LC1 - LC2_{steel\ pulleys\ at\ 300\ N\ of\ tension} = 6\ N$). Nevertheless, the pulleys are not perfect, and a sinusoidal trend is still observed. This trend depends on the position of the pulleys (see Figure 4.7), therefore, the pulleys were marked so each test will have the same similar trend. Deriving a correction function is difficult, as the tension is not constant when the ball is penetrating the sample: the tension will decrease on one side of the ball and increase on the other, and these increments reduces with increasing cycles. Hence, the lower the constant tension, the lower the correction for the system compliance. Based on chapter 3.6, 50 N of tension seems enough to keep the POM balls on position while testing. For the aluminium ball, a minimum tension of 100 N is required.

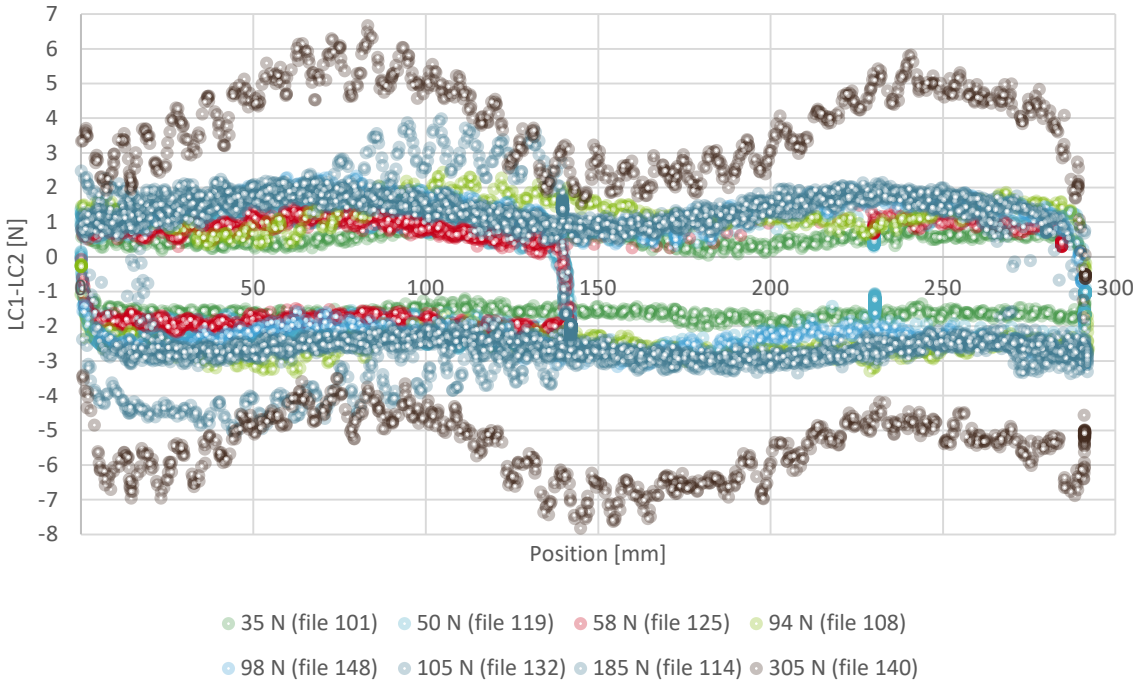

Figure 4.6 - Difference in load cells readings as function of position for different tensions

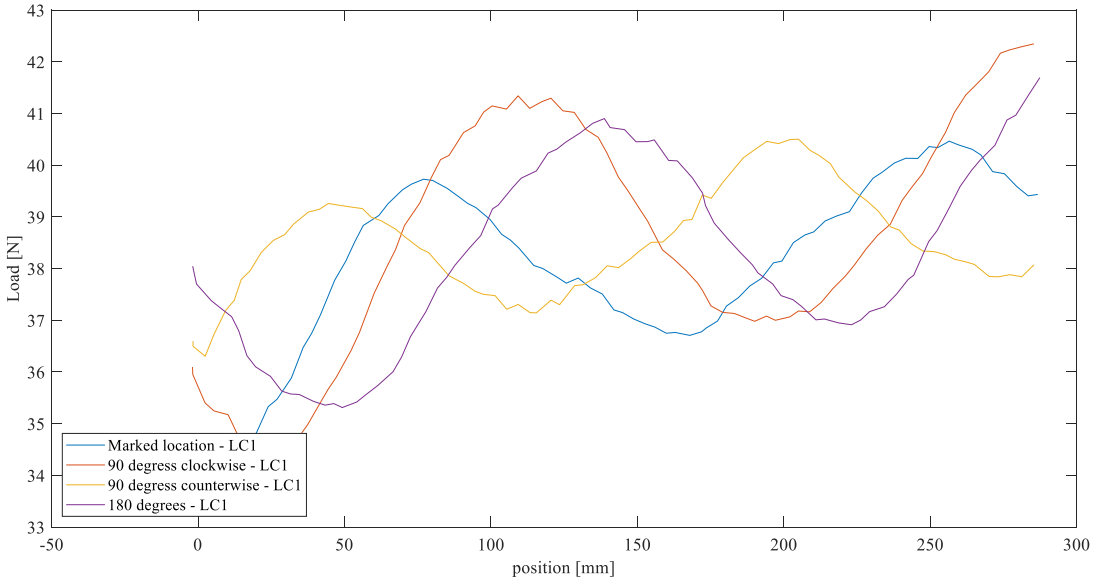

Figure 4.7. Variability of the load when varying the initial position of the pulleys

4.3 Stitch test

Six samples were prepared to test the stitch concept. The general characteristics of the samples and the tests are summarised in Table 5. The water content and unit weight profiles of the samples are plotted in Figure 4.8; note that Test 4 and 5 are not plotted as surcharge was applied during these tests, consolidating the upper centimetres of the sample, hence changing the undisturbed properties. The reference for the x coordinate was taken at the inner surface of the front plate of the box, and the reference depth at the top of the box, hence the horizontal penetration will be always at 112 mm deep, no matter the final settlement of the sample.

Table 5 – General characteristics of the samples and tests

Test		**1**	**2**	**3**	**4**	**5**	**6**
Centrifuge velocity	RPM	330	366	430	360	360	250
Water content of clay slurry (w)	[%]	117.65%	77.05%	67.12%	69.23%	65.91%	71.43%
Surface depth*	[mm]	70	50	35	30	30	35
Pre-consolidation stress $N * \sigma_v'$ (z=112 mm)**	[kPa]	12.2	21.3	37.6	27.8	27.8	19.33
σ_v' (z=112 mm)**	[kPa]	0.252	0.372	0.462	0.492	0.492	0.462
OCR(z=112 mm)**	[-]	48	57	81	57	57	42
Surcharge	[kg]	0	0	0	10	0	0
σ_v (z=112 mm)**	[kPa]	0.672	0.992	1.232	2.72	1.312	1.232
Undrained shear strength***	[kPa]	1.45	1.86	2.04	2.69	2.02	1.65
Remoulded undrained shear Strength***	[kPa]	0.68	0.85	0.85	1.22	0.97	0.86
Sensitivity (S_t)***	[-]	2.13	2.18	2.49	2.22	2.09	1.87
Ball diameter	[mm]	35	35	35	35	30	30
Initial tension	[N]	50.2	40	43	40	100	115
Penetration speed	[mm/s]	10	10	10	10	10	10

* The top of the test box is taken as the reference point (0 mm)
** The horizontal penetration was performed in al tests at z=112 mm (centre of the penetrometer)
*** Estimated with laboratory vane shear test

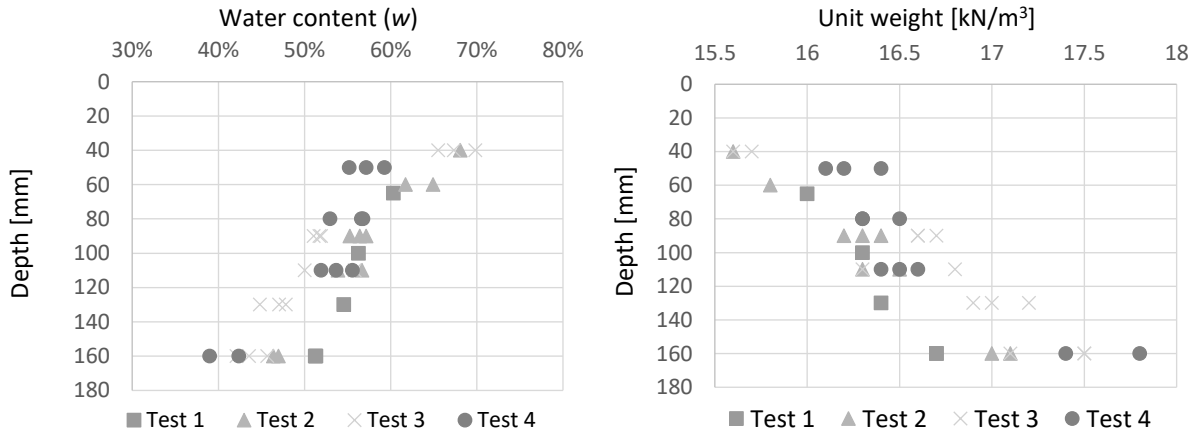

Figure 4.8 - Water content and unit weight profile of the samples

Before the insertion of the ball penetrometer unzipping of the rope was allowed to prevent the overestimation of the initial penetration. The rope was cycled 10 times to guarantee that the surrounded soil was remoulded. The results are shown in Figure 4.9. The intact measurement ranges from 4 to 5 N. With two cycles the soil is remoulded and the measured value is close to the system compliance (see figure 4.2), ranging from 0.5 N to 2N.

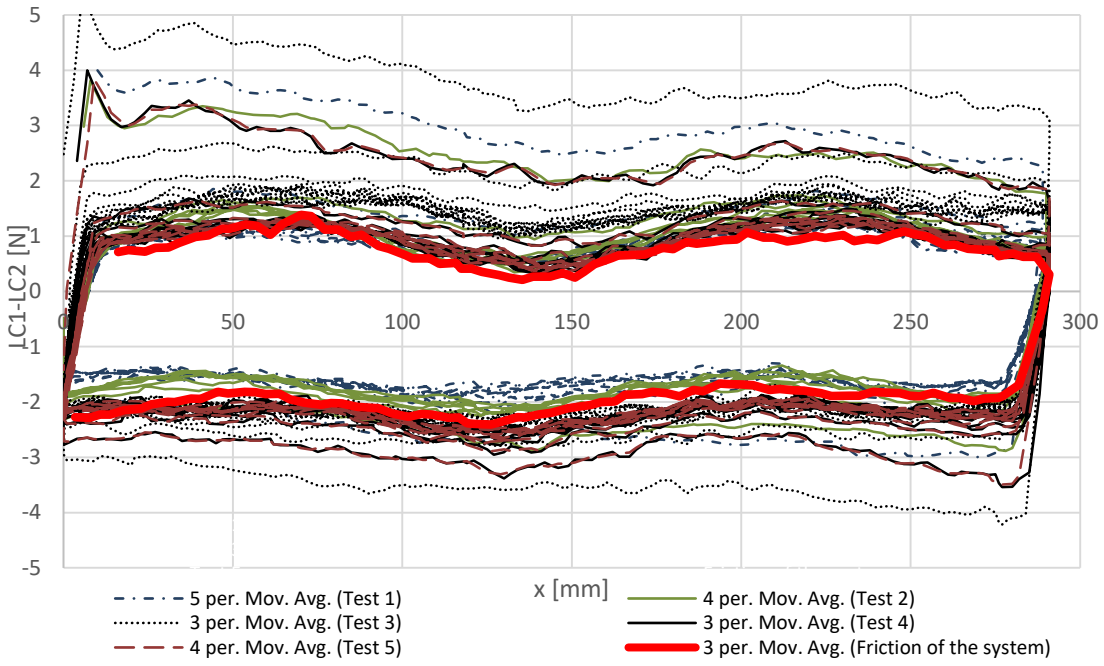

Figure 4.9 - Shaft resistance of the rope

After remoulding the soil around the rope shaft, the ball penetrometer was inserted an equivalent of 1 diameter in the sample at 0.3 mm/s, followed by the closure of the opening (see Figure 4.10). The stitch monotonic test is performed at 10 mm/s from $x = 0\,mm\ to\ x = 250\,mm$, and its followed by the cyclic and variable penetration rate tests performed from $x = 110\,mm\ to\ x = 250mm$ (see Figure 4.11). To capture the effect of partial drainage and rate effect during with the variable penetration rate tests, the speed was systematically increased after each cycle; the selected penetration rates are: 0.3, 0.5, 0.8, 1, 1.2, 1.5, 2, 5, 8, 10, 13, 15, 18, 20, 23, 25 and 29 mm/s. The duration of the variable penetration rate test was 50 minutes. The factual data of all the monotonic, cyclic and variable penetration rate tests are presented in Appendix B.

Figure 4.10 - Insertion of the stitch penetrometer

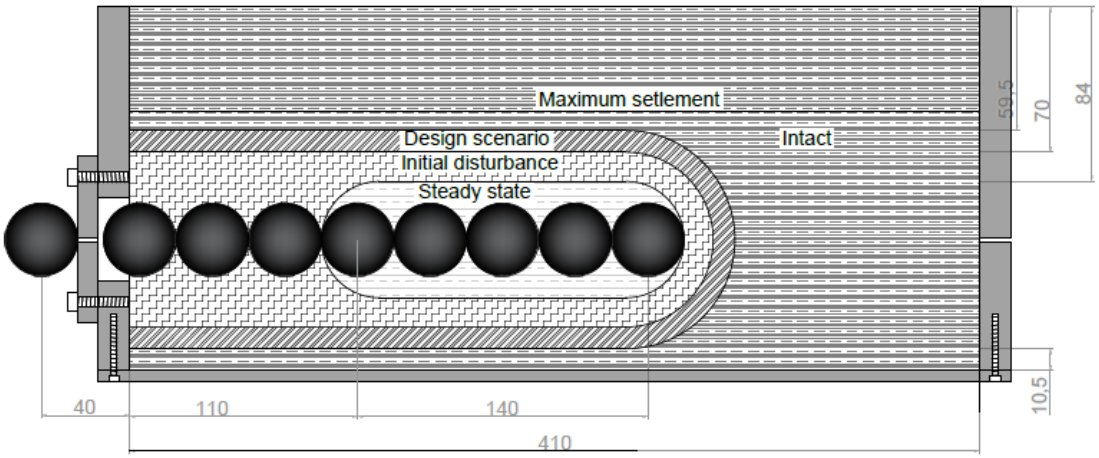

Figure 4.11 – Lateral view of the cyclic range and influence zones (dimensions in mm)

4.3.1 Test 1

Due to the high-water content of the slurry prepared for this Test (118%), the sample settled to a depth of 70 mm, hence only 25 mm of clay was left on top of the ball. In the design stage, it was desired to have at least 40 mm of soil on top of the ball, consequently for the other samples, the water content of the slurry was reduced. To prevent additional softening the water on top of the sample was removed. Due to the low soil cover, the failure mechanism reached the surface during this test, hence, the resistance of the soil is underestimated by the stitch. Initially the failure was not observed, but with increasing number of cycles the failure mechanism and the flow behaviour was clearly identified halfway the cycle (Figure 4.12), confirming that the selected cyclic range was long enough to have full flow around the penetrometer.

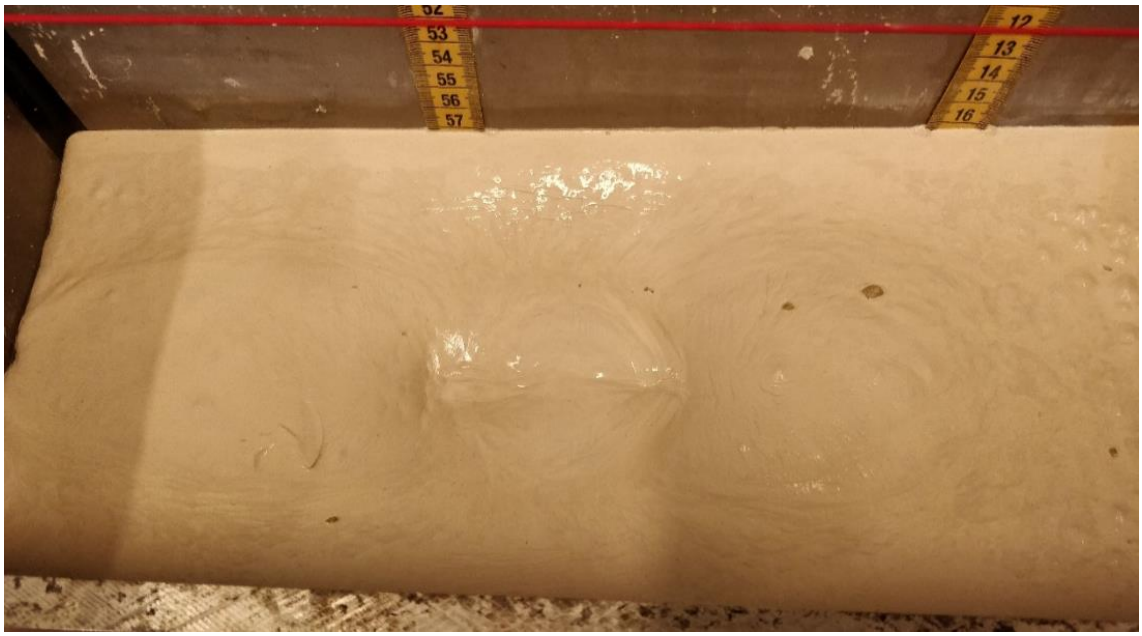

Figure 4.12 - Full flow mechanism observed in Test 1 (top view)

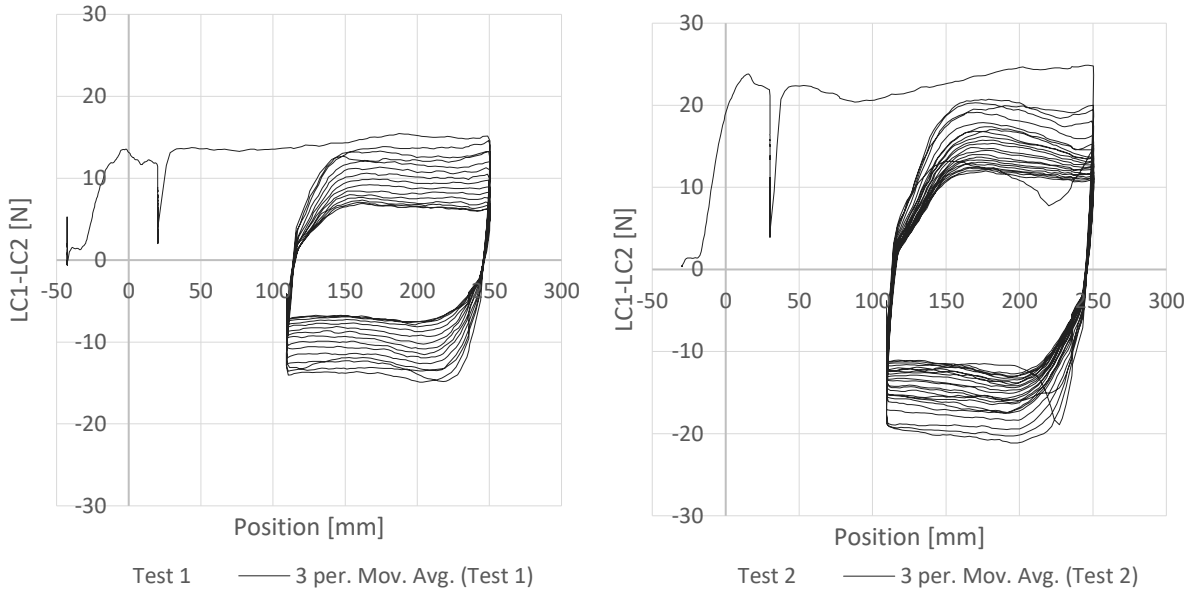

Figure 4.13 - Factual data. Left: test 1. Right: test 2

4.3.2 Test 2

Clay slurry with water content of 77%, was consolidated at 366 RPM in the centrifuge, therefore a higher resistance than Test 1 was expected (see Figure 4.13). The surface of the sample after consolidation was at 50 mm deep, which means there was 60 mm of soil on top of the ball. During the test the failure mechanism did not reach the surface, but heave was observed. The volume change of the sample is an issue as it can create a cavity if the soil flow-back is not fast enough. If a cavity is created, the measured resistance after the first penetration will be underestimated. The factual data (Figure 4.14) shows a strange behaviour in the second and third cycle, where the resistance dropped, and in the third cycle went back to the degrading trend. These behaviour is most likely related to a slow soil flow-back after the initial penetration.

A variable penetration rate test was performed on the remoulded soil by varying the penetration after each cycle (Figure 4.15). the transition from partially-drained to undrained behaviour was captured; hence the selected penetration rates (0.3, 0.5, 0.8, 1, 1.2, 1.5, 2, 5, 8, 10, 13, 15, 18, 20, 23, 25 and 29 mm/s) are used for the variable penetration rate tests.

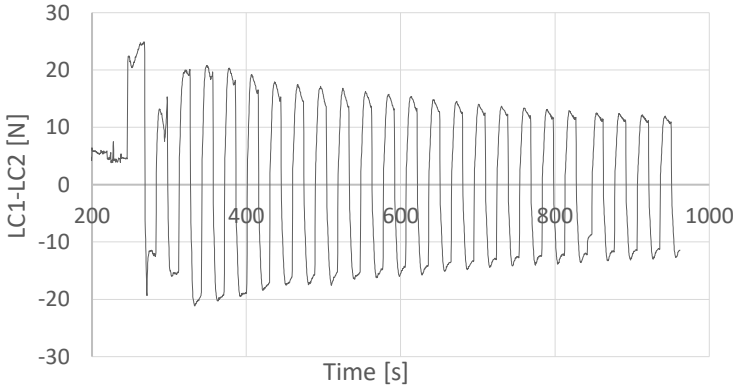

Figure 4.14 - LC1 - LC2 as function of time for Test 2

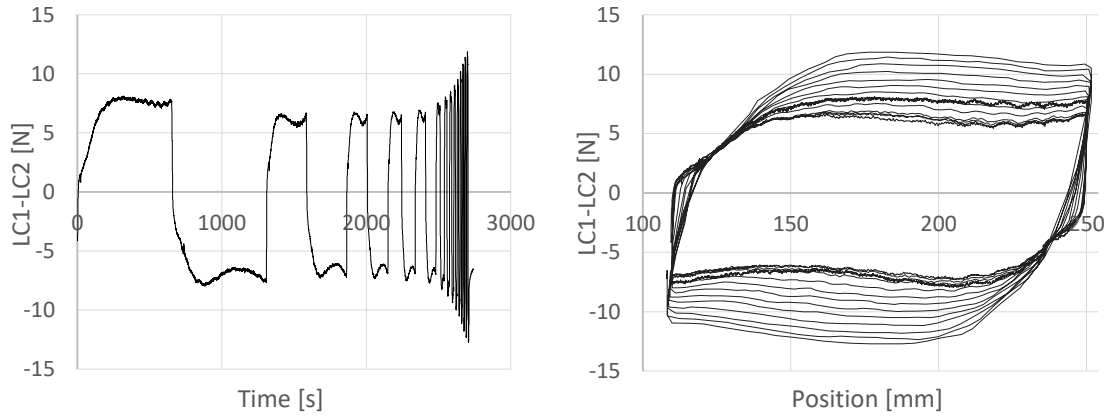

Figure 4.15 - Variable penetration rate Test 2. Left figure shows LC1-LC2 as function of time and the figure at the right shows LC1-LC2 as function of position

4.3.3 Test 3

The third sample was consolidated at 430 RPM, which is the maximum velocity of the small TU Delft centrifuge, hence, the strongest sample was expected. The sample had a settlement of 15 mm and the final depth of the surface was 35 mm, giving a higher pre-consolidation stress than the previous samples. Similar to Test 2, the failure mechanism did not reach the surface but heave was again observed. The intact resistance seems reasonable, as it is higher than the previous two tests and has a relatively constant value. With the first extraction, the resistance dropped almost to the remoulded value of the previous tests and with further cycling it reached the lowest measured value of all the stitch test (see Figure 4.16), which is unexpected for the sample consolidated at the highest RPM. The variable penetration rate test was performed on the remoulded clay, giving also an odd behaviour (see Figure 4.16). When the laboratory vane shear tests were performed at the depth of the penetration, zero values were obtained. Additionally, when the sample was scraped-away to take water contents and do fall cones at different depths, voids where found at the depth of the stitch penetration. This confirmed that full flow around the penetrometer did not occurred, and instead a cavity was created. This behaviour also occurred in Test 1 and 2 but only in the second and third cycle. Therefore, the measured data of Test 3 will not be used for the analysis and interpretation of the cyclic behaviour or rate effects.

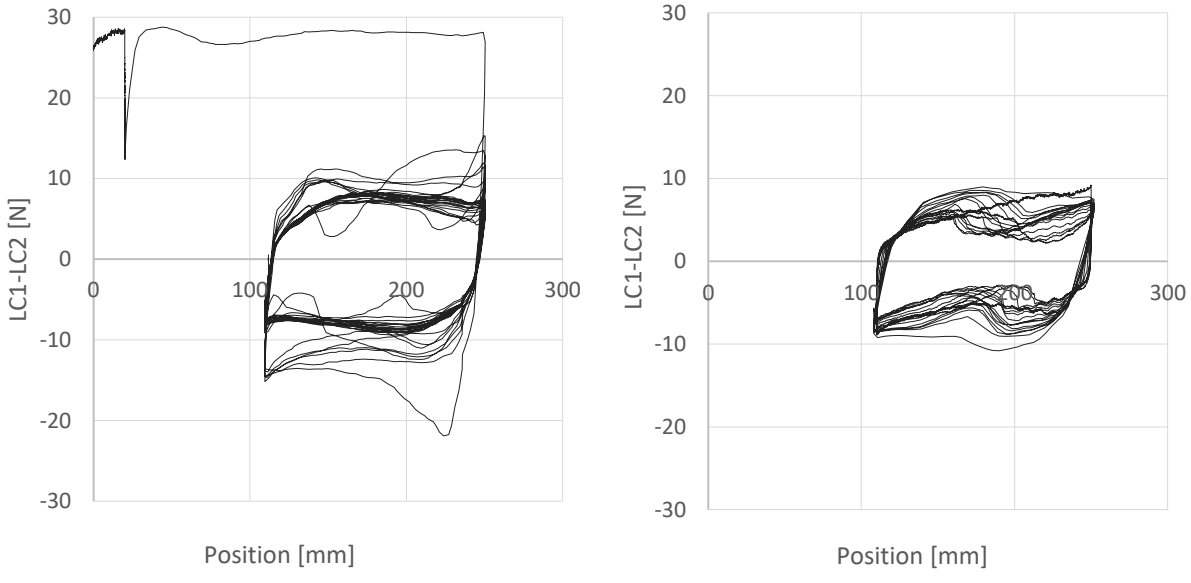

Figure 4.16 – Left: factual data of cyclic Test 3. Right: factual data of variable penetration rate Test 3

4.3.4 Test 4

For this test, the confining stress was increased by placing 1.4 kPa of surcharge, aiming to decrease the likeability of the creation of a cavity. But then again, low resistances were measured during the first extraction and second and third cycle (see Figure 4.17). During this test, it was observed that the resistance was decreasing at a low rate with increasing cycles. After the 20th cycle the resistance dropped rapidly until it reached a constant value (see Figure 4.17). The reason of this behaviour is not known. A possible explanation is that the penetrometer is changing the penetration path with every cycle due to a low tension on the rope. During the first penetration, the ball might tend to move upwards as the soil underneath is stronger; with further cycling the resistance of the soil reduces and the ball will tend to move downwards until equilibrium is reached. For the next sample, it was decided to increase the tension to 100N to analyse if the degradation behaviour changes.

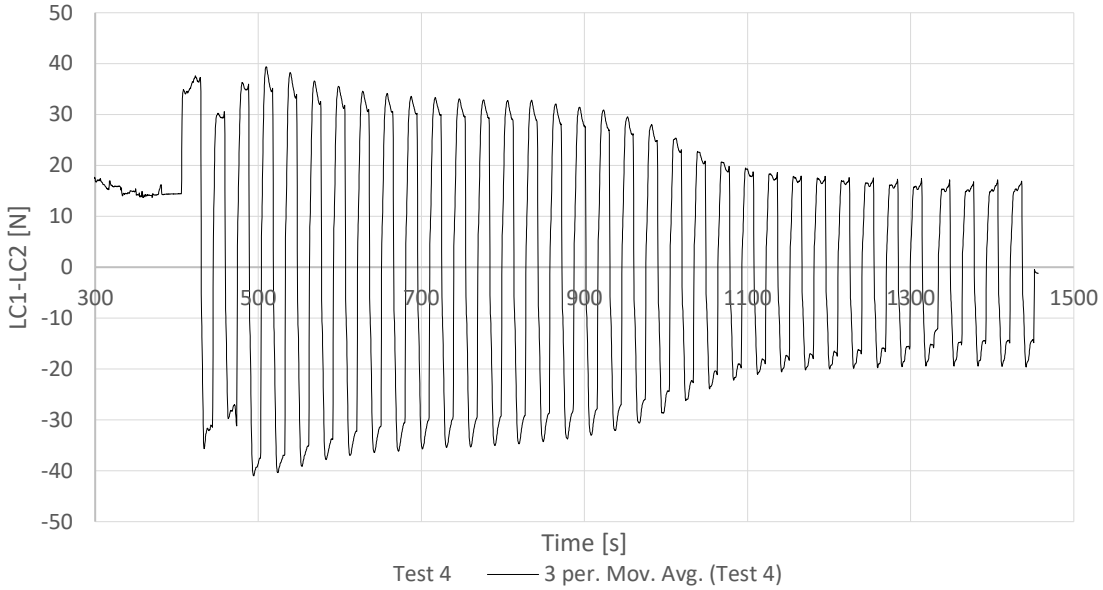

Figure 4.17 - LC1-LC2 vs time for cyclic Test 4

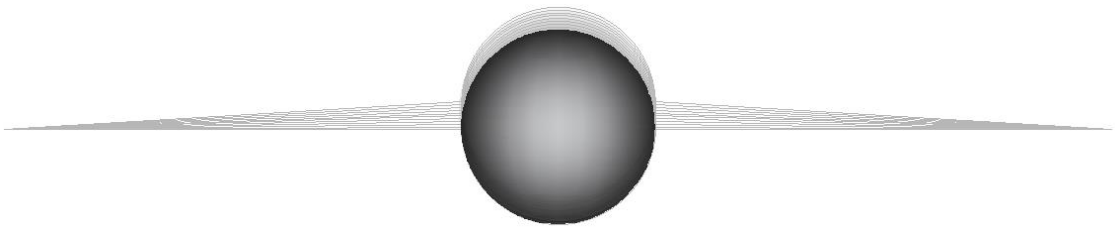

Figure 4.18 - Change of penetration path during cyclic test

4.3.5 Test 5

This test was performed with the 30 mm-diameter ball to reduce the volume change and to compare the results with the 35mm-diameter ball. The monotonic, cyclic and variable penetration rate test were performed without surcharge. After the variable penetration rate test 2 cm of dry sand ($\sim 0.35\ kPa$) were evenly placed on top of the sample and then a cyclic test was performed on the remoulded soil. Four more tests were performed by adding an extra 5, 10, 15 and 20 kg of surcharge, which represents an increase in the total stress of 1, 1.75, 2.11 and 3.15 kPa, respectively. **Figure 4.19** shows the measured resistance as function of position for the test with 10 kg (2.5 kPa) of surcharge. The initial penetration is

lower than the following cycles due to the decrease in effective stress caused by the increase in pore water pressure. With further cycling the pore pressure dissipates and the measured resistance reaches the remoulded strength. **Figure 4.20** compares the last cycle of the tests with varying surcharge, and all converge to the same remoulded resistance. Therefore, the remoulded resistance is not influenced by the increase in the confining stress; this is because the resistance is mainly due to flow around the penetrometer, rather than volume displacement. Additionally, a variable penetration rate test was performed with 20 kg of surcharge giving similar results to the one performed without surcharge, hence, the viscous effect is also not influenced by the confining stress.

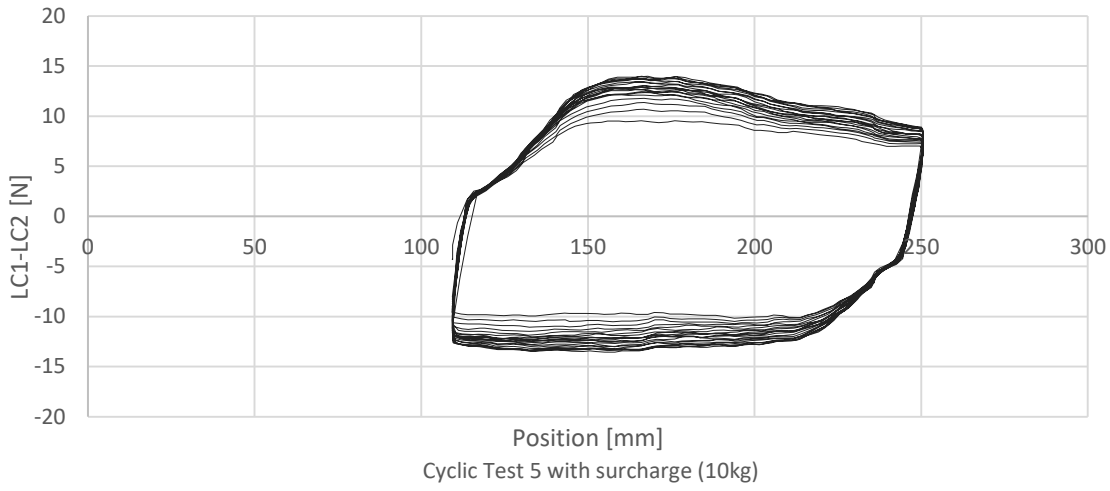

Figure 4.19 - Cyclic test 5 on remoulded clay with 10kg of surcharge

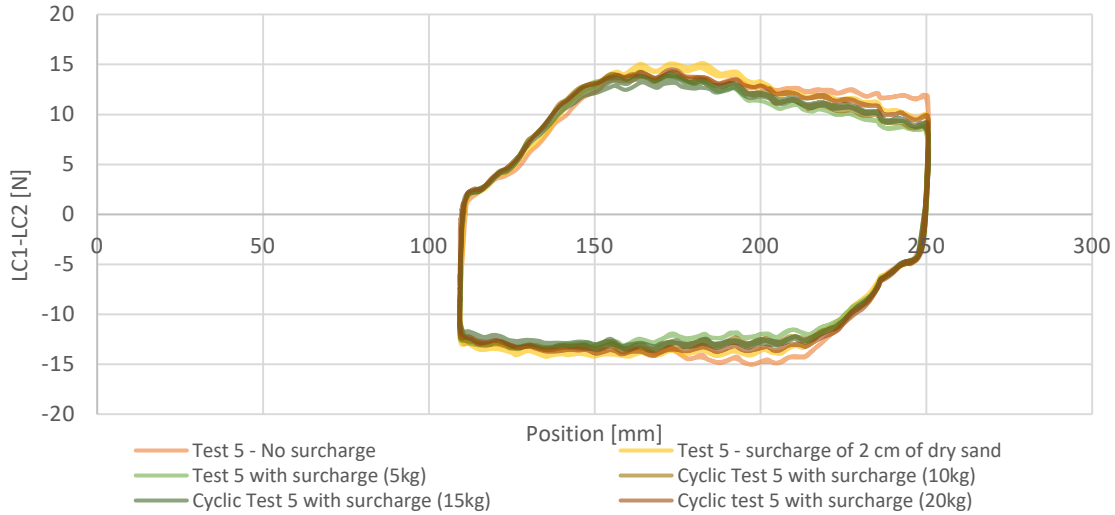

Figure 4.20 - Comparison of cyclic test on the same remoulded sample with varying surcharge

All the previous tests, were performed with the opening for the insertion of the ball closed. In this case, it was desired to see the cavity created by the initial penetration and how it develops with further cycling. This is reflected in the measured data, where the first extraction and second cycle shows a lower resistance than the third cycle (see Figure 4.22).

Figure 4.21 – Left: cavity created during the initial penetration. Right: cavity is closed with increasing cycles and time

Compared with the previous tests, the remoulded resistance was reached faster (5 cycles). It's important to note that for this test the 30 mm-diameter ball was used and the tension on the rope was increased to 100 N. The degradation with the 30mm-diameter ball should occur faster than for the 35mm-diameter ball as the volume of soil to be remoulded is lower, however, the degradation occurred 5 times faster, which is not believed to be only because of the size of the penetrometer. Instead, the degradation behaviour must have changed due to the increase in tension of the rope, which limits the misalignment during penetration.

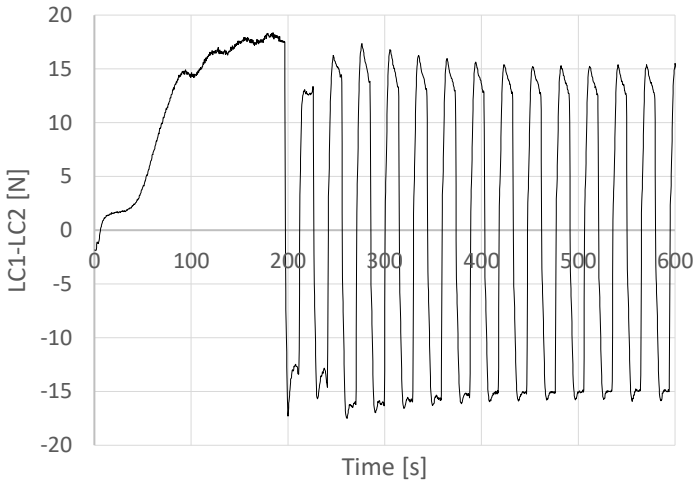

Figure 4.22 - LC1-LC2 vs time for cyclic Test 5

4.3.6 Test 6

It was aimed to test a softer sample to evaluate if the first extraction during the cyclic test can be accurately measured with the current set-up. The slurry was consolidated at 250 RPM and the surface after consolidation was at 35 mm. The test was performed with the 30mm-diameter ball and with 115N of tension. Similar to Test 5, the degradation occurred rather quick compared with the previous tests, but the decrease in tension during the second and third test was again observed.

4.3.7 Laboratory tests

After the monotonic, cyclic and variable penetration rate tests were completed, the rope was removed from the box, and several laboratory tests were performed on the sample. First miniature laboratory vane shear test with the 25.4x 25.4 mm vane blade in combination with a spring category 1, were performed at same depth of the stitch penetration (110 mm from the top of the box) to determine Intact and remoulded strength. At the locations that the vane was not inserted, fall cone was performed creating a grid to evaluate the variability of undrained shear strength after the stitch test. The sample was scraped away and the grid of fall cones was repeated at varying depth. Around 100 fall cones were performed per stitch test; the 60° cone with a mass of 60 g was used. Water content was taken at different depths. The laboratory classification tests results are presented in Appendix E.

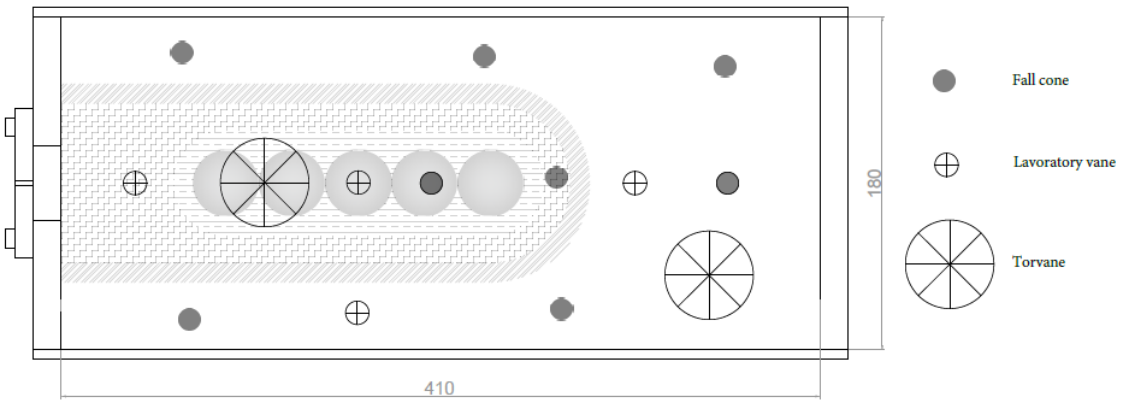

Figure 4.23 - Sketch of the testing approach (top view)

5. DATA PROCESSING, ANALYSES AND INTERPRETATION

5.1 Initial, remoulded and extraction resistances

To obtain the penetration resistance, the difference between the measurements of the two load cells (LC1-LC2) is divided by the projected area of the penetrometer (A_p). The initial penetration resistance (q_{in}) is chosen as the average of the measured values halfway the penetration cycle ($x = 180\,mm$). The first penetration for all the test created a cavity, hence, the first extraction during the cyclic test was not accurately measured. Alternatively, the extraction resistance (q_{ext}) was taken as the resistance at $x = 30mm$ measured during the extraction of the penetrometer at the end of the test. The remoulded resistance (q_{rem}) is the value of the penetration when further softening within each cycle is essentially negligible. Table 6 summarises the penetration resistances for the six tests.

Table 6 – Net initial, extraction and remoulded resistances for all tests

Test		1	2	3	4	5	6
Ball diameter	[mm]	35	35	35	35	30	30
q_{in}	[kPa]	15.77	24.83	29.17	38.75	26.38	20.44
q_{ext}	[kPa]	14.21	22.25	22.25*	37.91	25.38	18.70
q_{rem}	[kPa]	7.03	12.27	8.48*	15.77	21.47	12.32
q_{in}/q_{ext}	[-]	1.16	1.12	1.31*	1.02	1.04	1.09
q_{in}/q_{rem}	[-]	2.24	2.02	3.44*	2.46	1.23	1.66

*Invalid measurements

5.2 Extraction ratio

Figure 5.1 shows the variation of the resistance ratio of the extraction to the previous penetration for each cycle. The ratio after 2 cycles is very close to 1 for all tests, which was expected as the penetrometer can be considered as “shaft less”. This is in accordance with the numerical analyses performed by Zhou and Randolph (2011). The scatter of Test 3 is due the cavity created in the soil after the first penetration.

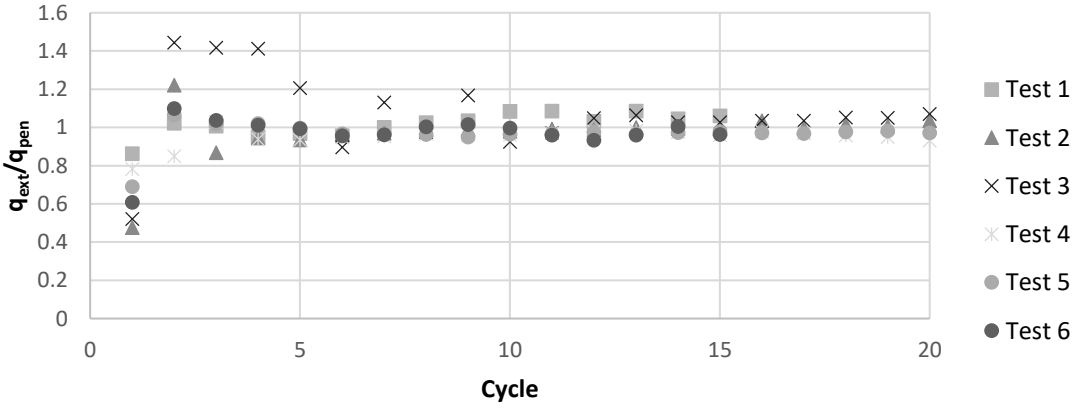

Figure 5.1 - Resistance ratios of extraction to penetration for each cycle

5.3 Undrained shear strength

The estimated undrained shear strengths of the samples are plotted in Figure 5.2 as function of the pre-consolidation stress and compared with the trend derived in Figure 4.3. Test 1, 2, 5 and 6 seems to be in agreement with the trends derived in Section 4.1. s_u increases with increasing pre-consolidation

stress. The strength of Test 3 seems to have been underestimated. and the strength of Test 4 overestimated by the laboratory vane shear test.

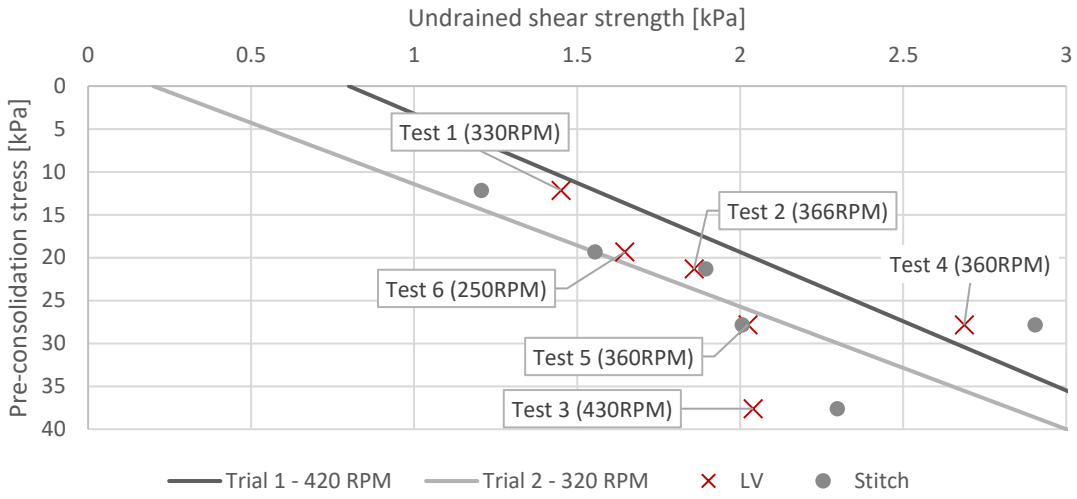

Figure 5.2 - Undrained shear strength of the test samples vs vertical effective stress "in-flight"

The interpretation process of the ball penetrometer was explained in section 2.3.2.5, and it was discussed that for a ball with no shaft - or at least a negligible value of it - the measured soil resistance does not need to be corrected for the pore water pressure (as the ball does not have a o-ring on top) nor the in-situ stress ratio, as there is no shaft on top. Therefore, the measured resistance correlates to undrained shear strength by a simple linear relationship:

$$q_b = N_b s_u \qquad 5.1$$

The bearing factor N_b is defined as function of surface roughness ($\alpha = f_s/s_u$) where f_s is the limiting interface friction (Einav & Randolph, 2005; Lu, et al., 2000), area ratio (Zhou & Randolph, 2011; Zhou, et al., 2013; 2016) soil sensitivity and viscous rate effect (Peuchen, et al., 2005; Lu, et al., 2000). In section 2.3.2.5, the formulas proposed by Yafrate, et al. (2009) to calculate the sensitivity were presented (equations **2.22**, **2.23** and **2.29**); these equations are based on data of 16 samples, and BPT and TPT measurements of four sites. It is important to note that the regression is based on a large range of sensitivities.

Table 7 – Results of sensitivity based on existent relationships

Relationship		Test1	Test2	Test3	Test4	Test5	Test6
q_{in}/q_{ext}		1.1	1.1	~~1.3~~	1.0	~~1.2~~	1.1
st	Equation **2.22** from (Yafrate, et al., 2009)	3.1	2.7	~~5.6~~	3.5	~~1.3~~	2.0
st	Equation **2.23** from (Yafrate, et al., 2009)	1.5	1.5	~~2.7~~	1.1	~~1.9~~	1.4
st	Equation **2.29** from (Einav & Randolph, 2005)	2.3	2.0	~~3.6~~	2.5	~~1.3~~	1.8
st	Laboratory vane shear test (LV)	2.13	2.18	2.49	2.22	2.09	1.87
st	Equation **5.2**	2.24	2.02	-	2.41	-	1.66
st	Equation **5.3**	2.07	2.15	-	-	-	1.87

The estimated sensitivities of the soil by the stitch using these equations are shown in Table 7. They do not match with the sensitivities derived by the laboratory vane shear tests. Equation **2.22** (remoulded

ratio), gives a higher value of sensitivity than Equation **2.23** (extraction ratio). and the value calculated using the fully degrading ratio (Einav & Randolph, 2005) is always in between. Equation **2.29** is the closest to the sensitivity derived with LV.

$$S_t = \frac{q_{in}}{q_{rem}} \qquad 5.2$$

$$S_t = \left(\frac{q_{in}}{q_{rem}}\right)^7 \qquad 5.3$$

Equations **5.2** and **5.3** were derived with the measurements of Test 1, 2, 4 and 6. Test 3 and 5 were discarded as they fall outside the expected degradation behaviour. The sensitivity estimated with the proposed equations matches better with the sensitivity derived with the laboratory vane shear test (see Figure 5.3), therefore they are used for the calculation of the bearing factor. The sensitivity for all the tests is close to 2, therefore is not proven that the equations will work with larger or lower sensitivities. Future work should test materials with varying sensitivity to have a wider and stronger database and validate or modified the proposed equations.

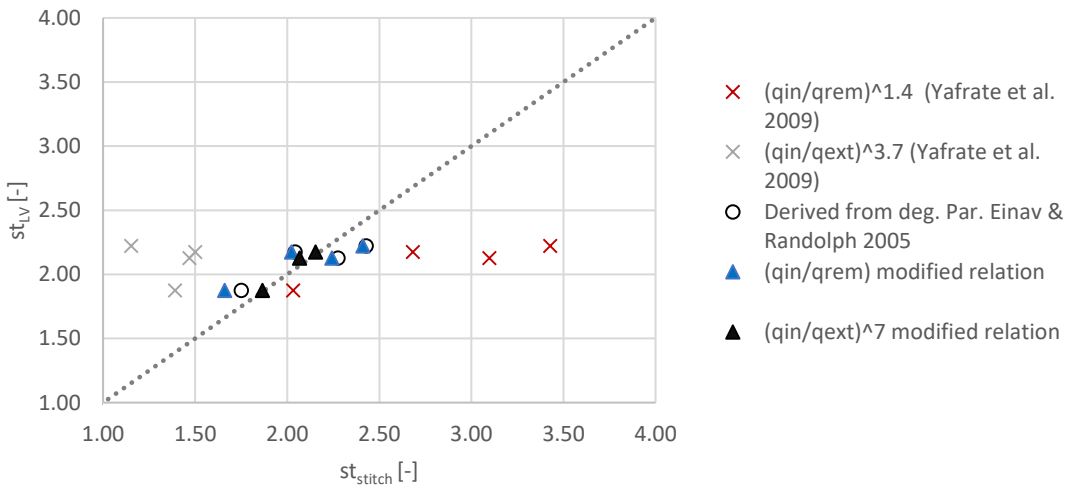

Figure 5.3 - Comparison of the derived soil sensitivity derived by LV, the Yafrate, et al. (2009) correlations and the modified correlations

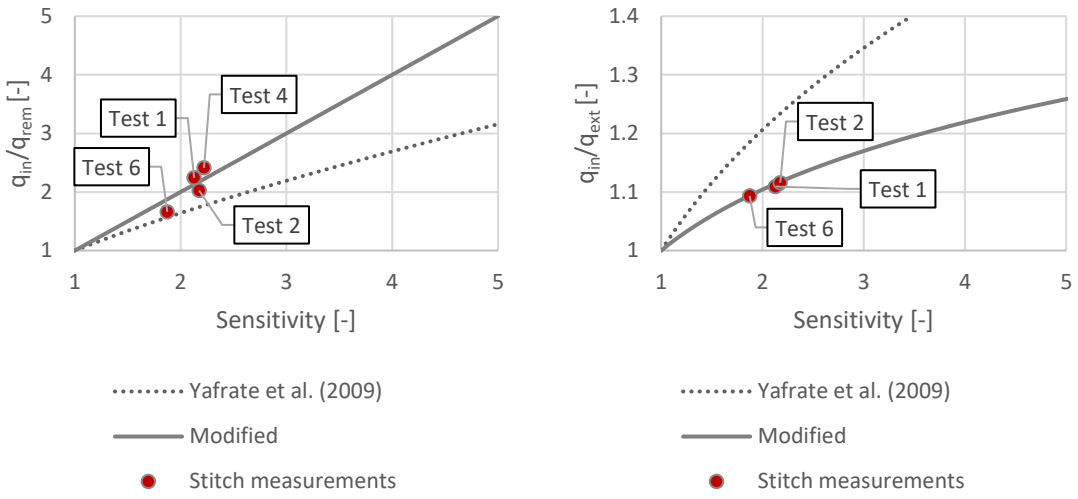

Figure 5.4 – Left: proposed relationship of q_{in}/q_{rem} with sensitivity. Right: proposed relationship of q_{in}/q_{ext} with sensitivity

The bearing factor was estimated by using equations **2.24**, **2.25**, **2.26** and **2.27** combined with the different methods to obtain the sensitivity of the soil (Table 8). The variability of the bearing factor is very low and the best estimate for the bearing factor for the type of penetrometer used combine with the TU Delft kaolin clay is 13.1.

Table 8 - Results of the bearing factor calculated with existing empirical relationships

Method		Relationship	Test 1	Test 2	Test 3	Test 4	Test 5	Test 6
1.1	N_b	Eq. **2.24** (Yafrate, et al., 2009) and S_t from LV	13.1	13.1	13.0	13.1	13.1	13.1
1.2	N_b	Eq. **2.24** (Yafrate, et al., 2009) and S_t from Eq. 2.22	13.0	13.1	-	13.0	-	13.1
1.3	N_b	Eq. **2.25** (Yafrate, et al., 2009) and q_{in}/q_{ext}	13.2	13.2	-	13.2	13.2	13.2
1.4	N_b	Eq. **2.24** (Yafrate, et al., 2009) and S_t from eq. **5.3**	13.1	13.1	-	13.2	-	13.1
1.5	N_b	Eq. **2.24** (Yafrate, et al., 2009) and S_t from eq. **2.29**	13.0	13.1	-	13.0	13.2	13.1
2.1	N_b	Eq. **2.26** (DeJong, et al., 2011) and S_t from LV	13.1	13.1	13.1	13.1	13.1	13.2
2.2	N_b	Eq. **2.26** (DeJong, et al., 2011) and S_t from Eq. 2.22	13.1	13.1	-	13.1	-	13.2
2.3	N_b	Eq. **2.27** (DeJong, et al., 2011) and q_{in}/q_{ext}	13.2	13.2	-	13.2	13.2	13.2
2.4	N_b	Eq. **2.26** (DeJong, et al., 2011) and S_t from eq. **5.3**	13.1	13.1	-	13.2	-	13.2
2.5	N_b	Eq. **2.26** (DeJong, et al., 2011) and S_t from eq. **2.29**	13.1	13.1	-	13.1	13.2	13.2
Low estimate		$N_{b,\mathrm{LE}}$	13.0	13.1	13.0	13.0	13.1	13.1
High estimate		$N_{b,HE}$	13.2	13.2	13.1	13.2	13.2	13.2
Best estimate		$\boldsymbol{N_{b,BE}}$	13.1	13.1	13.0	13.1	13.2	13.1

Taking the friction ratio as the inverse of the sensitivity ($\alpha = 1/st$) the bearing factor derived for the ball penetrometers used (POM 35 mm & 30 mm) can be compared with the theoretical and computational relationships discussed in Chapter 2 (Figure 2.5). Figure 5.5 shows that the estimated N_b and α are close to the trend of a ball without a shaft proposed by Randolph, et al. (2000) and Einav & Randolph (2005), therefore $N_b = 13.1$ is used to estimate the intact and remoulded undrained shear strength. The results are presented in Figure 5.6 and Table 9. The intact and remoulded undrained shear strength determined by the stitch are in average around 3% and 6% larger than the LV, respectively.

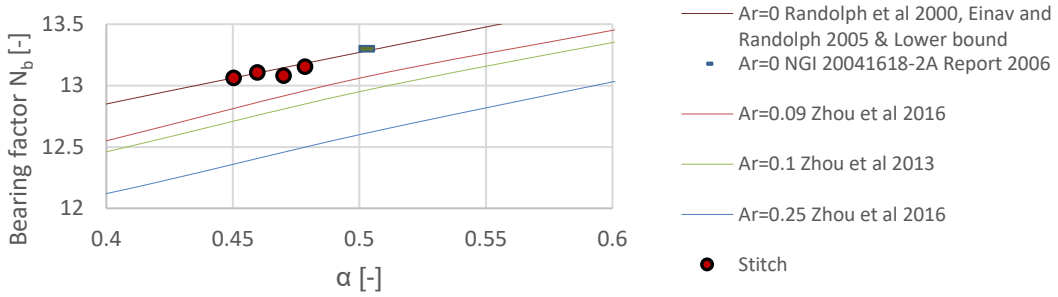

Figure 5.5 - Stitch bearing factor as function of friction ratio derived by the sensitivity from LV

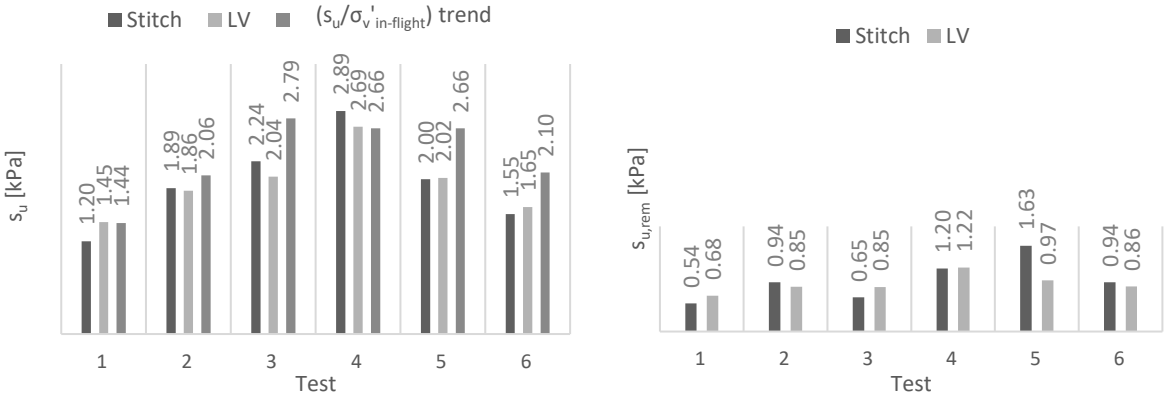

Figure 5.6 - Comparison of s_u and $s_{u,rem}$ obtained by the stitch and LV

Table 9 - Undrained shear strength intact for all the test and its variability due to the variability of N_b

Method	Parameter	Test 1	Test 2	Test 3	Test 4	Test 5	Test 6
Stitch	$s_u\ [kPa]$	~~1.20~~*	1.89	2.24	2.89	2.00	1.55
	$s_{u,rem}\ [kPa]$	~~0.54~~*	0.94	~~0.65~~*	1.20	~~1.63~~*	0.94
Laboratory vane	$s_{u,LV}\ [kPa]$	1.45	1.86	2.04	2.69	2.02	1.65
	$s_{u,rem,LV}\ [kPa]$	0.68	0.85	0.85	1.22	0.97	0.86

*Invalid measurements

Table 10 - Percental difference between the stitch measurements and the LV measurements

Test	1	2	3	4	5	6	Average
$s_{u,stitch}/s_{u,LV}$	~~83%~~	102%	110%	108%	99%	94%	103%
$s_{u,rem,stitch}/s_{u,rem,LV}$	~~79%~~	110%	~~77%~~	98%	~~168%~~	109%	106%
st_{stitch}/st_{LV}	~~107%~~	94%	~~144%~~	109%	~~60%~~	94%	99%

5.4 Degradation curve

Based on the corrected measured resistance, a model to simulate the degradation curve, proposed by (Einav & Randolph, 2005) is implemented in this section. For all the test, the degradation (Deg), the

number of cycles (N_{95}) needed to achieve 95% of degradation (Deg_{95}) and the remoulded resistance normalized by the initial penetration resistance (Δ_{rem}) were determined, and are reported in Table 12.

The normalized resistance as function of cycle (n) is calculated with equation **5.5**. Note that the first penetration cycle is taken as 0.5 and the first extraction as 1. Figure 5.2 plots the derived degradation curves with the measured values.

$$Deg = q_{in} - q_{rem} \quad 5.4$$

$$Deg_{95} = 0.95 * Deg \quad 5.5$$

With the soil resistance at which Deg_{95} is reached ($q_{b,95}$), N_{95} is chosen.

$$q_{b,95} = q_{in} - Deg_{95} \quad 5.6$$

Finally, the degradation curve is plotted with the following equation:

$$\Delta_{(n)} = \Delta_{rem} + (1 - \Delta_{rem})e^{-3(n-0.5)/N_{95}} \quad 5.7$$

The theoretical average shear strain per passage of the penetrometer (ξ_P) is taken from the UBSPM proposed by Einav & Randolph (2005). The cumulative plastic shear strain to achieve 95% of degradation (ξ_{95}) may then be deduced from:

$$\xi_{95} = 2\xi_P N_{95} \quad 5.8$$

Table 11 - Calculated strain values with the UBSPM (Einav & Randolph, 2005)

α	ξ_p
0	2.41
0.25	2
0.5	1.71
0.75	1.45
1	1.35

The fully remoulded strength ratio δ_{rem} is taken as equal to the friction ratio (α) or as the inverse of the sensitivity ($1/S_T$) for the first iteration (i). Then $\delta_{rem,i+1}$ is back-calculated using equation **2.13** and iterated until it reaches a constant value.

$$\delta_{rem,i+1} = \left[\delta_{rem,i} + (1 - \delta_{rem,i})e^{-1.5\xi_P/\xi_{95}}\right]\Delta_{rem} \quad 5.9$$

Table 12 - Derived degradation parameters

Test	Unit	1	2	3	4	5	6
Deg	[kPa]	8.74	12.55	20.70*	22.20	4.91	8.12
Deg_{95}	[kPa]	8.30	11.93	19.66*	21.09	4.66	7.72
N_{95}	[-]	14	20.5	6.5*	26	5.5	4
Δ_{rem}	[-]	0.45	0.49	0.29*	0.41	0.81	0.60
α	[-]	0.44	0.49	0.28*	0.41	0.81	0.57
ξ_{95}	[-]	50	71	26*	94	16	13
δ_{rem} (3)	[-]	0.44	0.49	0.28*	0.41	0.80	0.57

*Invalid measurements

Figure 5.8 shows the degradation curves for all tests. The degradation curves of Test 1, 2 and 4 seems to converge at q_{rem}/q_{in} between 0.4 and 0.5. Test 5 and 6 which were performed with the 30-mm diameter ball and with a higher tension on the rope than the previous tests, degraded faster. As discuss in Section 4.1, the undrained shear strength gradient is high in the samples consolidated in the centrifuge. The degradation with the 30mm-diameter ball should occur faster than for the 35mm-diameter ball as the volume of soil to be remoulded is lower, however, the degradation occurred 5 times faster, which is not believed to be only because of the size of the penetrometer. Instead, the degradation behaviour must have changed due to the increase in tension of the rope, which limits the misalignment of the penetration.

the shear strains (ξ_{95}) needed to cause Deg_{95} for Test 1, 2 and 4 are high compared with the theory, which suggests typical values for ξ_{95} of around 10-50 (Randolph & Zhou, 2006); $\xi_{95} = 10$ is a rapidly softening soil and $\xi_{95} = 50$ is a ductile soil (Randolph, et al., 2005). The reason behind the large amount of strain needed to degrade the material might be related to the tension of the rope. It was concluded that during the initial penetration the ball moved upwards of the idealised position due to the high s_u gradient of the sample. With further cyclic, the penetrometer slowly move downwards until equilibrium is reached. The measured resistance on each cycle must have been a combination of intact, disturbed and remoulded strength. This behaviour could be similar for as-laid pipeline, which induced cyclic shear strains to the soft sediments by means of axial expansion, pipeline walking, or thermal expansion among others. For Test 5 and 6 ξ_{95} is within the typical range and the estimated value for Test 6 is lower than for Test 5.

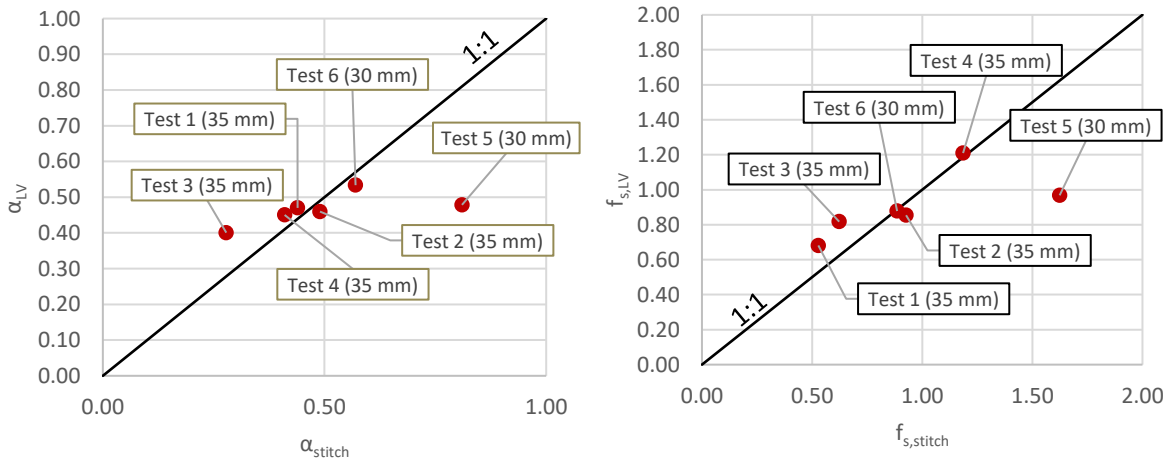

Figure 5.7 - Comparison of the estimated friction ratio (α) (left) and the limiting interface friction (f_s) (right) derived from the sensitivity of the soil

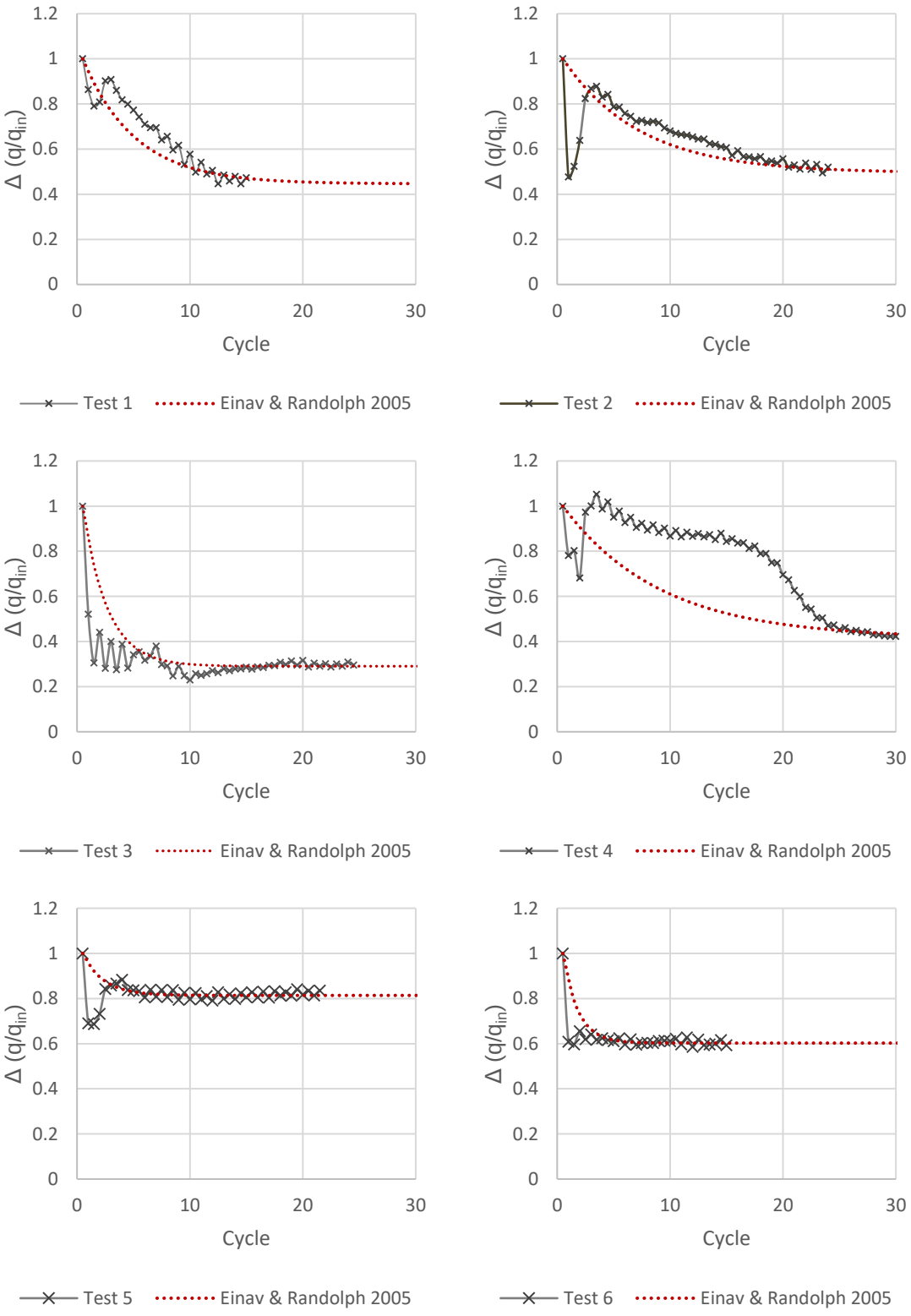

Figure 5.8 - Degradation curves

The derived friction ratios (α) are consistent for Test 1, 2 and 4 which were performed with the same penetrometer. Figure 5.7 compares the stitch friction ratio (α_{stitch}) with the friction ratio estimated with the sensitivity obtained by laboratory vane (α_{LV}Table 5). Good agreement is seen with Tests 1, 2, 4 and 6. The friction ratio of Test 3 and 5 are wrongly estimated by the measurements of the stitch. The degradation of Test 3 was overestimated due to issue explain in section 4.3.3. The degradation of Test

5 seems to have been underestimated, and no explanation was found for this behaviour. With the friction ratio and the undrained shear strength the interface friction can be estimated ($f_s = \alpha / s_u$) by both the laboratory vane and the stitch (Figure 5.7).

5.5 S_u variability after the stitch test

After performing the laboratory vane shear test, several fall cones were performed at different locations and depths to analyse the variability of undrained shear strength in the disturbed sample after performing the stitch test. The results are just indicative, as the soil is disturbed by the removal of the soil. In average 25 fall cones at 4 depths were taken per sample to create contour plots. The strength of the soil is locally lower at the location of the stitch. The horizontal and vertical domain selected during the design stage seem correct for the application.

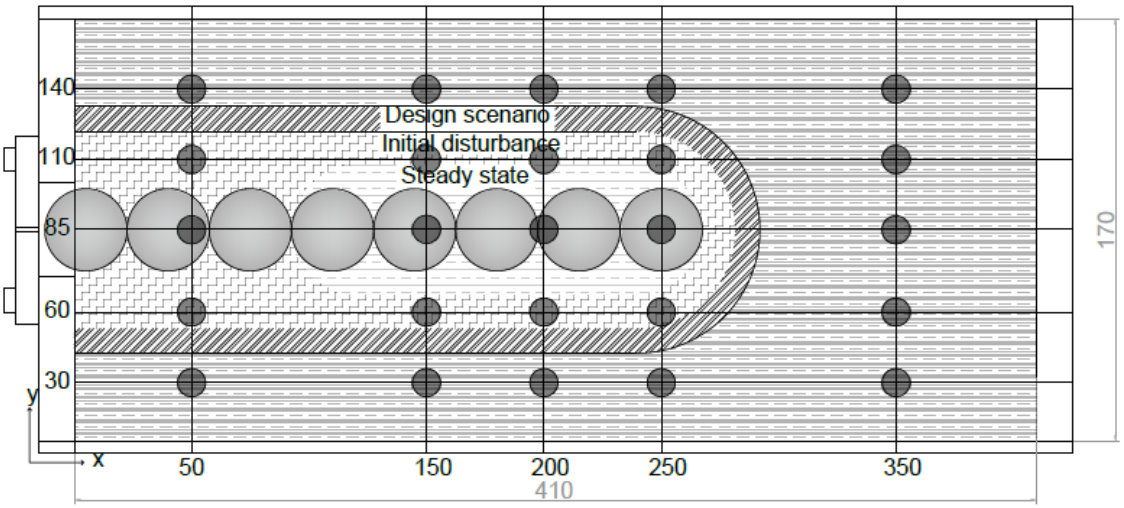

Figure 5.9 - Grid of fall cones to create contour plots (top view)

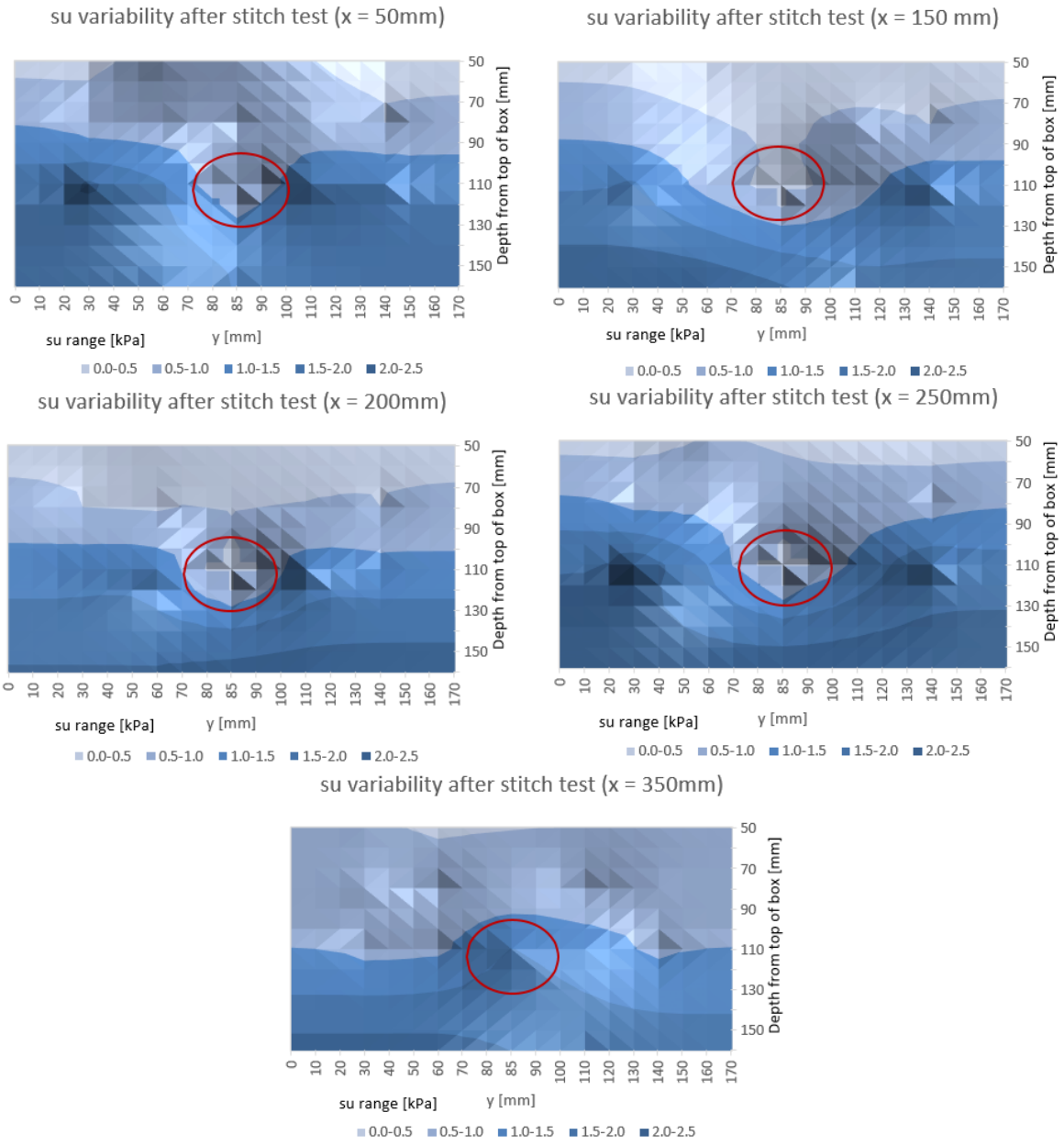

Figure 5.10 - Contour plots of the variability of s_u for test 2

5.6 Penetration rate effect

The measured resistance of each cycle was plotted as function of the penetration rate (Figure 5.12) and the normalized velocity (Figure 5.13). The individual plots can be found in the Appendix D. The reference penetration resistance (q_{ref}) was selected as the one measured at a penetration rate of 10 mm/s. A similar behaviour was identified for all tests: first the measured resistance start to decrease with increasing speed, until it reaches a plateau between 0.5 and 2 mm/s ($30 < V < 80$); with increasing speed the measured resistance start to gradually increase until a maximum value at 29 mm/s ($V = 1067$). The increase in penetration at low rates relates to partial drainage of the soil, which allows to estimate the consolidation coefficient. The plateau represents the penetration rate at which the viscous rate effect is zero; this region can be describe as the transition from partially drained to undrained behaviour. For penetration rates above 2 mm/s, the soil behaves as a viscous fluid, therefore the incremental rate is dependent on the strength and density of the soil.

To investigate how relevant is the penetration rate effect measured with the stitch, the resistance at the standard penetration rate of the BPT and MBPT (20mm/s) was normalized with the measured resistance at 10, 8, 5 and 2 mm/s. The normalized resistances are plotted in **Figure 5.11** as function of the remoulded undrained shear strength. The normalized resistance q_{20}/q_{ref}, where q_{20} is the penetration resistance measure with a penetration rate of 20 mm/s, increases with increasing undrained shear strength. q_{20}/q_{10} varies from 1.1 to 1.6, q_{20}/q_2 varies from 1.3 to 2.4, q_1/q_{10} varies from 0.6 to 0.9 and q_1/q_2 varies from 0.86 to 0.98. The measured resistance at 10 mm/s is 10-60% larger than the resistance measured at v_0. The measured resistance at 20 mm/s is 20-170% larger than the resistance measured at v_0. A penetration rate of 10 mm/s with the 30 and 35mm-diameter balls used during this research shows good agreement with strength derived by the laboratory vane, which is known to have a higher rate of shearing than other tests (e.g. triaxial test).

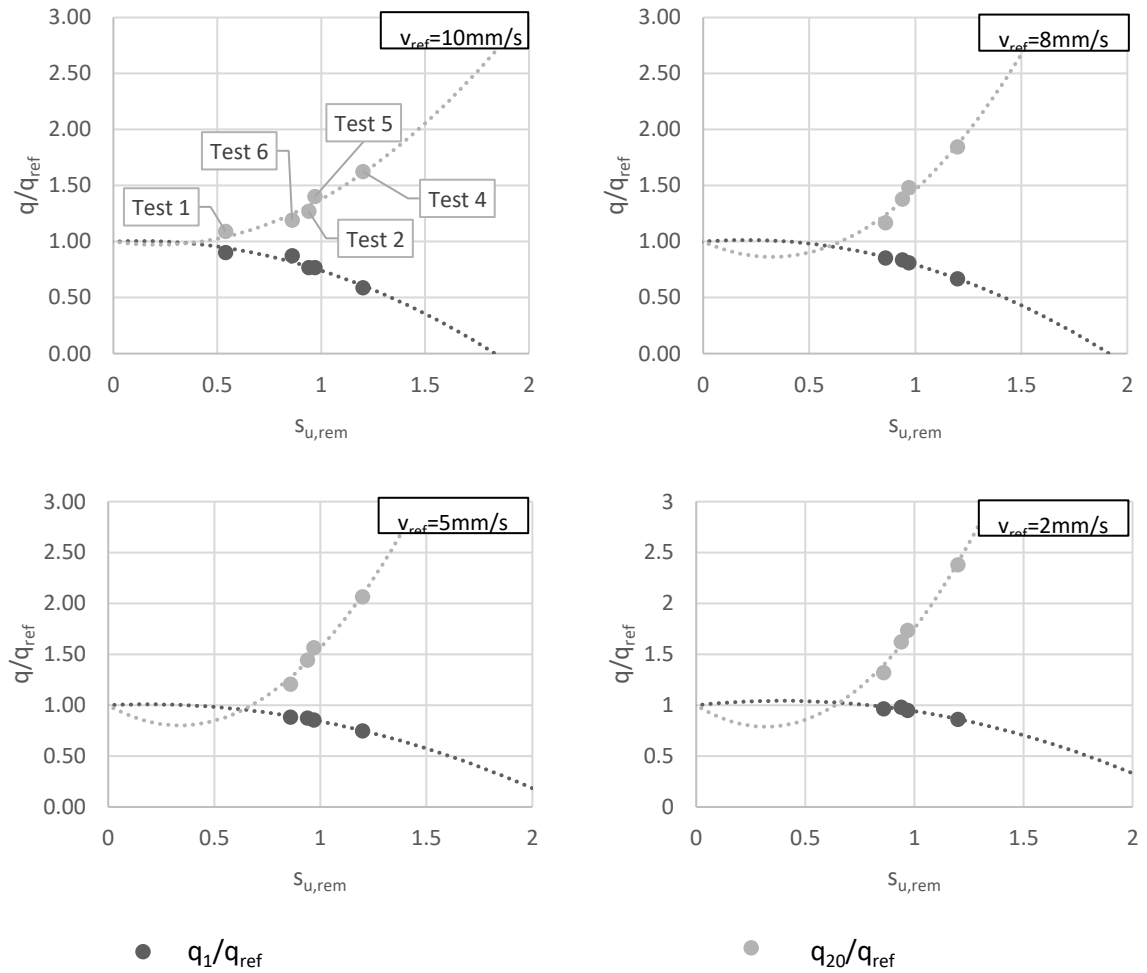

Figure 5.11 - Normalized penetration resistance at 1 mm/s and 20 mm/s as function of remoulded undrained shear strength for v_{ref} = 10, 8, 5 and 2

A hyperbolic sine curve combined with factors for consolidation coefficient proposed by (Watson, et al., 2000; Low, et al., 2008b) was fitted to the data by assigning c_v, v_o and μ. The selected parameters are summarised in Table 13 and the individual plots are shown in Appendix D.

The strain rate parameter for natural soft clays has been determined by BPT, TPT, MBPT or MTPT ranging from 0.05 to 0.3 (Randolph & Zhou, 2006) (Zhou & Randolph, 2007; 2009b) (Lunne, et al., 2011) (Low, et al., 2008b) (Taukoor & Rutherford, 2017) which is significantly smaller than the one determined

by the stitch (3-15). The remoulded soil behaves like a viscous fluid, consequently, the resistance is mainly due to the viscous drag force which is proportional to the fluid viscosity, object size and velocity. With low penetration rates, the flow should be laminar, and with increasing speed the drag force increases dramatically and its behaviour is more complex. The shaft of the MBPT might reduce de drag force during both, penetration and extraction, hence, it might be reasonable that the derived strain rate parameter from the stitch is larger than the range estimated for natural soft clays by the MBPT.

Table 13 - derived parameter from the variable penetration rate test

		Test 2	Test 4	Test 5	Test 6
c_v	[m²/year]	17	20	25	17
	[m²/s]	5.47E-07	2.0E+07	8.04E-07	5.47E-07
μ	[-]	3	15	15	5
v_0	[mm/s]	0.5	1	2	1.4
V_0	[-]	32.46	55.19	75.69	77.91

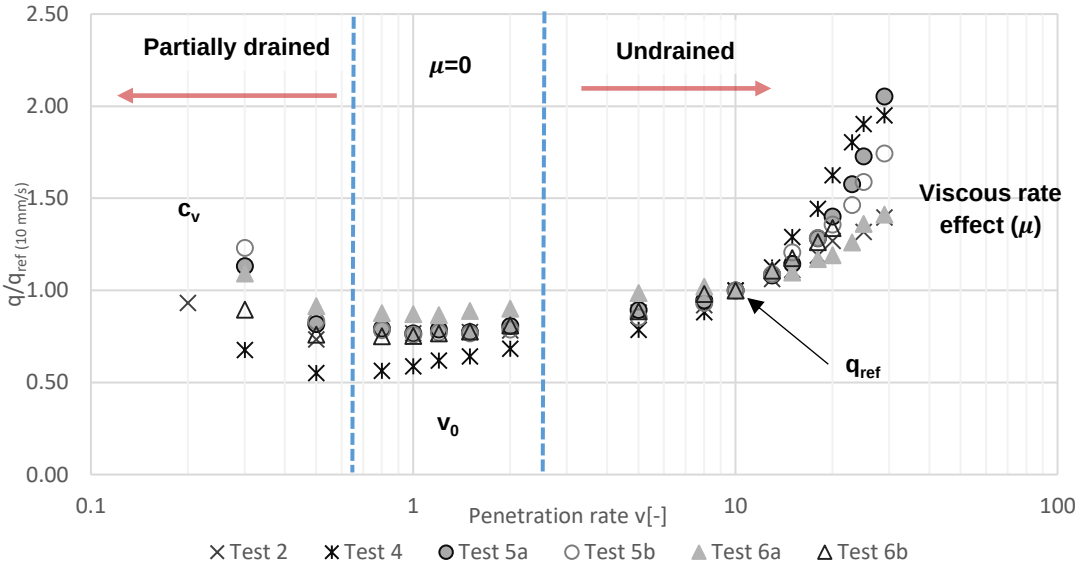

Figure 5.12 – Normalized resistance as function of penetration rate v_0

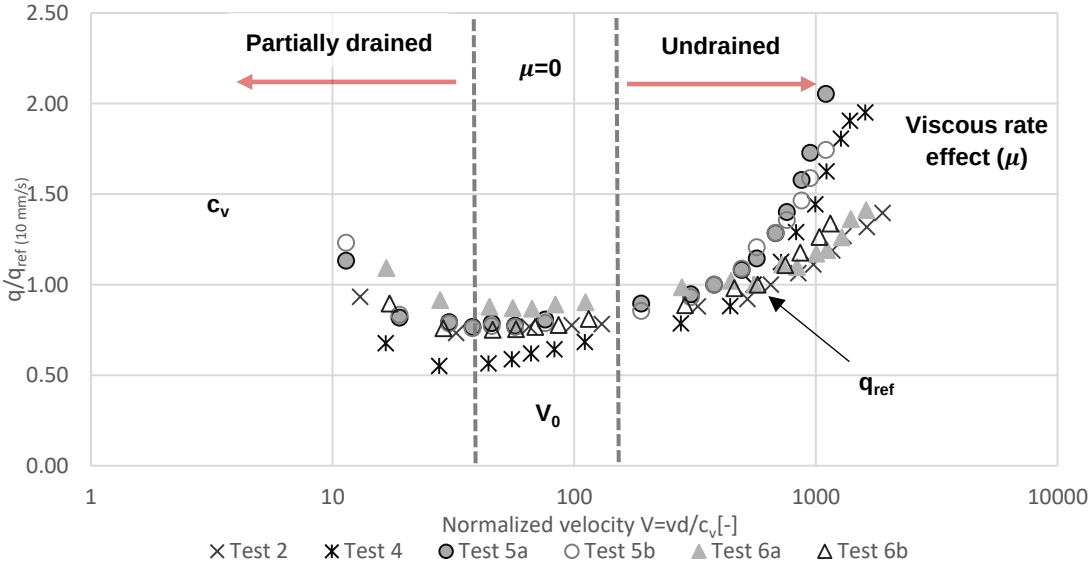

Figure 5.13 – Normalized resistance as function of the normalized velocity

6. FUTURE DEVELOPMENT, RESEARCH AND ENGINEERING APPLICATIONS

6.1 Future development of the prototype

- As-laid pipelines are often at high temperature high pressure (HTHP) and they not only induce cyclic shear to the soil but also heat transfer. The ball penetrometer of the stitch prototype does not have any instrumentation, which makes it easy to change the material, shape or physical characteristics of the penetrometer. An interesting experiment would be to install a penetrometer with a heating system, and investigate the response of the soil to a combination of cyclic shear and temperature change.

- Soil-structure interaction is a key element to model correctly the response of the soil to an excitation from a structure. Typical pipe-soil interactions are pipeline walking, lateral buckling, end expansion, route-curve, pull-out, free spans, among others. Therefore, accurate estimation of the strength parameters is crucial. Any ball penetrometer, made of any material can be installed in the stitch set up, it could be even possible to make a penetrometer with the same coating of the pipeline to be installed, to estimate a more realistic pipe-soil interaction. It will be interesting to investigate the effect of the friction ratio and material on the response of the soil.

- The quality of the pulleys can be improved to reduce the system compliance. An option is to install shielded pulleys.

- The current set up can be modified to allow vertical penetration and diagonal penetration. This can be accomplished by installing a rail on the upper plate of the set-up to change the location of the pulleys. The test box can be placed on an aluminium frame to install a pulley underneath, aligned with the main trolley. A possible issue will be the size of the sample. With the small centrifuge, a maximum sample of 145 mm height was obtained; in average, it weighted 25 kg. To have a bigger sample, the main TU Delft drum centrifuge can be used. The maximum load that can be placed in this centrifuge is 30 kg, therefore the biggest sample that can be obtained will be around 190 mm height.

- A force-controlled option can be incorporated in the control unit of the stitch. It is important to remember that the response of the soil is equal to the difference of the measurements of the two loadcells. This option could be interesting to investigate self-burial of the penetrometer by a constant force or by cyclic loading, and can be important to estimate the embedment depth of as-laid pipelines.

- The soil resistance does not depend on the size of the penetrometer. The ball selected for this research was limited by the size of the test box. If a bigger samples is available (e.g. box core), the size of the penetrometer can be increased to increase the resolution of the measurements. With kaolin clay, the stitch showed a high increase of resistance due to the rate effects, therefore the penetration speed should be carefully selected depending on the size of the penetrometer. The penetration rate for this research was selected within the range (0.2-0.3 diameters per second) recommended by DeJong, et al. (2010) and Lunne, et al. (2011). The measured resistance at 10 mm/s shows good agreement with strength derived by the laboratory vane,

which is known to have a higher rate of shearing than other tests (e.g. triaxial test). Therefore, it is encouraged to do a variable penetration rate test on the remoulded samples.

6.2 Future Research

- The test set-up could be used for the assessment of pull-out capacity of anchors, roots, tension piles, suction cans, spud can extraction, among others

- Investigate the effect of trenching and back-filling, by performing a stitch test on the disturbed specimen. This is relevant for pipelines that are buried by ploughing or jetting, where the largest uncertainty is related to how the trenching method has affected the intact strength and stiffness of the backfilled soil (DNV-GL, 2017).

- Investigate the effect of the size of the penetrometer and area ratio.

- Analyse change in pore pressure during monotonic, cyclic and variable penetration rate tests by installing a pore pressure transducer in the ball and in key locations of the sample

- Test balls of different materials to build a database of the influence of the interface friction on the soil response

- Test fine grained material with different sensitivities to develop on the correlations of sensitivity with penetration ratio and extraction ratio. Additionally, the variability of the bearing factor can be assessed.

- Perform monotonic rate testing (multiple tests performed at different penetration rates) and compare with variable penetration rate test on the remoulded sample. To optimize the sample preparation, it is suggested to have two test box for consolidation in the centrifuge.

6.3 Engineering applications

- Strength characterization of extremely low strength clays is challenging and highly important for many engineering applications. In the marine environment is suitable to determine a continuous profile of intact and remoulded undrained shear strength from a large sample (e.g. box core). It has the potential to determine the penetration rate effects, degradation rate and consolidation coefficient, but further investigation must be done to validate the accuracy and repeatability on the determination of these parameters.

- The versatility of testing in multiple directions can provide information about vertical, axial, and lateral response to monotonic, cyclic or variable penetration rate tests on intact and remoulded specimens, leading to a reduction of the uncertainty of the engineering models and the soil-structure interaction parameters. This is relevant for many engineering applications, like:

    - Deriving design parameters for pipeline riser, pipeline supports, shallow foundations. The shear strength in the upper meter of the surficial sediments is crucial (Low, et al., 2008a)

- Assessment of as-laid pipeline embedment depth, lateral and upheaval buckling, end expansion, pull-out capacity, flow line anchoring, on-bottom stability, development of free spans.

- The strength properties of the upper 0.1 to 0.7 m are crucial for the design calculations of pipelines with a diameter between 0.3 and 0.8 m, and a seabed penetration of less than 80% (White & Randolph, 2007). The as-laid pipeline embedment is a key design parameter determined by the strength within the upper half a meter (Yan, et al., 2011) (Stainer & White, 2015)(Westgate et al. 2012).

- Submarine slides can travel to velocities of 7 to 30 m/s (Bjerrun 1971; Imran et al. 2001; Canals et al. 2004; de Blasio et al. 2004b) (Sahdi, 2013). The dynamically installed anchor foundations hit the seabed at speeds ranging from 10 to 30 m/s (Nanda et al, 2017). The strain-rate effect of the soil under high rate of shearing is therefore interesting for these applications and hazards assessments. With the stitch is possible to study the soil response to a range of penetration speeds, capturing the partial drainage effect and the viscous rate effect. The current set up has a penetration rate of 0.3 to 29 mm/s.

7. RESEARCH CONCLUSIONS

- The prototype can perform horizontally monotonic, cyclic and variable penetration rate test with rates ranging from 0.3 to 29 mm/s. It has a maximum pulling force of 500N. The rope used has a diameter of 1.2 mm and a breaking load of 2kN. The friction of the pulleys at 100N ranges from 0.5 to 2 N. Two nickel plated alloy steel IP67 S-type load cells (AS4H) with 1 kN of capacity, 1.5 kN of safe overload, 3 kN of ultimate overload and accuracy of +/- 0.013N are installed. Two ball penetrometers were used during this thesis, a 30 and 35mm-diameter POM balls. A third 35mm-diameter aluminium penetrometer is available for testing. A logging frequency of 5 Hz or lower can be used.

- The surface depth of Test 1 was 70 mm, hence the ball penetrometer had only 20 mm of soil on top. The undrained shear strength in this test was underestimated as the failure mechanism reached the surface. During this test, it was possible to observe the flow behaviour confirming that the selected cyclic range was long enough for the development of the full flow mechanism. Heave was observed when testing the other five tests, but the failure mechanism did not reach the surface. These tests had a soil cover between 40 and 60 mm. As the measured resistance agrees with the strength derived with the laboratory vane, it can be concluded that heave (change in volume) did not have an influence on the soil response.

- The intact and remoulded undrained shear strength was underestimated in Test 1 as the failure mechanism reached the surface of the sample. The remoulded resistance of Test 3 was underestimated as it is believed the initial penetration created a cavity and due to the strength and structure of the clay of this sample the material did not fully flow back. The remoulded undrained shear strength of sample 5 was overestimated by 68% compared with the laboratory vane. Excluding the after mentioned tests, the intact and remoulded undrained shear strength determined by the stitch are in average around 3% and 6% larger than the LV, respectively.

- Low resistances during the first extraction, and second and third cycle were registered during all tests. The clay consolidated in the centrifuge is characterised of having a defined planar structure. When testing horizontally, the flow-back of the soil is limited, and it is believed that a cavity was created with the first penetration. With further cycling and de-structuration of the clay the cavity is filled and the measured resistance goes back to the degradation trend. In Test 4 the confining stress was increased as an attempt to increase the flow-back rate, nevertheless the same behaviour was observed.

- The variability of the bearing factor is very low and the best estimate for the bearing factor for the type of penetrometer used combined with the TU Delft kaolin clay is 13.1. Taking the friction ratio (α) as the inverse of the sensitivity, the estimated bearing factor is in accordance with the value suggested by Randolph, et al. (2000) and Einav & Randolph (2005) for a ball penetrometer with no shaft.

- The effect of the confining stress was evaluated in Test 5 by performing cyclic test with varying surcharge. It was found the remoulded strength and rate effects are not influenced by confining stress. The reason is that the measured resistance is mainly due to flow around the penetrometer rather than volume displacement.

- For the balls used during the tests (30 and 35 mm-diameter) no influence of the ball size on the soil response was observed as the results obtained were consistent with the results of the laboratory vane shear test.

- The number of cycles (N_{95}) required to reach 95% of degradation (Deg_{95}) for Test 1, 2 and 4 was 27, 40 and 50, respectively. The degradation of soft clays usually occurs within the first 10 cycles. Deg_{95} was reached after 11 cycles and 5 cycles for Test 4 and 5 respectively. It is believed that the tension on the rope for the first 4 tests was not high enough to prevent misalignment of the penetration. During the initial penetration, the ball might tend to move upwards as the soil underneath is stronger; with further cycling the resistance of the soil reduces and the ball tends to move downwards until equilibrium is reached. Therefore, the measured resistance on every cycle is a combination of undrained shear strength intact, disturbed and remoulded. The initial and remoulded penetrations are valid but the degradation curve is underestimating the degrading rate.

- the shear strains (ξ_{95}) needed to cause Deg_{95} for Test 1, 2 and 4 are high compared with the theory, which suggests typical values for ξ_{95} of around 10-50 (Randolph & Zhou, 2006). The reason behind the large amount of strain needed to degrade the material might be related to the tension of the rope. It is believed that the uplift force on the penetrometer displaced in the upward direction the ball. With further cyclic, the penetrometer slowly came back to the idealised position. The measured resistance on each cycle must have been a combination of intact, disturbed and remoulded strength. This behaviour could be similar for as-laid pipeline, which induced cyclic shear strains to the soft sediments by means of axial expansion, pipeline walking, or thermal expansion among others. For Test 5 and 6 ξ_{95} is within the typical range and the estimated value for Test 6 is lower than for Test 5, which is reasonable as the sample was stronger.

- The sensitivity of the soil estimated with the correlations from the extraction ratio ($st = (q_{in}/q_{ext})^{3.7}$) and remoulded ratio (($st = (q_{in}/q_{rem})^{1.4}$) proposed by Yafrate, et al. (2009) doesn't match with the sensitivities derived from the laboratory vane. Yafrate, et al. (2009) derived these equations based on data of 16 samples, and BPT and TPT measurements of four sites. It is important to note that the regression is based on a large range of sensitivities. A better fit was found by using $st = (q_{in}/q_{ext})^{7}\ and\ st = q_{in}/q_{rem}$. Nevertheless, the range of sensitivity used to derive these equations is very limited and further investigation with varying sensitivity is encouraged.

- Several fall cones were performed on the samples after the stitch test to study the area of influence of the penetrometer. It was found that the horizontal and vertical domain selected during the design stage are large enough for the penetrometers used, therefore the interface friction of the walls does not have an influence on the measured resistance.

- A similar behaviour was identified for all variable penetration rate tests: first the measured resistance start to decrease with increasing speed, until it reaches a plateau between 0.5 and 2 mm/s ($30 < V < 80$); with increasing speed the measured resistance starts to gradually increase until a max of value at 29 mm/s ($V = 1067$). The increase in penetration at low rates

relates to partial drainage of the soil, which allows to estimate the consolidation coefficient. The plateau represents the penetration rate at which the viscous rate effect is zero; this region can be describe as the transition from partially drained to undrained behaviour. For penetration rates above 2 mm/s, the soil behaves as a viscous fluid, therefore the incremental rate is dependent on the strength and density of the soil.

- The measured resistance at 10 mm/s and 20 mm/s are 10-60% and 30-140% larger than the resistance measured at 2 mm/s (minimum penetration rate for undrained behaviour). Nevertheless, there is not a big difference between the undrained shear strength derived by the stitch at 10 mm/s compared with the intact and remoulded undrained shear strength obtain by the laboratory vane. Is known that the laboratory vane has higher rate of shearing than other tests (e.g. triaxial test). It is extremely important to define correctly the rate of penetration when testing on clays as the rate of shearing can have a big influence on the response, as it was found when performing the variable penetration rate tests during this thesis. If the rate of shearing of the structure is not known, it is highly recommended to perform a variable penetration rate test to gain information of the rate effect of the material.

- A hyperbolic sine curve combined with factors of consolidation coefficient proposed by (Watson, et al., 2000; Low, et al., 2008b) was fitted to the data by assigning c_v, v_o and μ. The estimated consolidation coefficient ranges from 17 to 25 m^2/year. The penetration rate at which the viscous rate effect tends to zero (v_o) ranges from 0.5 to 2 mm/s. The viscous rate effect (μ) ranges from 3 to 15.

- The strain rate parameter for natural soft clays has been determined by BPT, TPT, MBPT or MTPT measurements ranging from 0.05 to 0.3 (Randolph & Zhou, 2006) (Zhou & Randolph, 2007; 2009b) (Lunne, et al., 2011) (Low, et al., 2008b) (Taukoor & Rutherford, 2017) which is significantly smaller than the one determined by the stitch (3 to 15). The remoulded soil behaves like a viscous fluid, consequently, the resistance is mainly due to the viscous drag force which is proportional to the fluid viscosity, object size and velocity. With low penetration rates, the flow should be laminar, and with increasing speed the drag force increases dramatically and its behaviour is more complex. The shaft of the BPT and MBPT might reduce de drag force during both, penetration and extraction, hence, it might be reasonable that the derived strain rate parameter from the stitch is larger than the range estimated for natural soft clays by the standard full flow penetrometers.

- For a cyclic test the penetration rate and the cyclic range decreases with decreasing ball diameter, therefore the duration of the test should not be dependent on the size of the penetrometer. For a variable penetration rate test the smaller the penetrometer, the smaller the cyclic range, thus the faster test. This is important when testing offshore, where time is highly valuable.

- In view of the benefits of the variable-penetration test in estimating the rate dependency of the remoulded clay, it is recommended that the industry starts planning site investigations including intervals or cyclic tests with varying rate penetration test. As the viscous effect is not dependent

on the size of the penetrometer, the test can be optimized by reducing the cyclic range, which can be accomplished by reducing the size of the penetrometer.

8. SOURCES OF INFORMATION AND REFERENCES

Andersen, K., 2006. *Shear strength parameters determined by in situ tests for deep water soft soils: finite element analyses of ball and T-bar penetrometers in intact and remoulded clay,* Oslo: Geotechnical Institute (NGI), NGI Report, 20041618-2A.

ASTM International, 2015. *D2573/D2573M - 15: Standard test method for field vane shear test in saturated fine-grained soils,* s.l.: s.n.

ASTM International, 2016. *D4648/D4648M - 16: Standard test methods for laboratory miniature vane shear test for saturated fine-grained clayey soil,* s.l.: s.n.

Barbosa-Cruz, E. & Randolph, M., 2005. Bearing capacity and large penetration of a cylindrical object at shallow embedment. *Frontiers in offshore geotechnics,* pp. 615-621.

Boggess, R. & Robertson, P., 2011. CPT for soft sediments and deepwater investigation. *OTC 21244.*

Boylan , N. & Long, M., 2007. Characterisation of peat using full flow penetrometers. *In Proceedings of the 4th International Conference of Soft Soil Engineering,* pp. 403-414.

Boylan, N., Long, M. & Mathijssen, F., 2011. In situ strength characterisation of peat and organic soil using full-flow penetrometers. *Can. Geotech. J. 48,* pp. 1085-1099.

Boylan, N., Long, M. & Mathijssen, F., 2011. In situ strength characterization of peat and organic soil using full-flow penetroemters. *Canadian Gotechnical Journal 48(7): 1085-1099.*

British Standard Institution, 1990. *BS 1377-7:1990 Methods of test for soils for civil engineering purposes - part 7: shear strength tests (total stress).* s.l.:s.n.

British Standard Institution, 2015. *BS 5930:2015 Code of practice for ground investigations,* s.l.: BSI Standards Limited 2015.

Cassidy, M. J. & Byrne, B. W., 2001. *Drum centrifuge model tests comparing the performance of spudcans and caissons in Kaolin Clay,* Oxford: University of Oxford.

Chung, S. F., 2005. *PhD Thesis, Characterisation of soft soils for deep water developments,* s.l.: s.n.

Chung, S. f., Randolph, M. F. & Schneider, J. A., 2006. Effect of penetration rate on penetrometer resistance in clay. *Journal of Geotechnical and Geoenviromental Engineering, ASCE,* Volume 132(9), pp. 1188-1196.

Chung, S. & Randolph, M., 2004. Penetration resistance in soft clay for different shapped penetrometers. *Proceedings ISC-2 on Geotechnical and Geophysical site characterization,* pp. 671-677.

Colreavy, C., O'Loughlin, C. & Randolph, M., 2016. Estimating consolidation parameters from field piezoball test. *Geotechnique 66,* pp. 333-343.

DeJong, J. T., Yafrate, N. J. & DeGroot, D. J., 2007. Design of a miniature piezoprobe for high resolution stratigraphic profiling. *Geotechnical Testing Journa;,* Volume 30.

DeJong, J. T., Yafrate, N. J. & DeGroot, D. J., 2011. Evaluation of undrained shear strength using full-flow penetrometers. *Journal of geotechnical and geoenviromental engineering ASCE.*

DeJong, J., Yafrate , N. & Randolph, M., 2008. *Use of pore pressure measurements in a ball full-flow penetrometer.* Taipei, s.n., pp. 1269-1275.

DeJong, J. et al., 2010. Recommended practice for full flow penetrometer testing and analysis. *Geotechnical Testing Journal 33(2): 1-13.*

DeJong, J. et al., 2010. Recommended practice for full flow penetrometer testing and analysis. *Geotechnical Testing Journal,* Volume 33(2), pp. 1-13.

DNV-GL, 2017. *Recommended practice: DNV-GL-RP-F114 Pipe-soil interaction for submarine pipelines.* Edition may 2017 ed. s.l.:DNV GL AS.

Einav, I. & Randolph, M. F., 2005. Combining upper bound and strain path methods for evaluating penetration resistance. *Int. J. Numer. Meth. Engng,* Volume 63, pp. 1991-2016.

Fugro Engineers B.V., 2011. *Deckscout operations for geotechnical staff - interal document,* s.l.: s.n.

Fugro Netherlands Marine - Internal document, 2017. *FNLM/GEO/TEK/117 Clay remoulded shear strength and sensitiviy,* s.l.: s.n.

Fugro Netherlands Marine - Internal document, 2018. *FNLM/GEO/APP/001 - Cone penetration test ,* s.l.: s.n.

Hird, C. C., Johnson, P. & Sangtian, N., 2001. Performance of a miniature piezocone in profiling thinly layered soil. *Proc. 15th Int. Conf. Soil Mech. Geotech. Engng.,* pp. 113-116.

House, A. R., Oliveira, J. R. M. S. & Randolph, M. F., 2001. Evaluating the coefficient of consolidation using penetration tests. *IJPMG-International Journal of Physical Modelling in Geotechnics,* Volume 3, pp. 17-26.

International Organization for Standarization, 2004. *ISO/TS 17892-6:2004 Geotechnical investigation and testing - Laboratory testing of soil - Part 6: Fall cone test.* s.l.:s.n.

International Organization for Standarization, 2014. *ISO 19901-8:2014 Preoleum and natural gas industries - Specific requirements for offshore structures - Part 8: Marine soil investigations.* s.l.:s.n.

ISO, 2014. *ISO/DIS 22476-9: Ground investigation and testing - Field testing - Part 9: Field vane testing,* s.l.: s.n.

Kelleher, P. & Randolph, M., 2005. Seabed geotechnical characterisation with a ball penetrometer deployed from the portable remotely operated drill. *Proceedings of the 1st international symposiu, on frontiers in offshore.*

Klar , A. & Osman, A. S., 2008. Continuous velocity fields for the T-bar problem. *International journal fro numerical and analytical methods in geomechanics,* pp. 949-963.

Lehane, B., O'Loughlin, C., Gaudin, C. & Randolph, M., 2009. Rate effects on penetrometer resistance in kaolin. *Geotechnique,* 59(1), pp. 41-52.

Low, H. E. et al., 2008a. Characterization of near seabed surface sediment. *Offshore technology conference.*

Low, H. E. & Randolph, M. F., 2010. Strength measurement for near-seabed surface soft soil using manually operated miniature full-flow penetrometer. *J. Geotech. Geoenviron. Eng.,* Volume 136(11), pp. 1565-1573.

Low, H. et al., 2010. Estimation of intact and remoulded undrained shear strengths from penetration tests in soft clays. *Geotechnique 60,* Volume No. 11, pp. 843-859.

Low, H., Randolph, M., DeJong, J. & Yafrate, N., 2008b. Variable rate full-flow penetration tests in intact and remoulded soil. *Geotechnical and gephysical site characterization,* pp. 1087-1092.

Lunne, T. et al., 2011. Guidelines for offshore in situ testing and interpretation in deep-water soft clays. *Canadian Geotechnical Journal 48(4): 543-556.*

Lu, Q., Hu, Y. & Dandolph, M., 2000. FE analysis for T-bar and spherical penetrometers in cohesive soil. *Proceedings of the tenth international offshore and polar engineering conference.*

Nakamura, A., Fukasawa, T. & Tanaka, H., 2007. Applicability of T-bar and ball peneration test to soft clay ground in Japan. *Proceedings of the seventeenth (2007) international offshore and polar engineering conference,* pp. 1307-1314.

Nguyen, T. D. & Chung, S. G., 2015. Effect of shaft area on ball resistance in soft clays. *Proccedings of the institution of Civil Engineers - Geotechnical engineering,* 168(GE2), pp. 103-119.

Nguyen, T. D. & Chung, S. G., 2017. Ball penetration test for characterisation of soft clays. *Proceedings of the institution of civil engineers.*

NORSOK, 2004. *Marine soil investigations. NORSOK standard G-001.* Rev. 2 ed. Lysaker, Norway: Standards Norway.

Oliveira, J. & Almeida, S., 2010. Pore-pressure generation in cyclic T-bar tests on clayey soil. *Internation journalof physical modellingin geotechnics,* 10(1), pp. 19-24.

Osman, A. S. & Randolph, M. F., 2015. On the calculation of umulative strain around full-flow penetrometers in steady-state conditions. *Int. J. Numer. Anal. Meth. Geomech. ,* Volume 39, pp. 368-387.

Peuchen , J. & Terwindt, J., 2014. *Introduction to CPT accuracy.* Las Vegas, Nevada, USA, 3rd International symposium on cone penetration testing.

Peuchen, J., Adrichem, J. & Hefer, P. A., 2005. Practice notes on puch-in penetrometers for offshore geotechnical. *Frontiers in Offshore Geotechnics,* pp. 973-979.

Peuchen, J. & Mayne, P., 2007. Rate effects in vane shear testing. *Proceedings of the 6th international offshore site investigation and geotechnics conference: confronting new challenges and sharing knowledge,* pp. 187-194.

Peuchen, J. & Terwindt, J., 2016. *Conference proceedengs: Critical appraisal of T-bar penetration tests.* Sydney, Australia, Australian geomechanics society, pp. 351-356.

Peuchen, J. & Westgate, Z., 2018. *Conference proceedings CPT'18. Defining geotechnical parameters for surface-laid subsea pipe-soil interaction.* Delft, The Netherlands, Delft University of Technology.

Puech, A., Orozco-Calderón, M. & Foray, P., 2011. Mini T-bar testing at shallow penetration. *Frontiers in offshore geotechnics II,* pp. 305-310.

Randolph, M., 2004. Characterisation of soft sediments for offshore applications. *In proceedings of the 2nd international conference on geotechnical and geophysical site characterization (ISC-2),* pp. 209-231.

Randolph, M., Cassidy, M., Gourvenec, S. & Erbrich, C., 2005. Challenges of offshore geotechnical engineering.

Randolph, M. F., 2016. *Conference proccedings "Geotechnical and geophysical site characterisation 5". New tools and directions in offshore site investigation.* Sydney, Australia, Australian geomechanics society.

Randolph, M. F., 2016. New tools and directions in offshore site investigation. *Geotechnical and geophysical site characterisation 5,* pp. 57-67.

Randolph, M. F. & Andersen, K. H., 2006. Numerical analysis of T-bar penetration in soft clay. *International Journal of Geomechanics ASCE,* Volume 6(6), pp. 411-420.

Randolph, M. F. & Houlsby, G. T., 1984. The limiting pressure on a circular pile loaded laterally in cohesive soil. *Géotechnique,* 34(4), pp. 613-623.

Randolph, M. F., Low, H. E. & Zhou, H., 2007. *In situ testing for design of pipeline and anchoring system.* London, Society for underwater technology, pp. 17-34.

Randolph, M. F., Martin, C. M. & Hu, Y., 2000. Limiting resistance of a spherical penetrometer in cohesive material. *Géotechnique,* 50(5), pp. 573-582.

Randolph, M. & Gourvenec, S., 2011. *Offshore geotechnical engineering.* s.l.:Spon Press.

Randolph, M., Hefer, P., Geise, J. & Watson, P., 1998. Improved seabed strength profiling using T-bar penetrometer. *Offshore site and foundation behaviour,* pp. 221-235.

Randolph, M. & Hope, S., 2004. Effect of cone velocity on cone resistance and excess pore pressure. *Engineering practice and performance of soil deposits,* pp. 147-152.

Randolph, M., Martin, C. & Hu, Y., 2000. Limiting resistance of a spherical penetrometer in cohesive material. *Géotechnique,* 50(5), pp. 573-582.

Randolph, M. & Zhou, H., 2006. *Shear strength parameters determined by in situ tests for deep water soft soils - Large deformation finite element analysis of T-bar and ball resistnce,* s.l.: s.n.

Sahdi, F., 2013. *PhD thesis: The changing strength of clay and its application to offshore pipeline design,* s.l.: The university of western Australia.

Sahdi, F. & Gaudin, C., 2014. Interpreting T-bar tests in ultra-soft clay. *International journal of physical modelling in geotechnics,* 14(1), pp. 13-19.

Stainer, S. A. & White, D. J., 2015. Shallow penetrometer penetration resistance. *Journal of geotechnical and geoenviromental engineering,* 141(3).

Taukoor, V. & Rutherford, C., 2017. Displacement rate effects during T-bar cycling in remoulded Gulf of Mexico clay. *Géotechnique 67,* Volume 6, pp. 553-557.

Watson, P., Suemasa, N. & Randolph, M., 2000. *Evaluating undrained shear strength using the vane shear apparatus.* Seattle, USA, The international society of offshore and polar engineers, pp. 485-493.

Weemees, I. et al., 2006. *Improved techniques for the in-situ determination of undrained shear strength in soft clays.* British Columbia, Canada, The Canadian and Vancouver Geotechnical Societies (CGS/VGS), pp. 89-95.

White, D. J. et al., 2017. The state of knowledge of pipe-soil interaction for on-bottom pipeline design. *Offshore technology conference OTC-27623-MS.*

White, D. J. & Randolph, M. F., 2007. Seabed characterisation and models for pipeline-soil interaction. *International journal of offshore and polar engineers,* 17(3), pp. 193-204.

White, D. J. et al., 2015. *Conference proceedings OTC-26026-MS. Best practice geotechnical characterization and pipe-soil interaction analysis for HPHT pipeline design.* Houston, Texas, Offshore Technology Conference.

Yafrate , N. & DeJong, J., 2007. Influence of penetration rate on measured resistance with full flow penetrometers in soft clay. *Advances in Measurement and Modeling of Soft Behaviour,* Volume 173, pp. 1-10.

Yafrate, N. & DeJong , J., 2006. *Interpretation of sensitivity and remoulded undrained shear strength with full flow penetrometers.* San Francisco, CA, USA, Proc. 16th Int. Offshore and Polar Engineering Conference, pp. 572-577.

Yafrate, N. & DeJong, J., 2005. Considerations in evaluating the remoulded undrained shear strength from full flow penetrometer cycling. *Frontiers in offshore geotechnics, ISFOG 2005,* pp. 997-997.

Yafrate, N., DeJong, J., DeGroot, D. & Mark, R., 2009. Evaluation of remoulded shear strength and sensitivity of soft clay using full-flow penetrometers. *Journal of geotechnical and enviromental engineering, ASCE,* Volume 135, pp. 1179-1189.

Yafrate, N. J., 2008. *PhD Dissertation: Use of full flow penetrometers in soft clay.* Davis: University of California.

Yafrate, N. J., DeJong, J. T. & DeGroot, D. J., 2001. The influence of full-flow penetrometer area ratio on penetration resistance and undrained and remoulded shear strength. *Proceedings of the 6th International Offshore Site Investigation and Geotechnics Conference: Confronting New Challenges and Sharing Knowledge,* pp. 461 - 468.

Yan, Y., White, D. J. & Randolph , M. F., 2011. Penetration resistance and stiffness factors for hemispherical and toroidal penetrometer in uniform clay. *International journal of geomechanics,* 11(4), pp. 236-275.

Yan, Y., White, D. J. & Randolph, M. F., 2017. Elastoplastic consolidation solutions for scaling from shallow penetrometers to pipelines. *canadian geotechnical journal,* Volume 54, pp. 881-895.

Zhang, C., White, D. & Randolph, M., 2011. Centrifuge modeling of the cyclic lateral response of a rigid pile in soft clay. *J. Geotech. Geoenviron. Eng.,* Volume 137, pp. 717-729.

Zhou, H. & Randolph, M., 2007. Computational techniques and shear band development for cylindrical and spherical penetrometers in strain-softening clay. *International Journal Geomechanics ASCE 7,* Volume 4, pp. 287-295.

Zhou, H. & Randolph, M., 2009a. Resistance of full-flow penetrometers in rate-dependent and strain-softening clay. *Géotechnique 59,* Volume 2, pp. 79-86.

Zhou, H. & Randolph, M., 2009b. Numerical investigations into cycling of full-flow penetrometers. *Géotechnique 59,* Volume 10, pp. 801-812.

Zhou, H. & Randolph, M., 2011. Effect of shaft on resistance of a ball penetrometer. *Géotechnique,* Volume 61(11), pp. 973-981.

Zhou, M., Hossain, M. s., Hu, Y. & Liu, H., 2016. Scale issues and interpretation of ball penetration in stratified deposits in centrifuge testing. *J. Geotech. Geoenviron. Eng.,* 145(5).

Zhou, M., Hossain, M. S. & Liu, H., 2013. Behaviour of ball penetrometer in uniform single- and double-layer clays. *Geotechnique ,* Volume 63, pp. 682-694.

A. TEST SET-UP

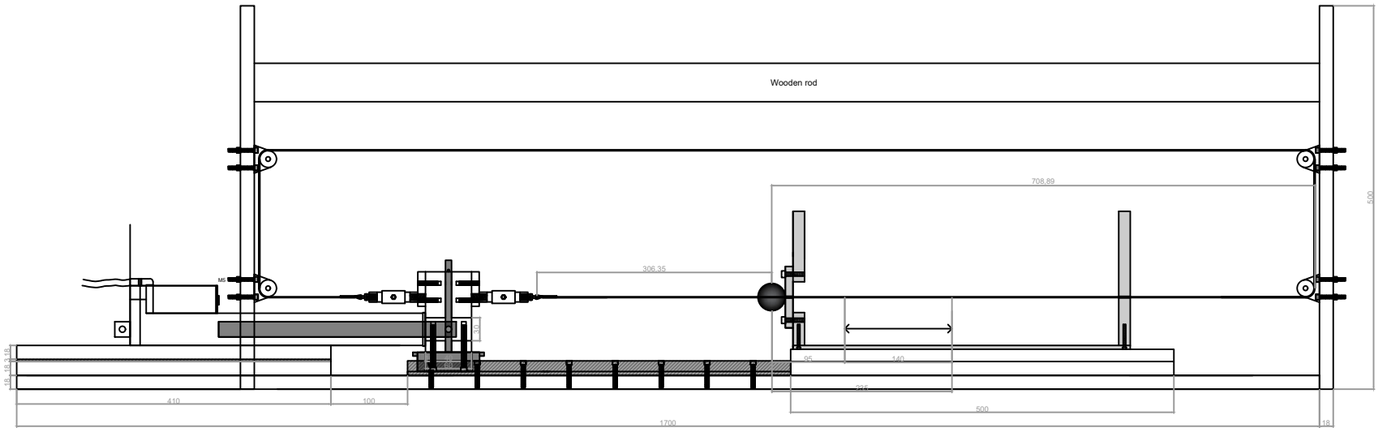

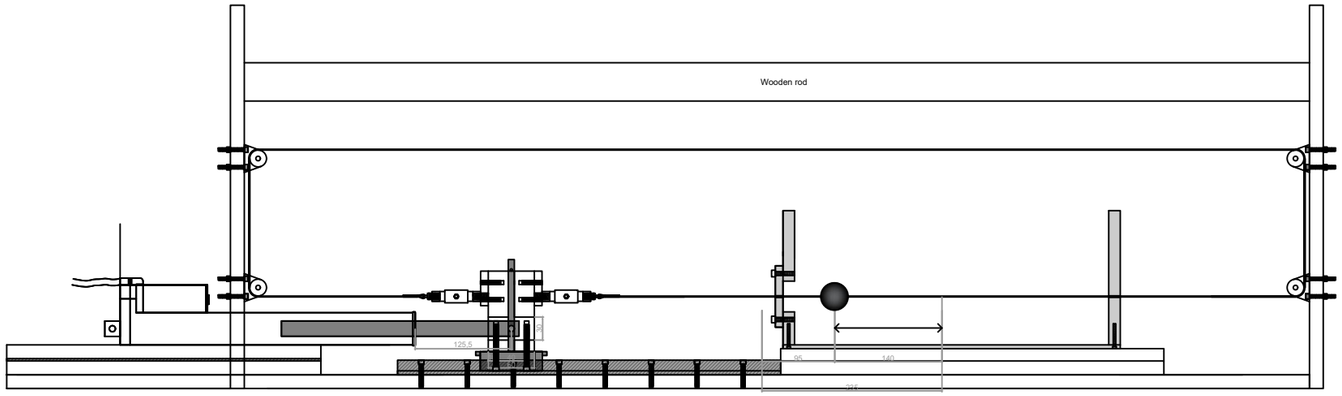

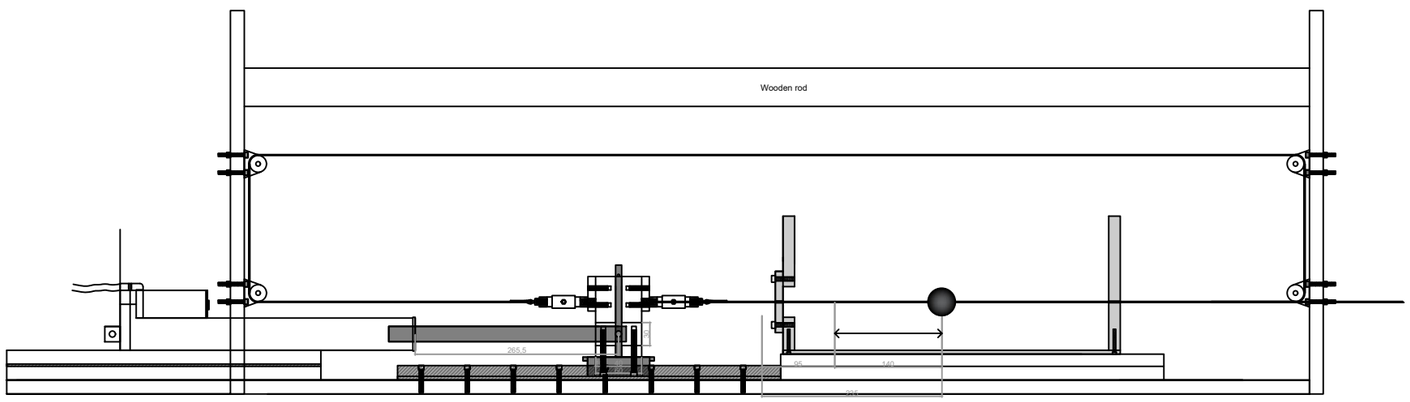

Ball penetrometers						
Diameter of the ball	D_b	30	35	34.925		mm
Projected area of the ball	A_p	706.9	962.1	958.0		mm^2
Volume	V_b	14137.2	22449.3	22305.3		mm^3
Buoyancy	B	14.4	22.9	22.7		g
Alluminium	$\rho_{b,alum}$			2.78		g/cm^3
Weight	Wg_b			62.0		g
Polyoxymethylene (POM)	$\rho_{b,PEEK}$	1.37	1.37			g/cm^3
Weight	Wg_b	19.4	30.8			g

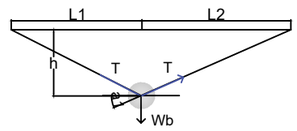

Minimum constant tenstion			
L1 [m]	0.307	0.307	0.307
L2 [m]	0.704	0.704	0.704
h [m]	0.0005	0.001	0.002
alpha 1	0.0016287	0.00326	0.00651
alpha2	0.0007102	0.00142	0.00284
Weight [g]	minimum constant tension [N]		
19.3679187	81.2	40.6	20.3
30.7555376	129.0	64.5	32.3
62.0087051	260.1	130.0	65.0

MOTOR		min	max	
Maximum force	Fmax	500.00		N
Workable loads	F	5.7	308	N
Excentricity	e	0.04	0.04	m
Moment	M	0.24	12.93	N*m
Stroke	S	300.00	300.00	mm
Rate		1.00	29.00	mm/s

Load cell specifications	**[N]**	**[kg]**
Minimum force applied	65	7
Maximum force applied	567	58
Capacity	981	100
Safe overload	1471.5	150
Ultimate overload	2943	300

TROLLEY		min	max	
Workable loads	F	5.7	308	N
Excentricity	e	0.09	0.09	
Moment	M	0.48	26.17	N*m
Maximum moment	Mmax	45.00		N*m
Excentricity	e	0.09		m
Maximum force	Fmax	529.41		N

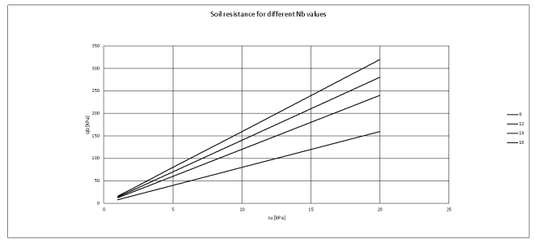

Pulling rope					
Diameter of the ball	D_b	30	35	34.925	mm
Minimum workable tension	Tmin	81.2	129.0	260.1	N
Maximum workable tension	Tmax	307.4	436.9	566.6	N
Breaking load	Tbreak	1900	1900	1900	N
Weight	Wc	3.6	3.6	3.6	g/m
Diameter of the wire	D_c	1.2	1.2	1.2	mm
Radius of disturbed area	$D_b=2*D_c$	2.40	2.40	2.40	mm
Cross-sectional area of the wire	A_{circle}	1.131	1.131	1.131	mm^2
A_{circle}/A_{cb}	A_r	0.0016	0.0012	0.0012	-

Penetrometer	Ball diameter	Shaft diameter	Ar
STITCH	30	1.2	0.0016
	35	1.2	0.0012
	34.925	1.2	0.0012
BPT	113	35.7	0.10
Mini BPT	33.9	11.3	0.11

Project: STITCH	Drawing: Test set-up	Date: 04/05/2018	FUGRO / TU Delft
Design by Eduardo Gómez Meyer	Checked by	Drawing 1 of 1	

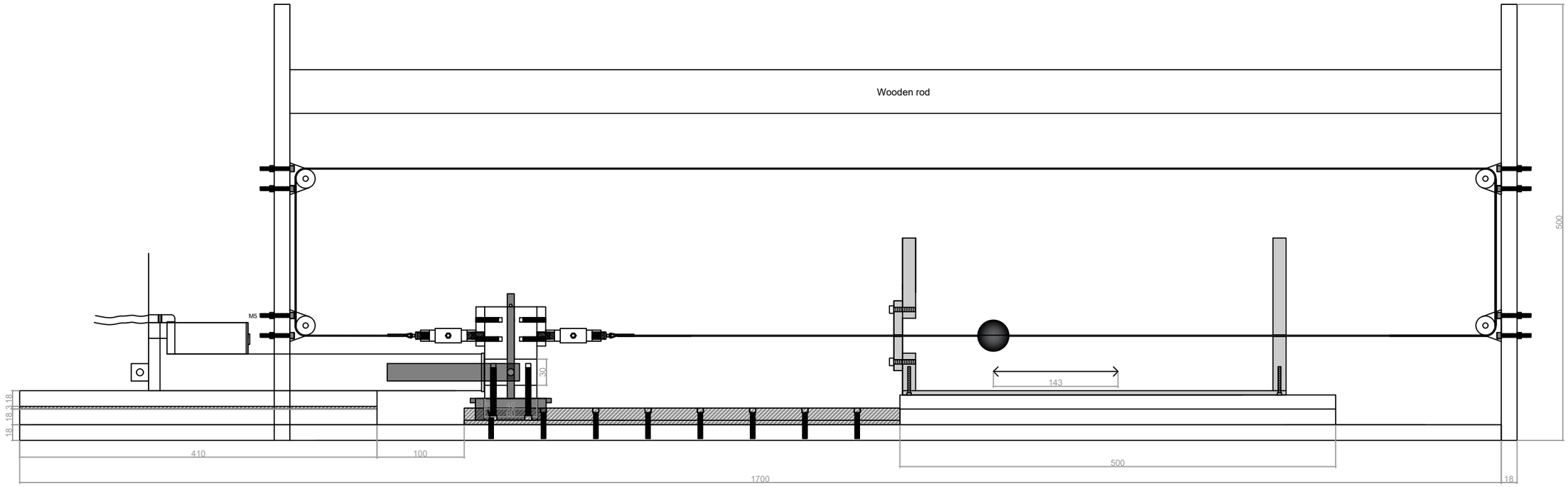

Block x 4

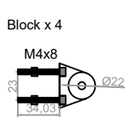

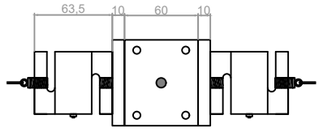

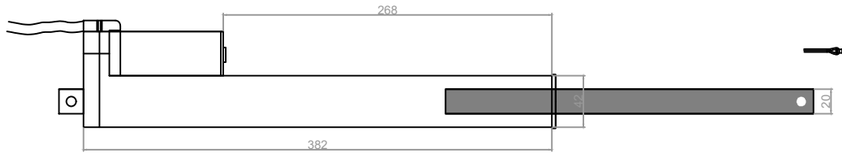

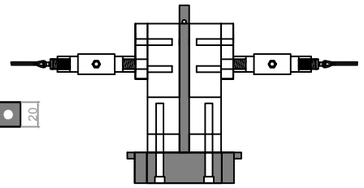

Rope connection

Connection plate x 2

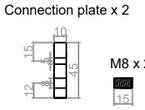

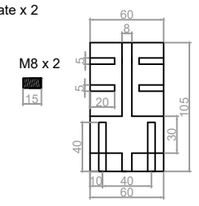

Pin 8 mm diameter

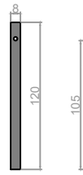

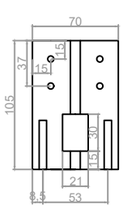

Connection plate x 2

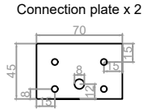

M5 x 8

Rail

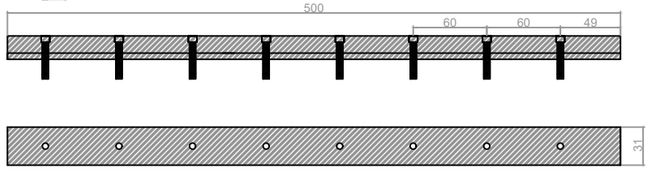

Trolley

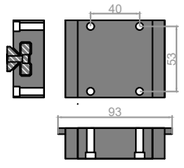

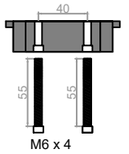

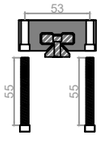

Project: STITCH	Drawing: Details of test set-up	Date: 29/04/2018	FUGRO / TU Delft
Design by: Eduardo Gómez Meyer	Checked by:	Drawing 1 of 1	

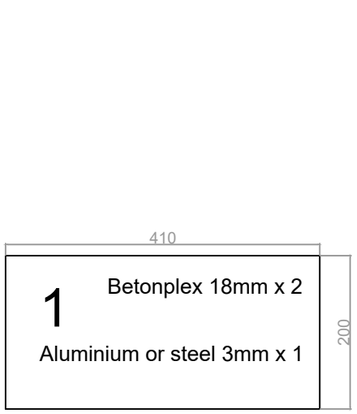

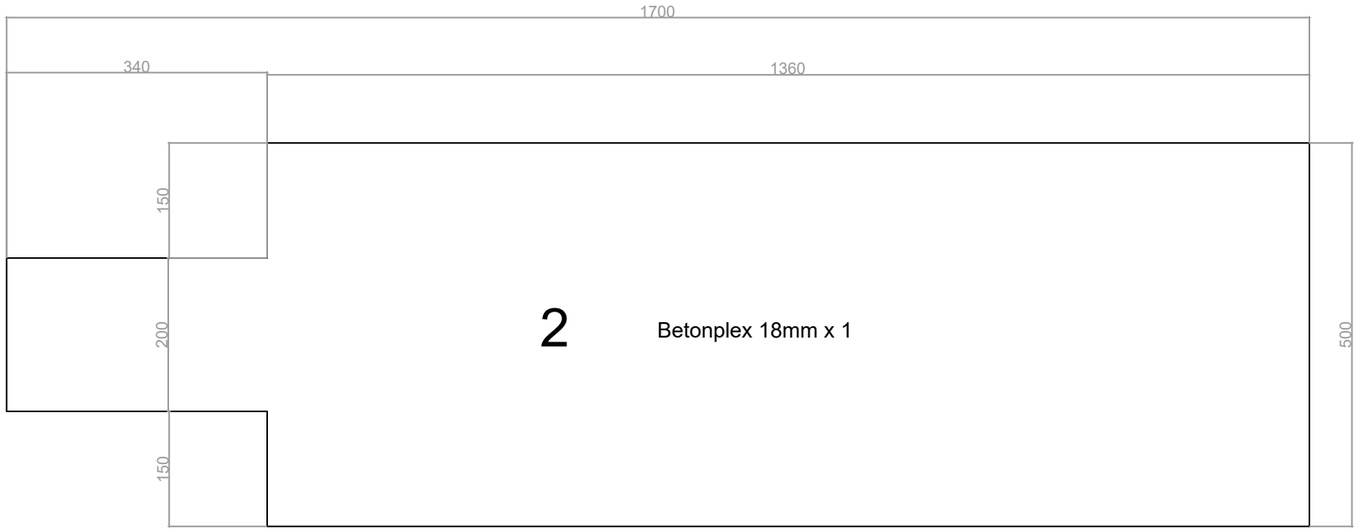

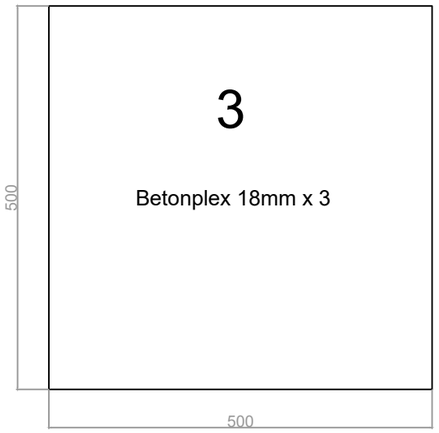

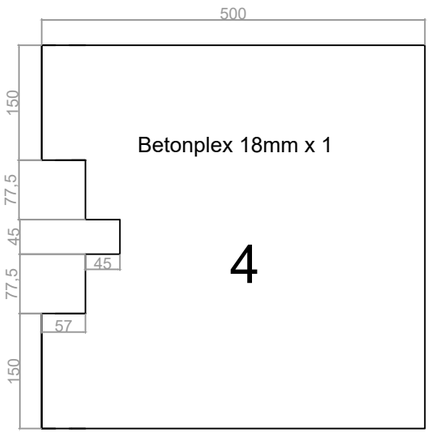

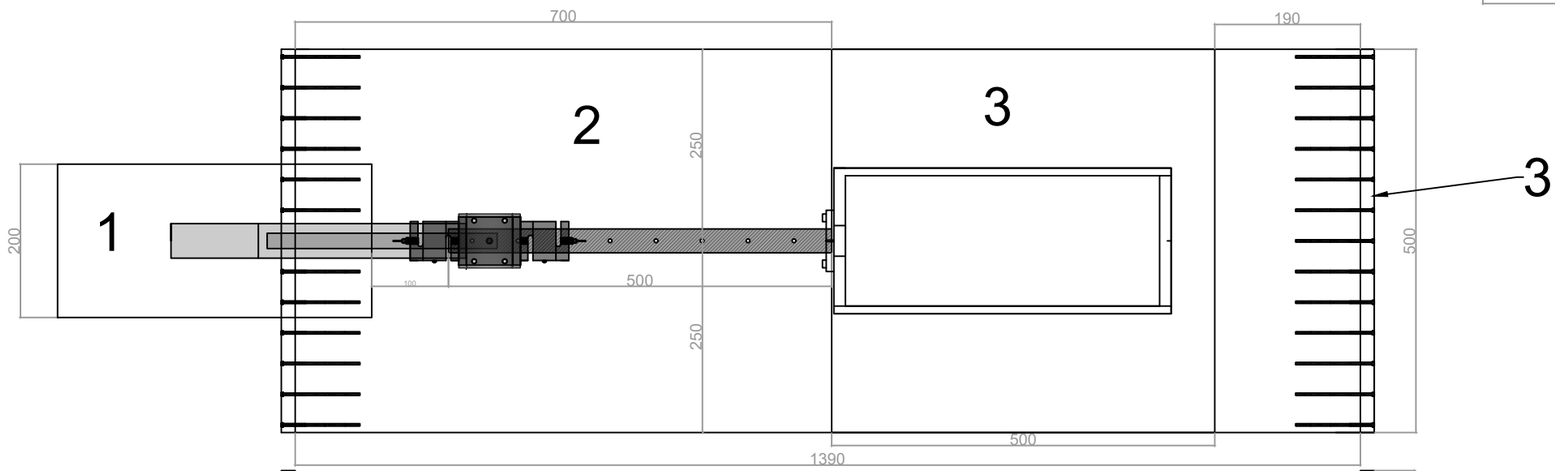

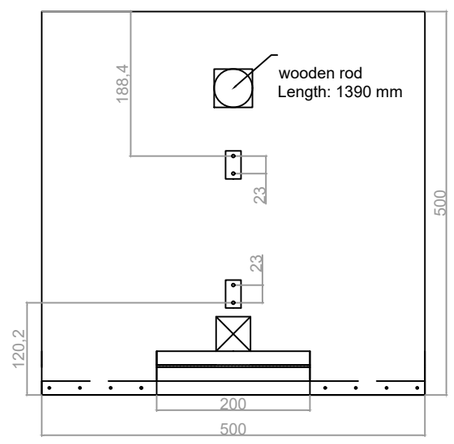

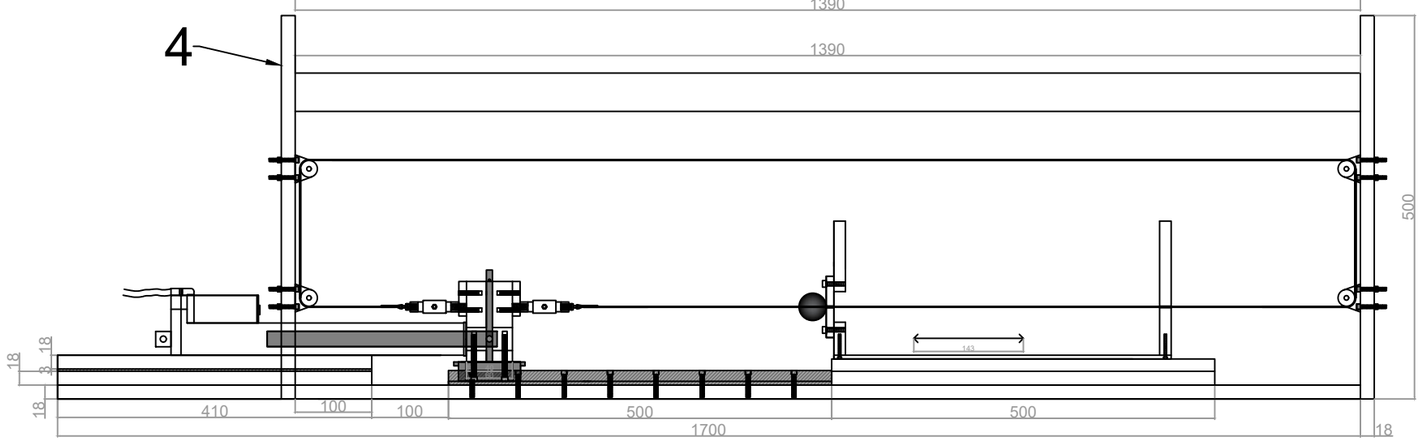

Project: STITCH	Drawing: Testing frame	Date: 24/04/2018	FUGRO / TU Delft
Design by: Eduardo Gómez Meyer	Checked by:	Drawing 1 of 1	

		Plate 1	Plate 2	Plate 3
Length 1	mm	440	440	170
Length 2	mm	190	175	175
Length 3	mm	5	10	15
Qt	mm	1	2	2
Volume	mm^3	418000	1540000	892500
Density of aluminium	g/cm^3	2.70	2.70	2.70
weight	kg	1.13	4.16	2.41

Rubber x2

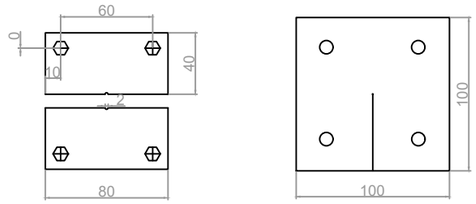

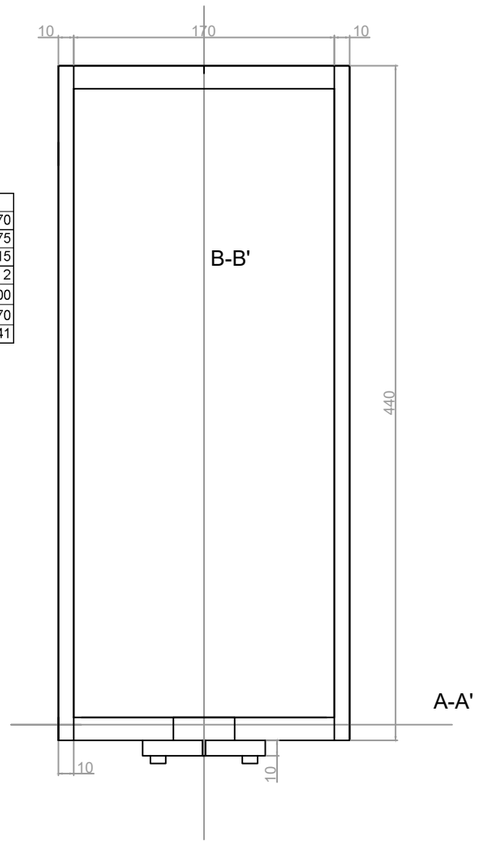

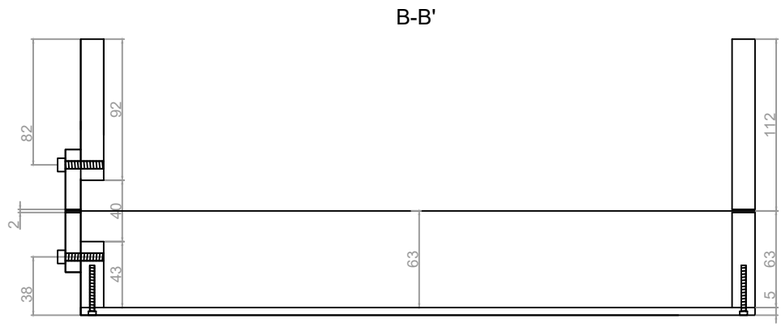

C-C'

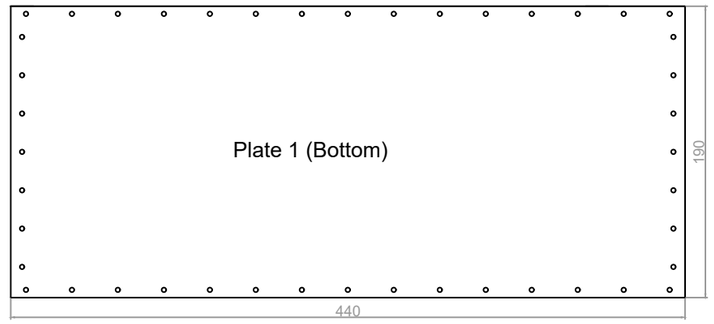

A-A'

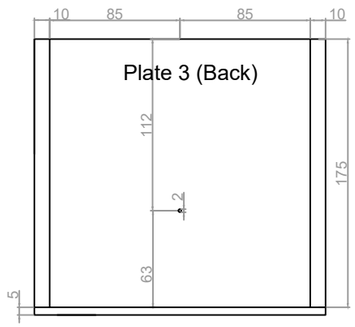

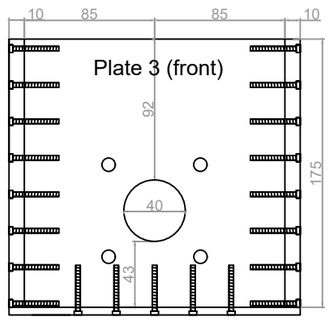

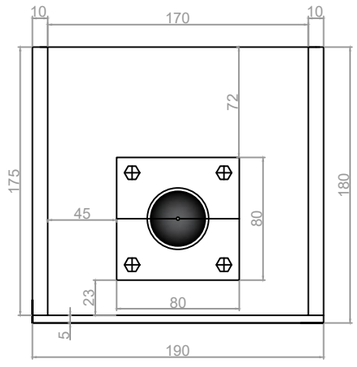

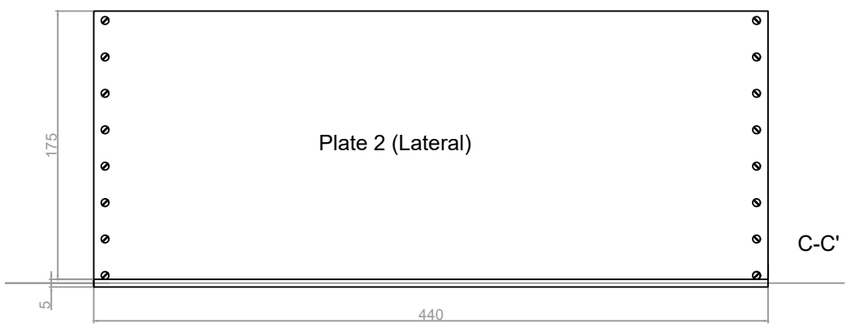

C-C'

Project: STITCH	Drawing: Testing box	Date: 06/04/2018	FUGRO / TU Delft
Design by: Eduardo Gómez Meyer	Checked by:	Drawing 1 of 1	

1

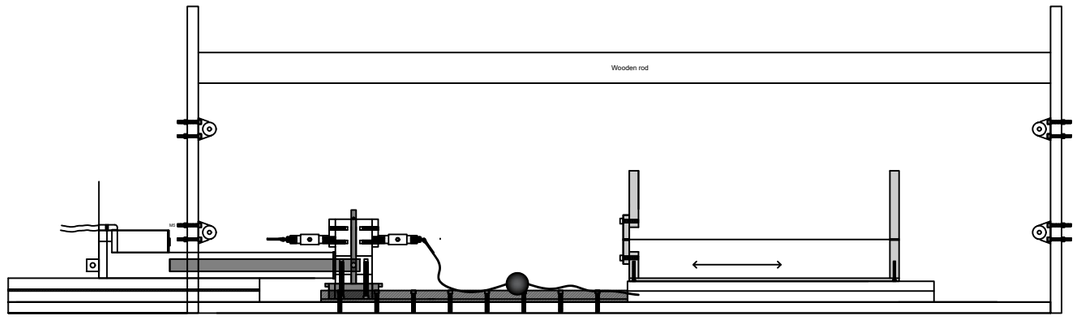

2

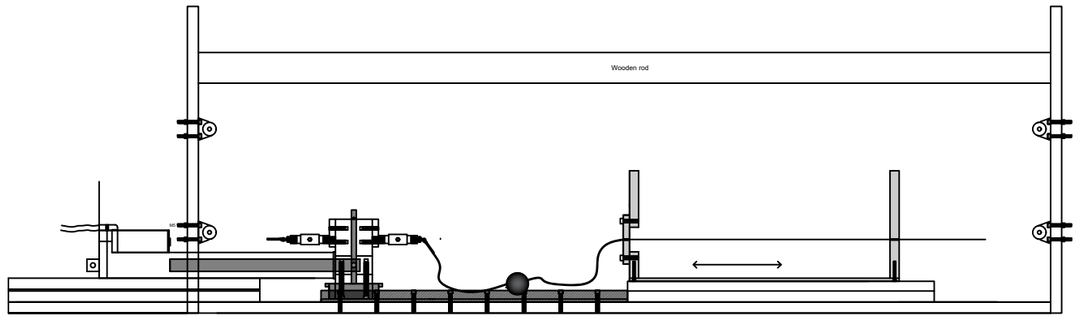

3

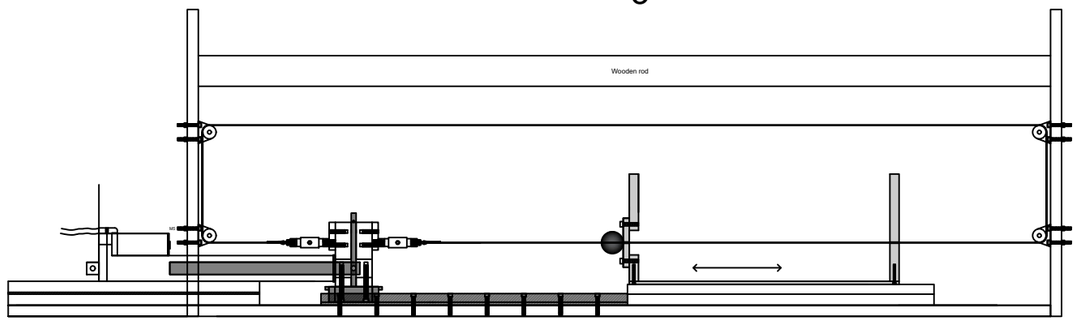

4

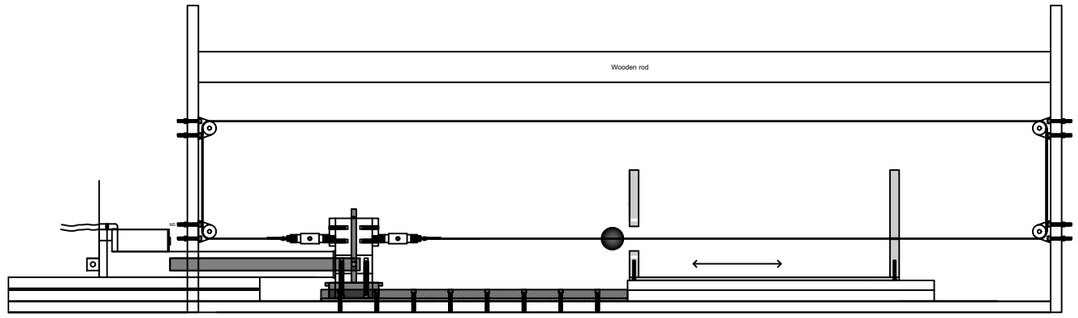

5

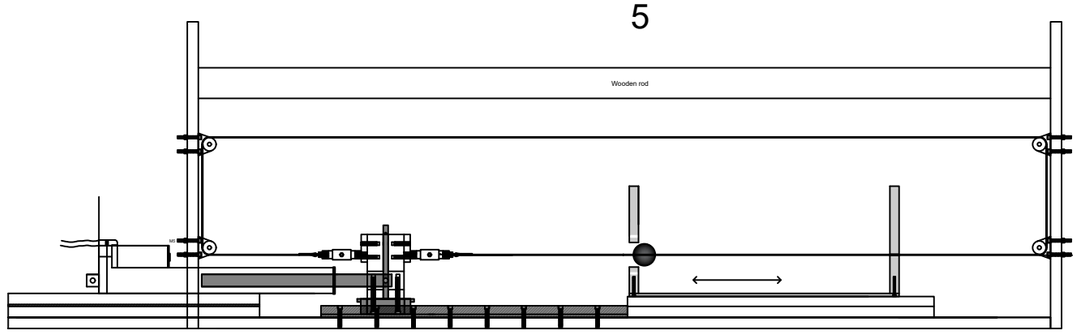

6

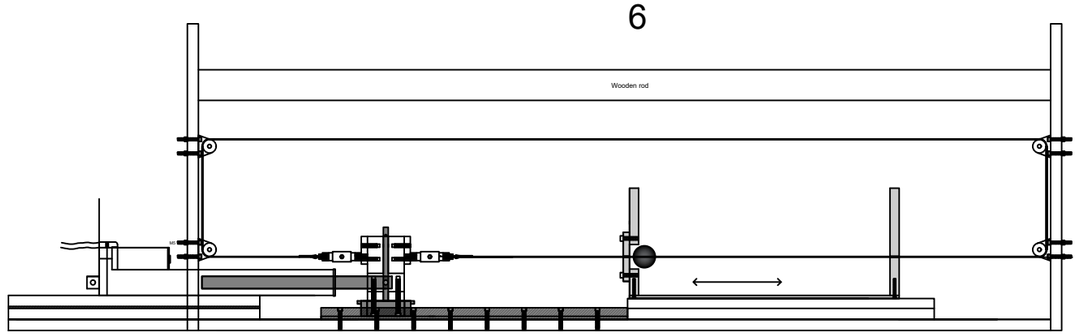

Project: STITCH	Drawing: Installation	Date: 09/04/2018	FUGRO / TU Delft
Design by Eduardo Gómez Meyer:	Checked by:	Drawing 1 of 1	

B. FACTUAL DATA

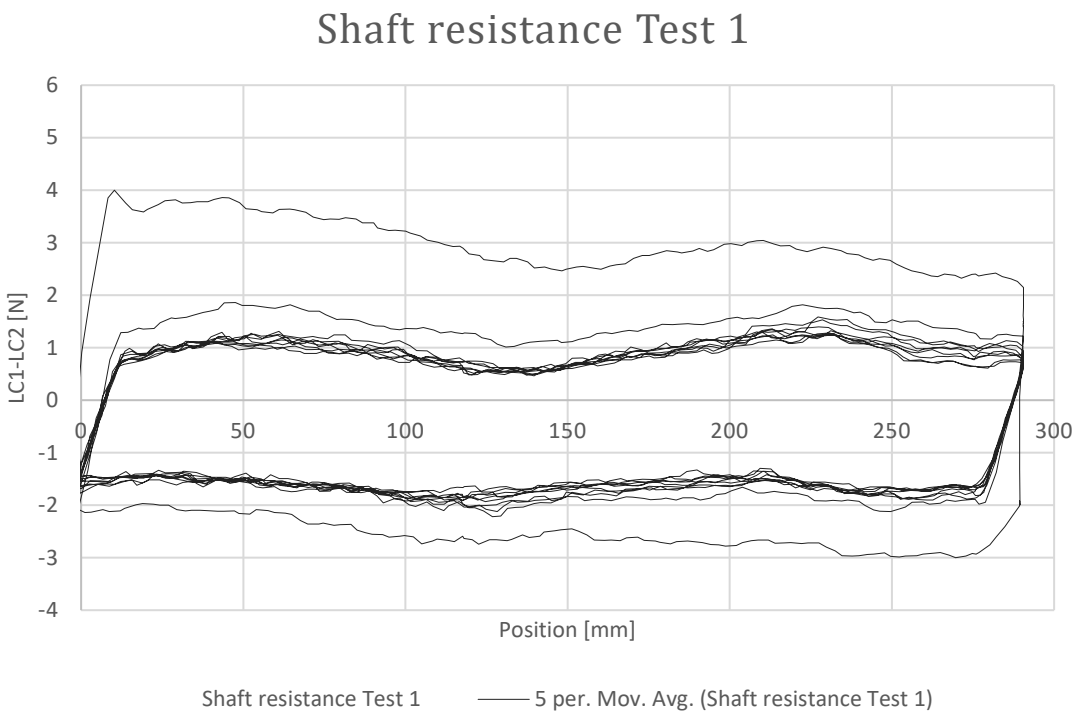

Figure A. 1 - Shaft resistance Test 1

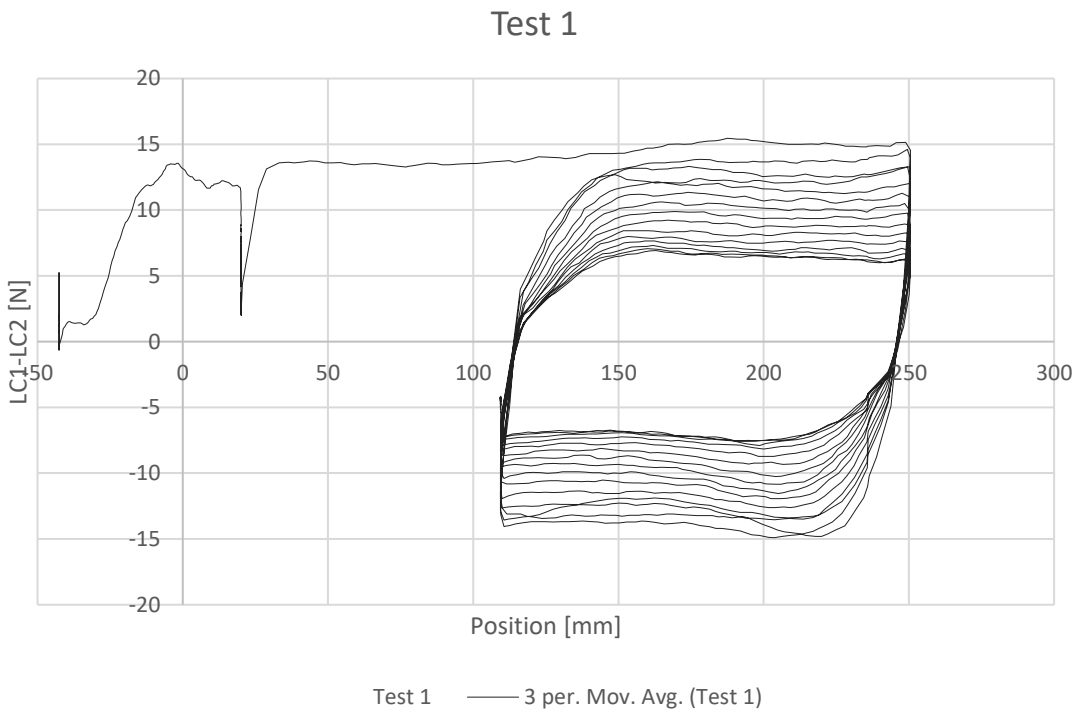

Figure A. 2 - cyclic Test 1

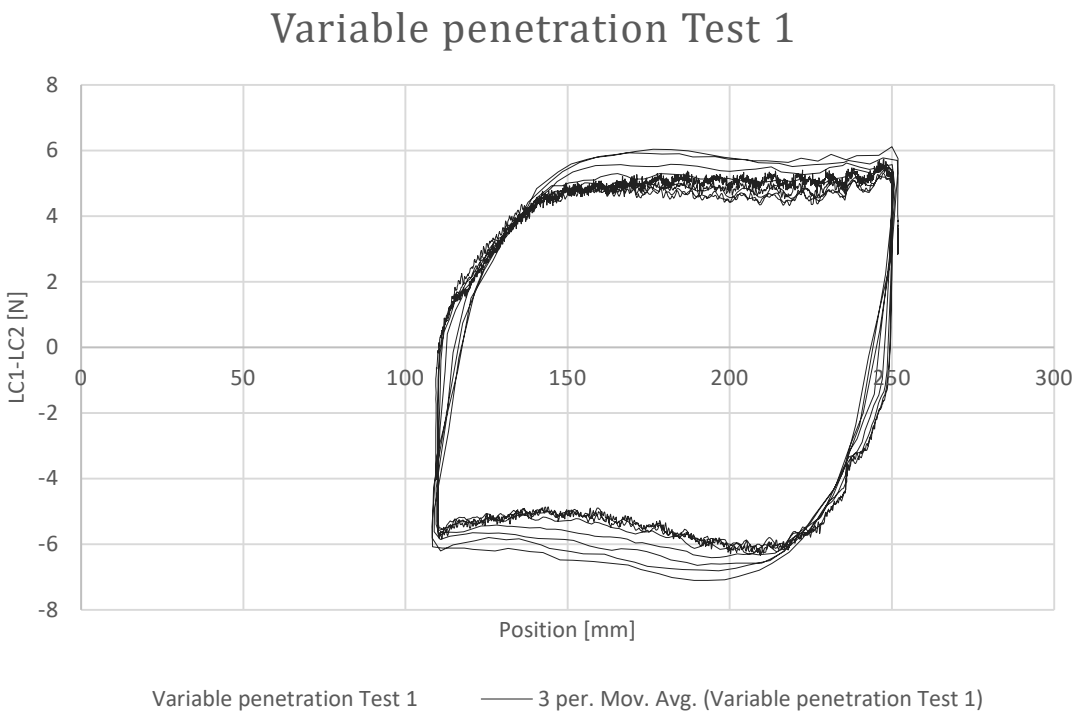

Figure A. 3 - Variable penetration rate Test 2

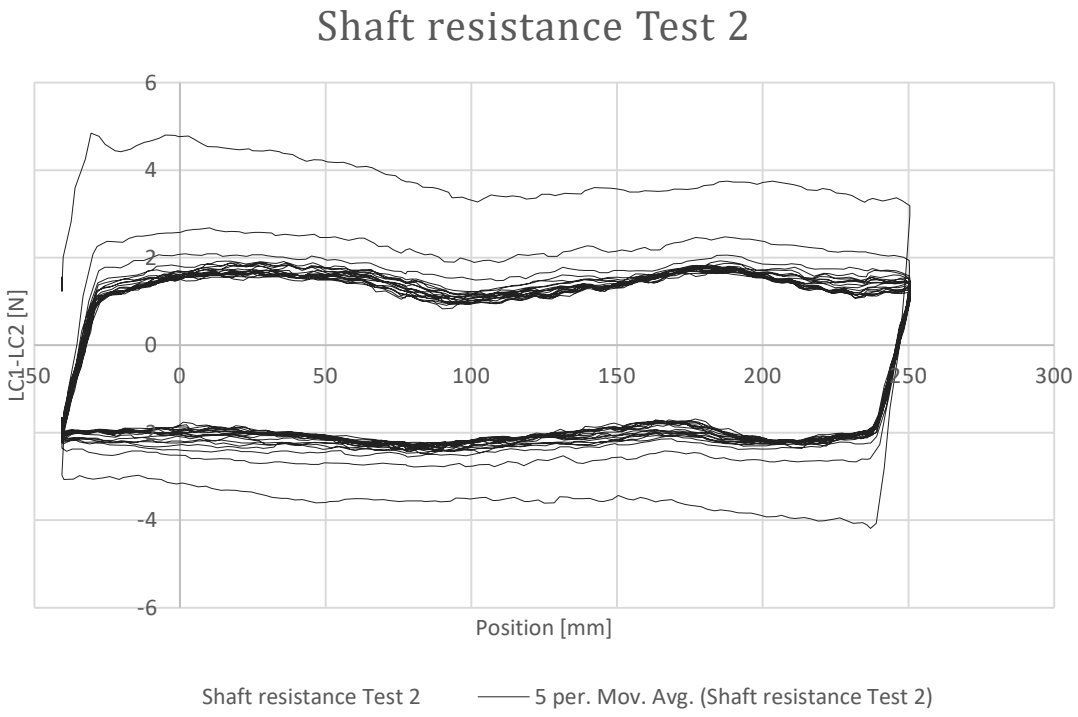

Figure A. 4 - Shaft resistance Test 2

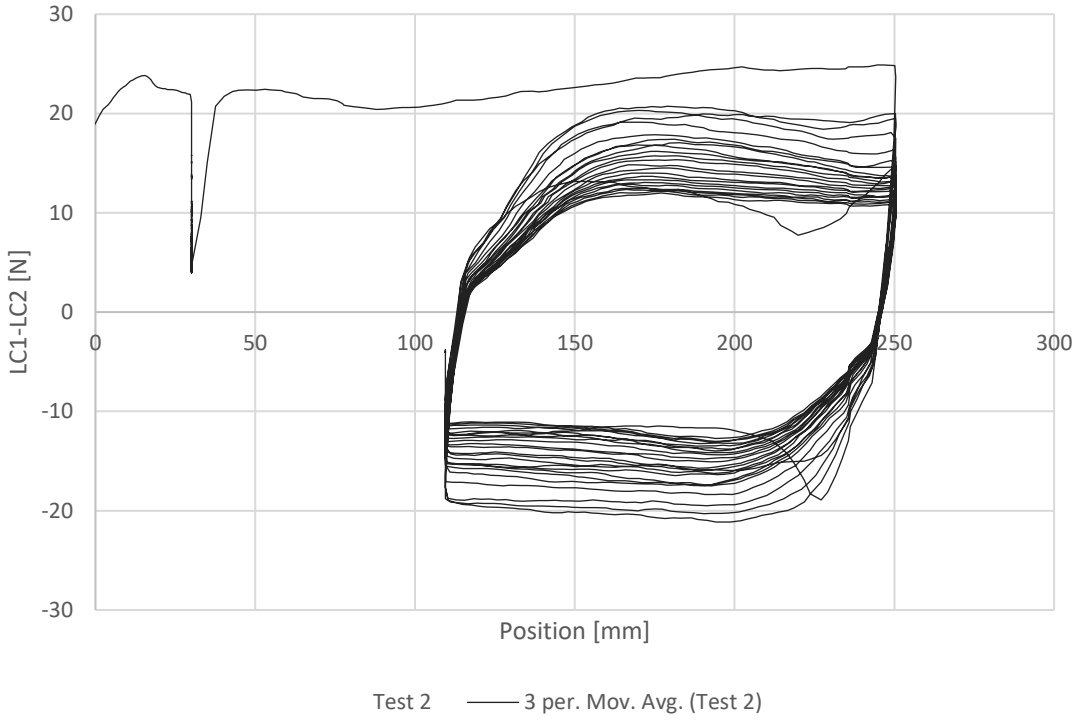

Figure A. 5 - cyclic Test 2

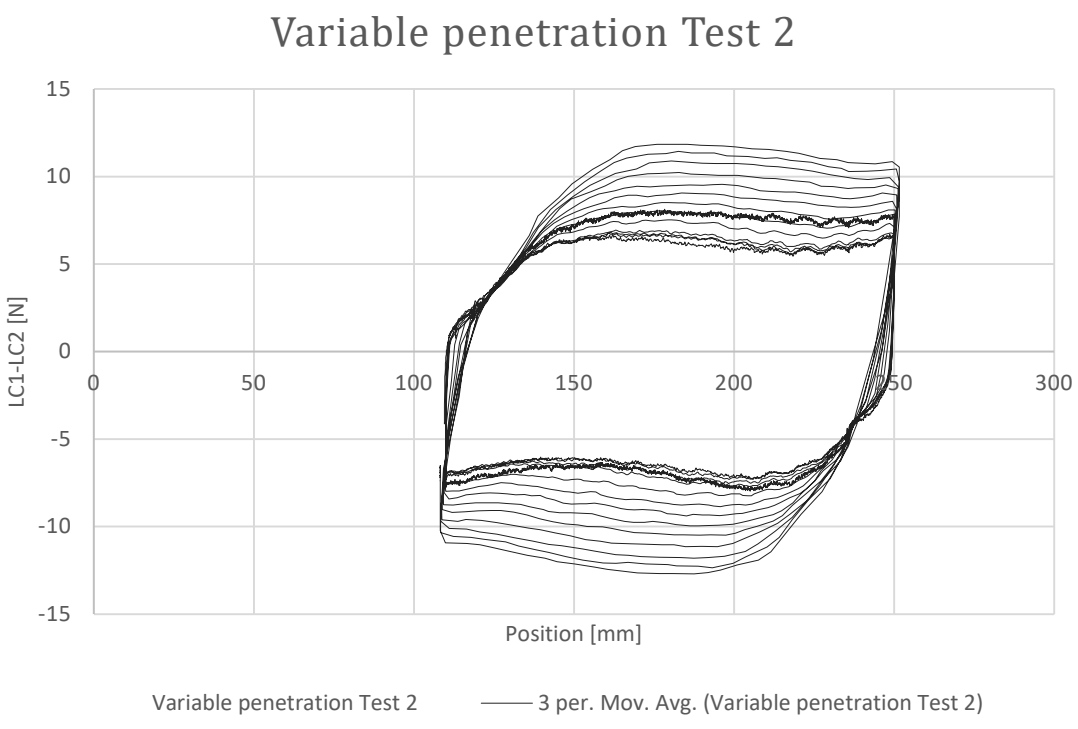

Figure A. 6 - Variable penetration rate Test 2

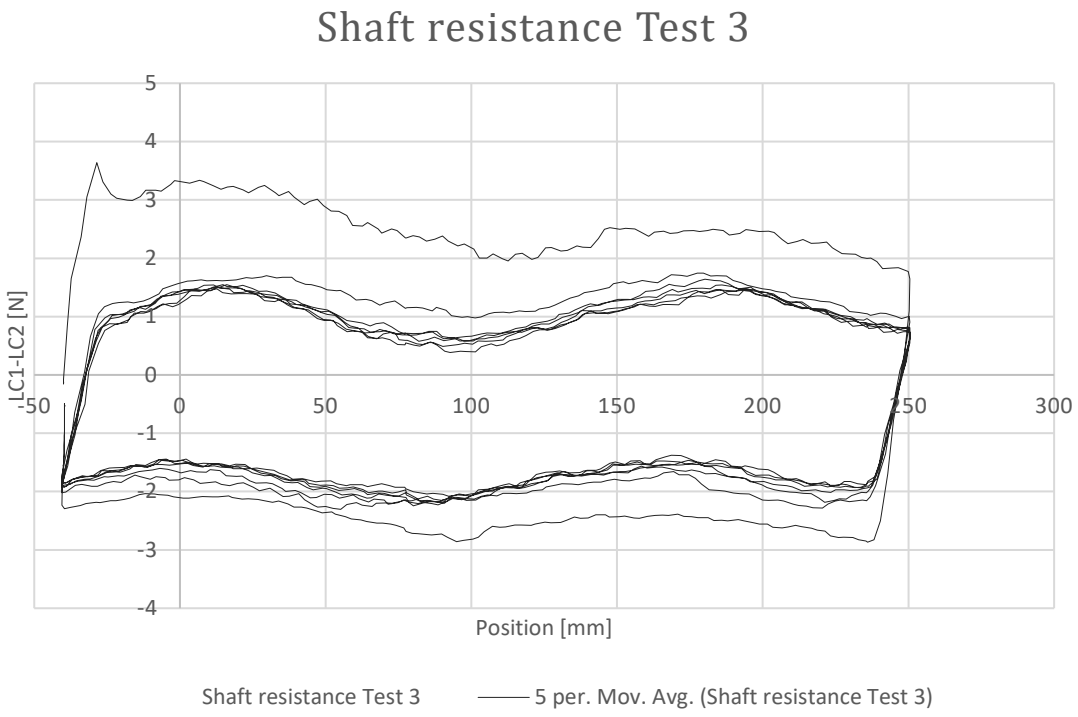

Figure A. 7 - Shaft resistance test 3

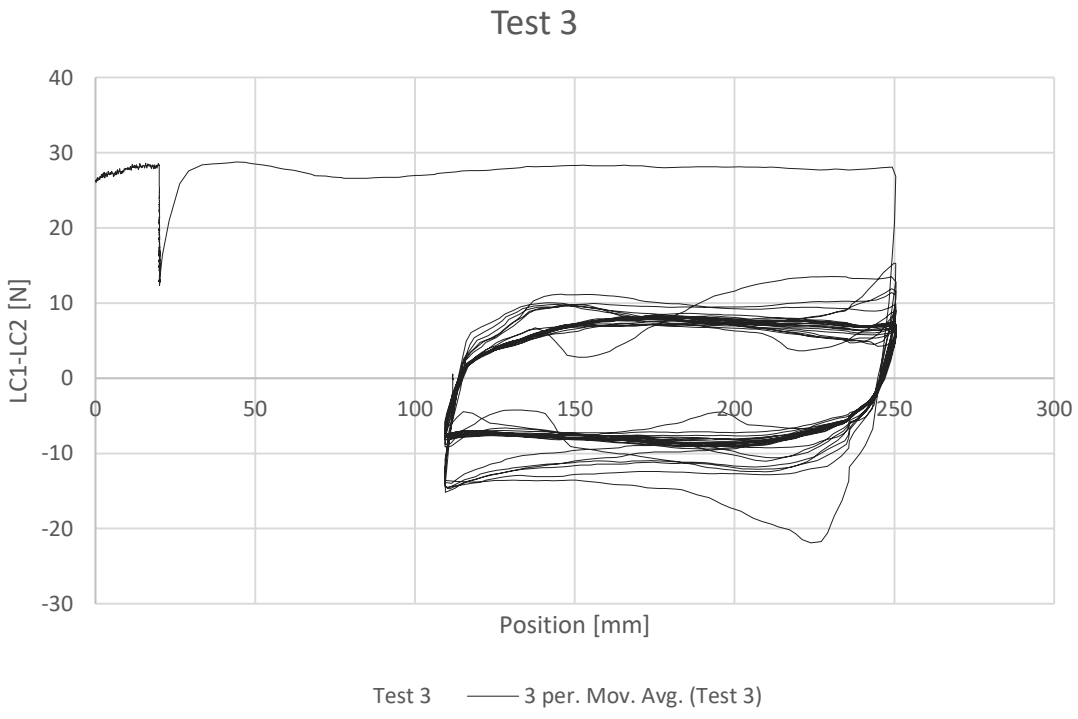

Figure A. 8 - Cyclic Test 3

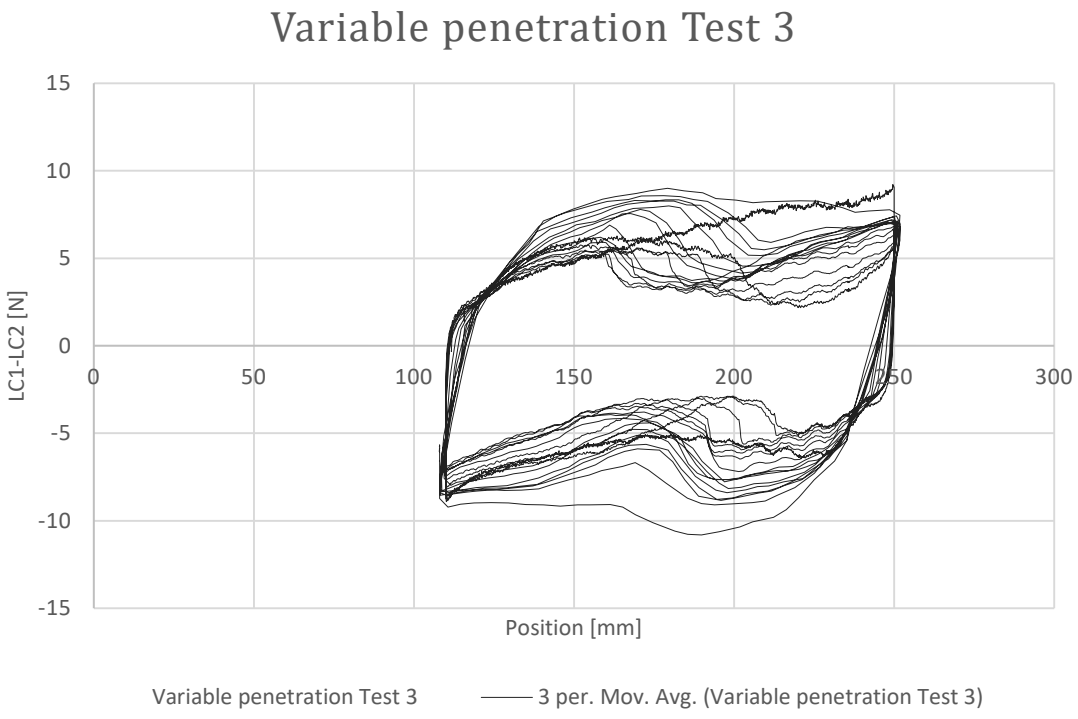

Figure A. 9 - Variable penetration rate Test 3

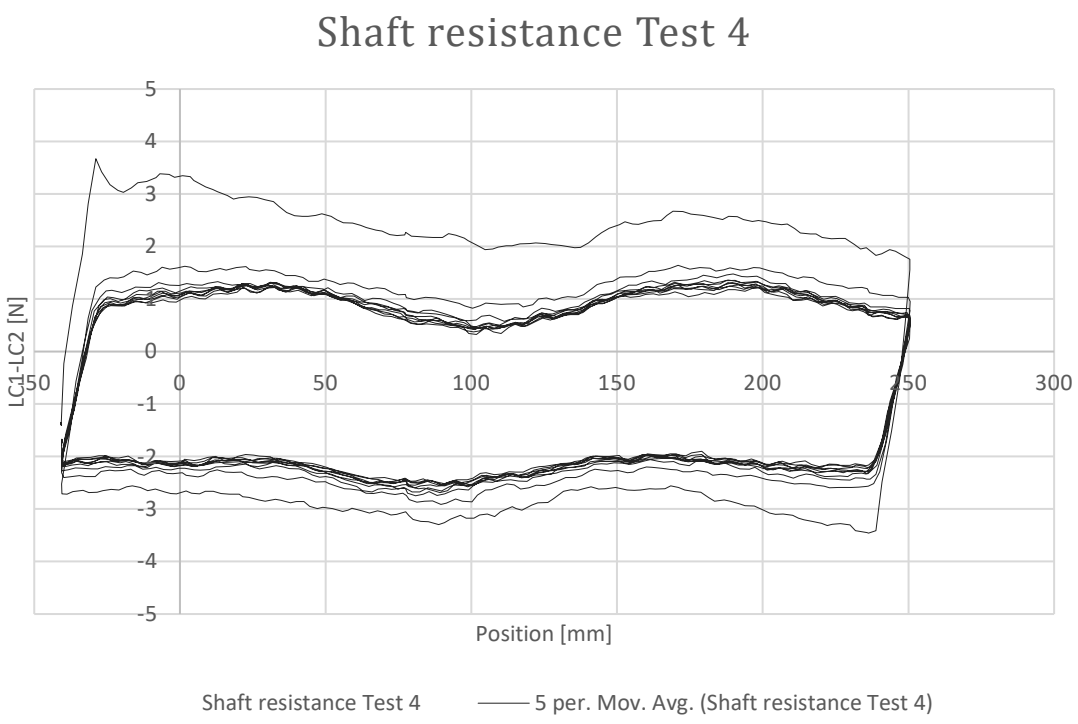

Figure A. 10 - Shaft resistance Test 4

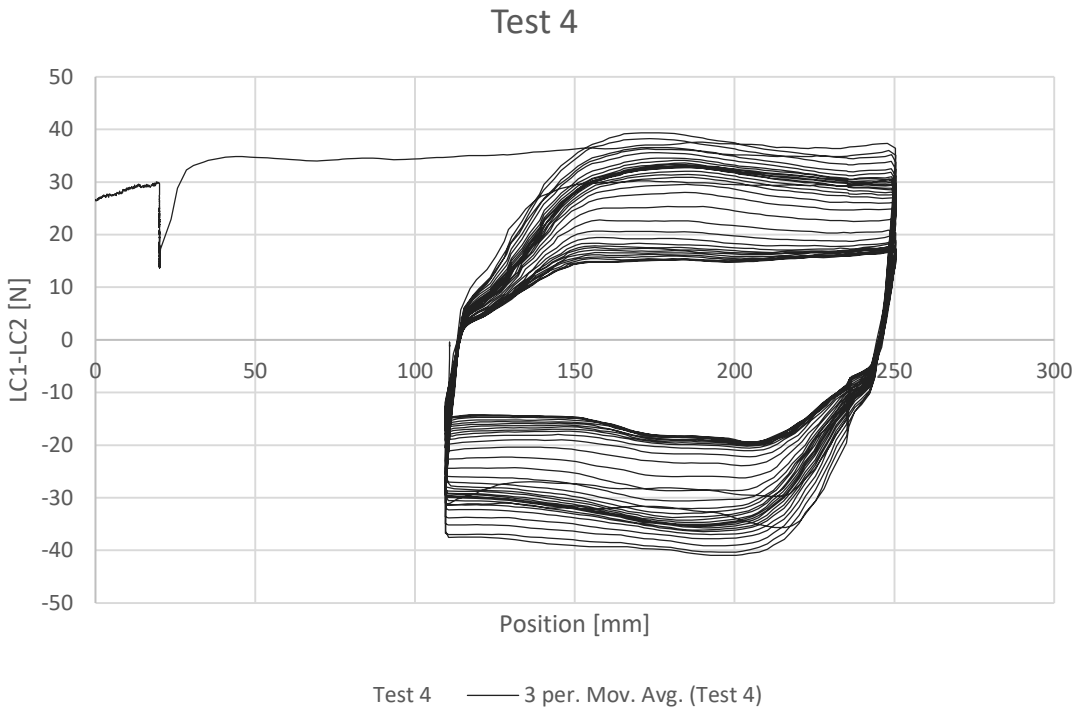

Figure A. 11 - Cyclic Test 3

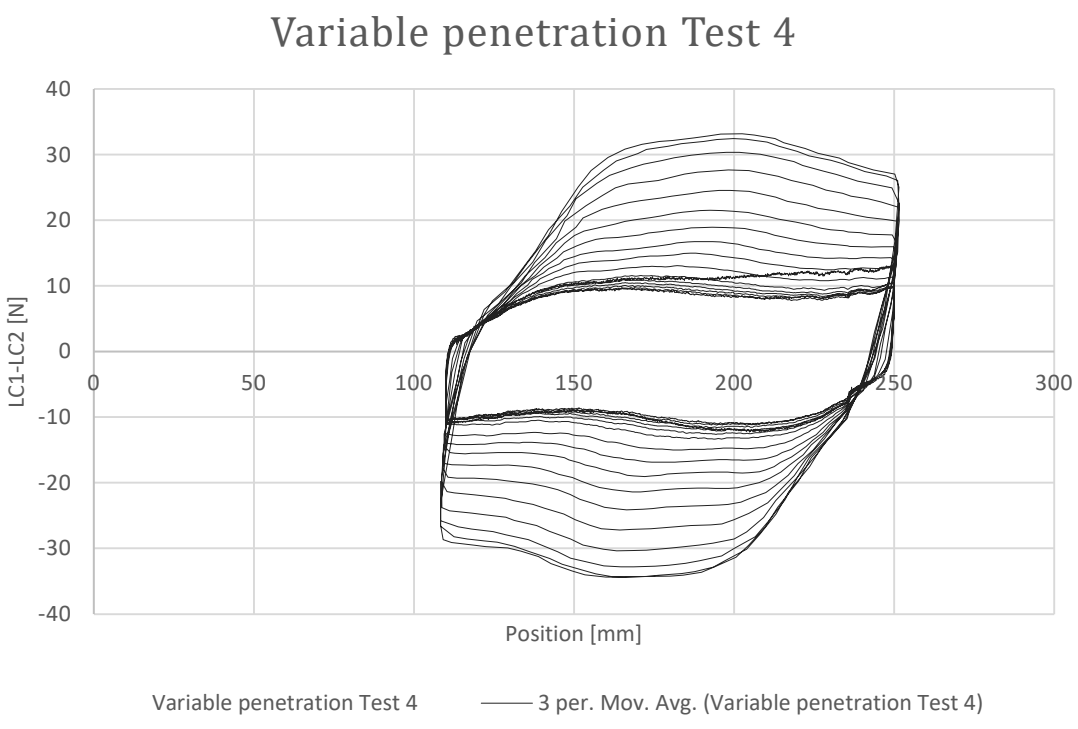

Figure A. 12 - Variable penetration rate Test 4

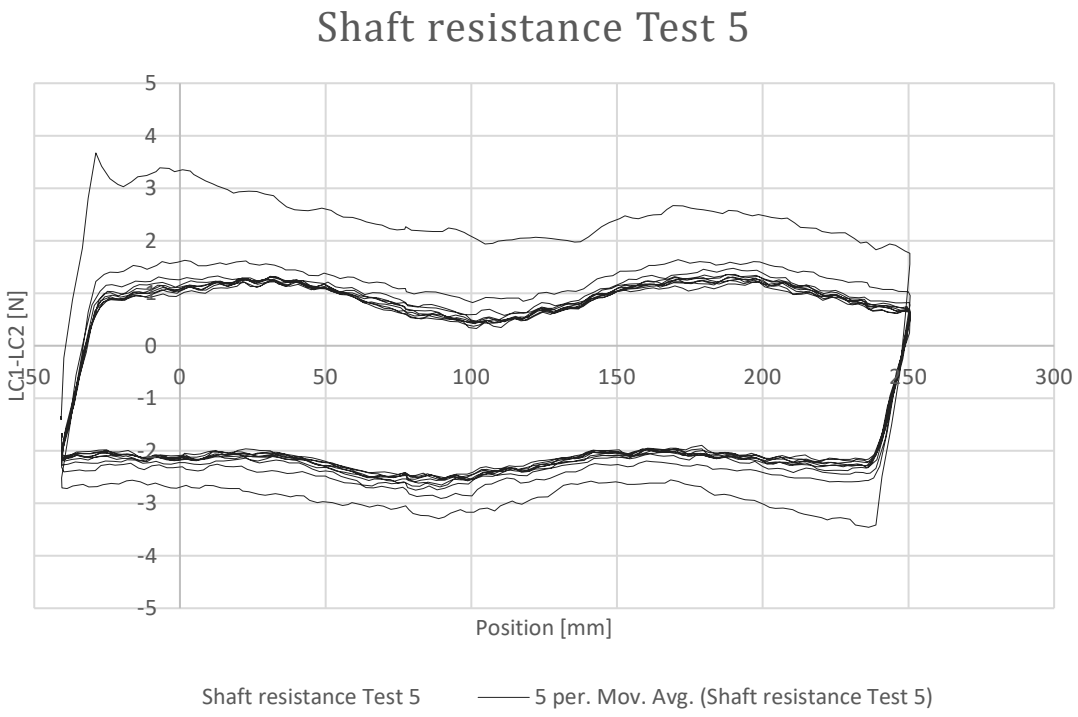

Figure A. 13 - Shaft resistance Test 5

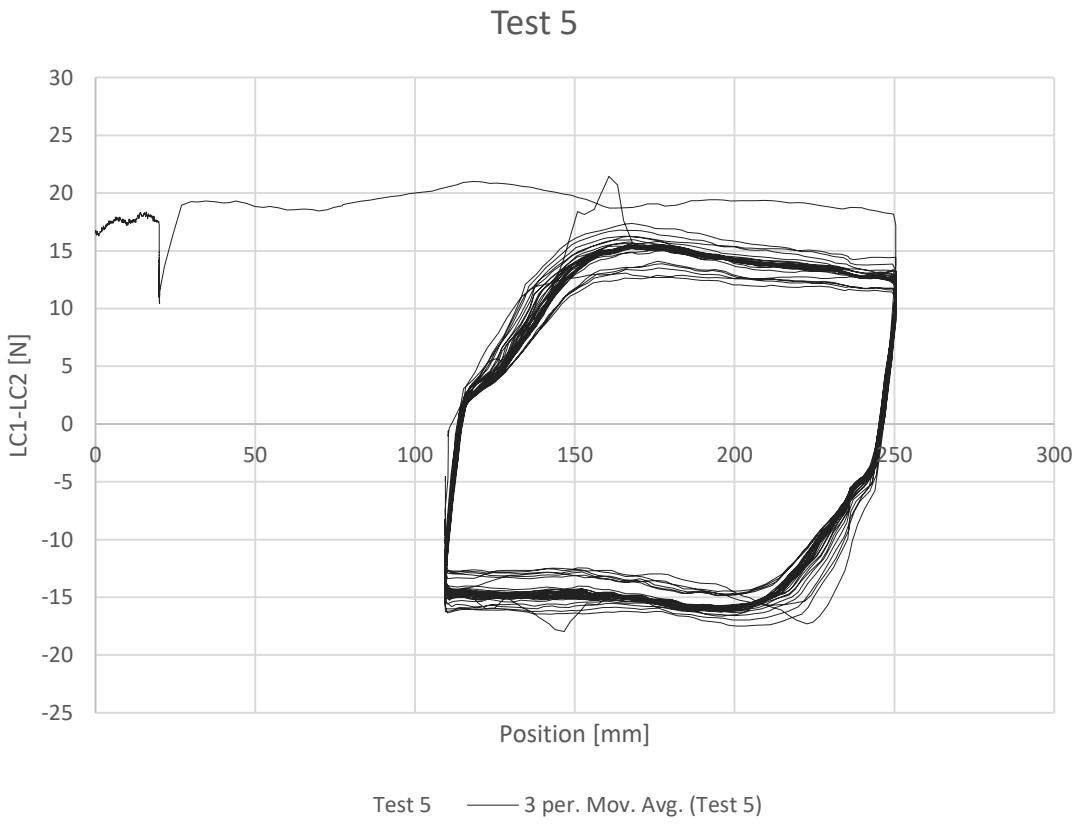

Figure A. 14 - Cyclic Test 5

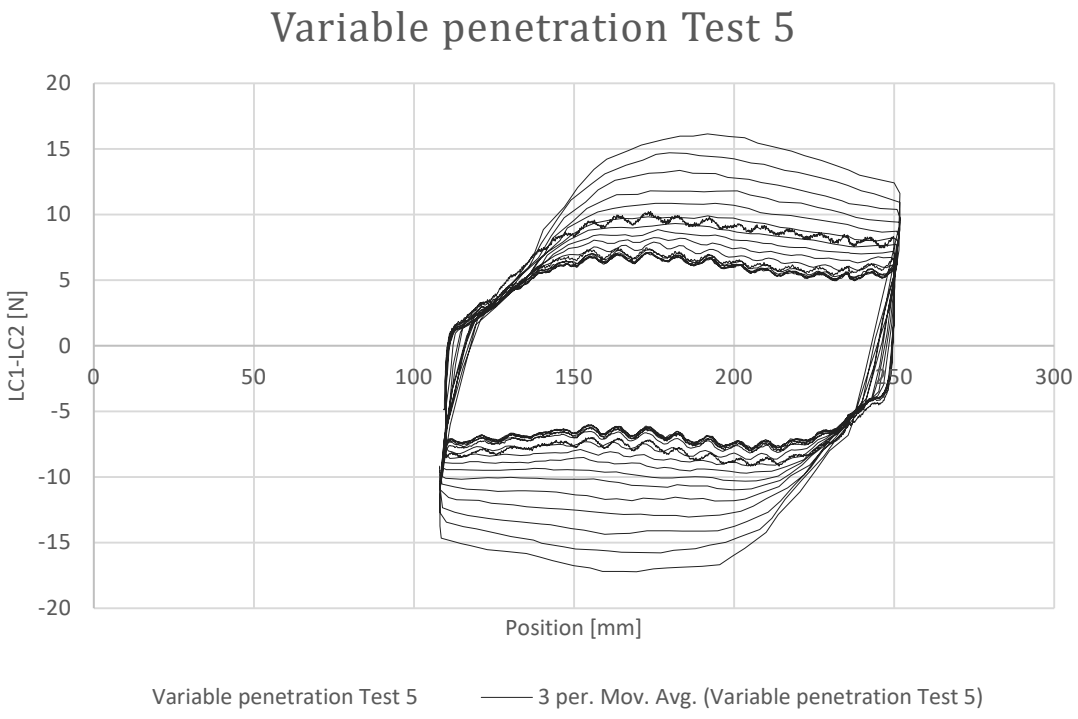

Figure A. 15 - Variable penetration rate Test 5

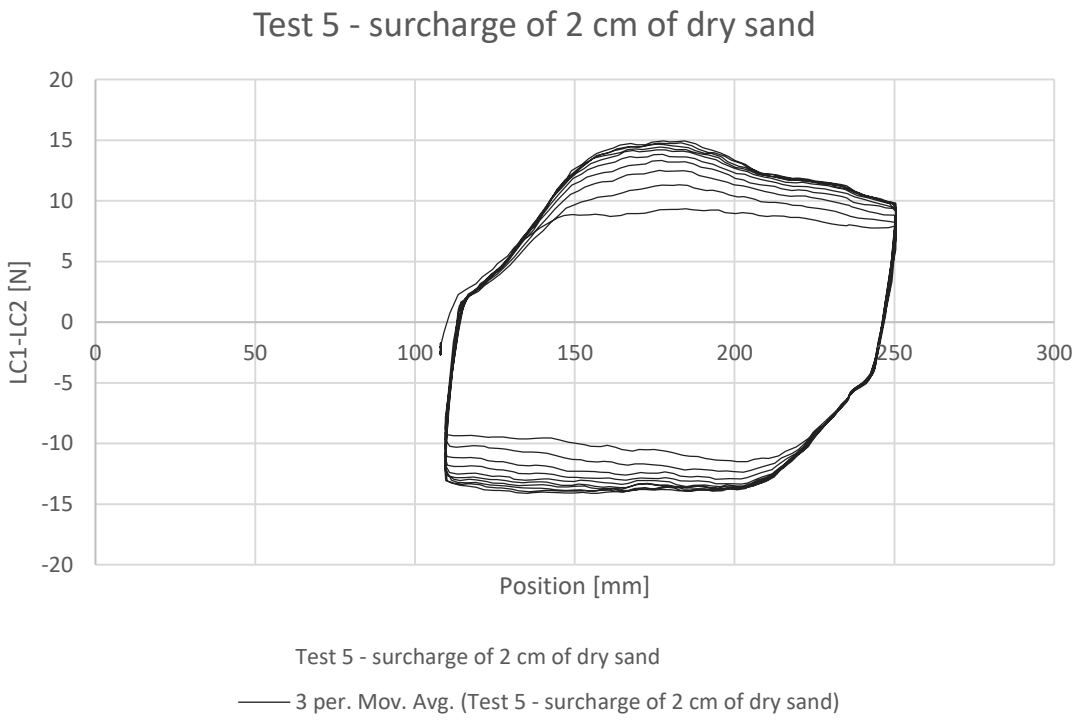

Figure A. 16 - Cyclic Test 5 with surcharge (2cm of dry sand)

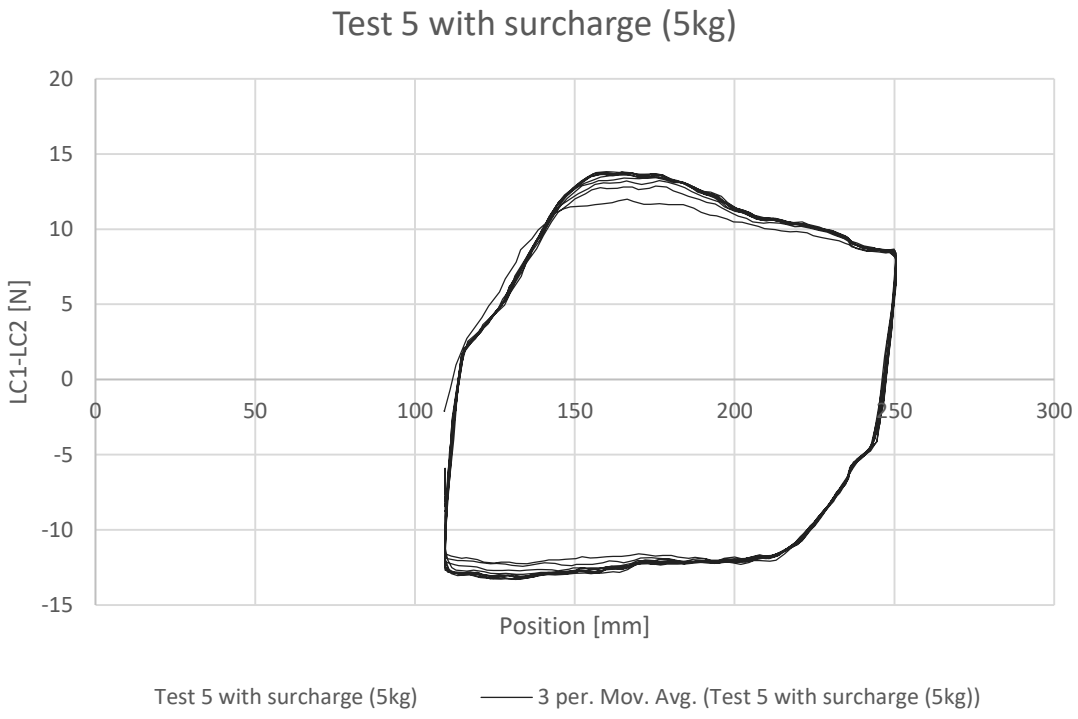

Figure A. 17 - Cyclic Test 5 with surcharge (5kg)

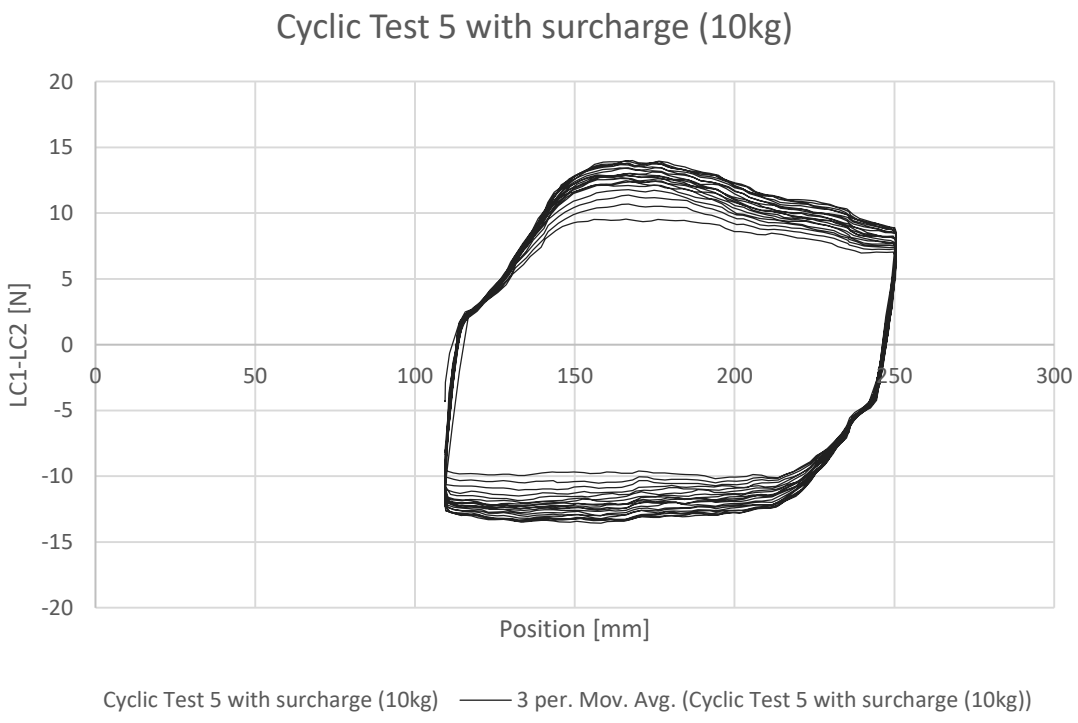

Figure A. 18 - Cyclic Test with surcharge (10kg)

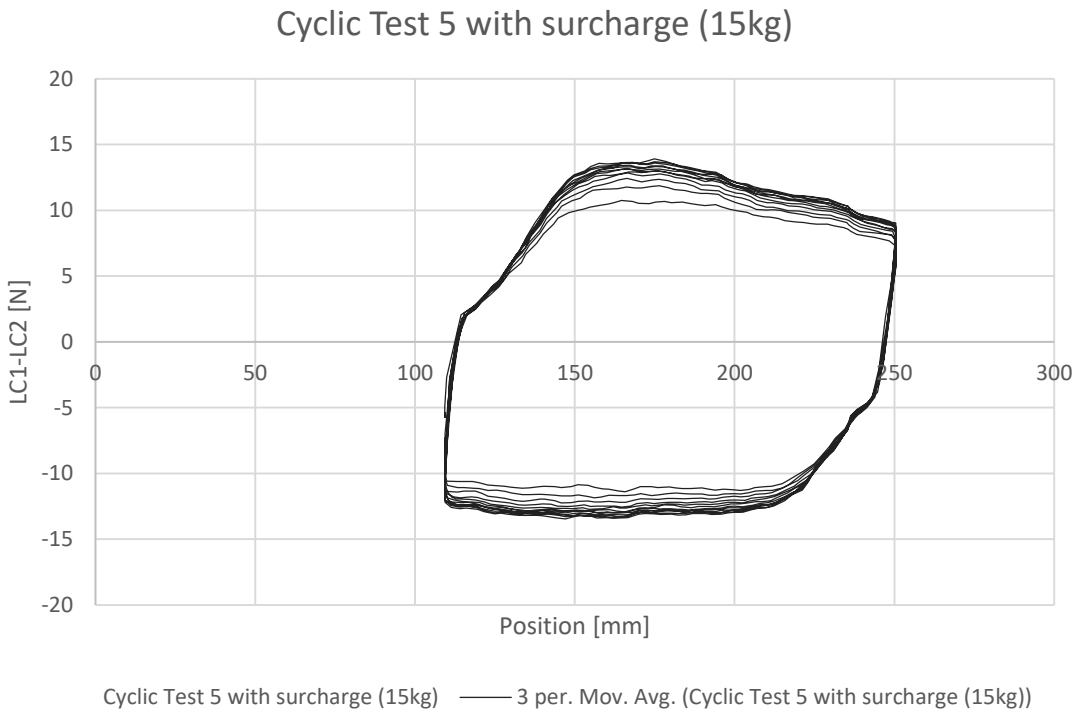

Figure A. 19 - Cyclic Test 5 with surcharge (15kg)

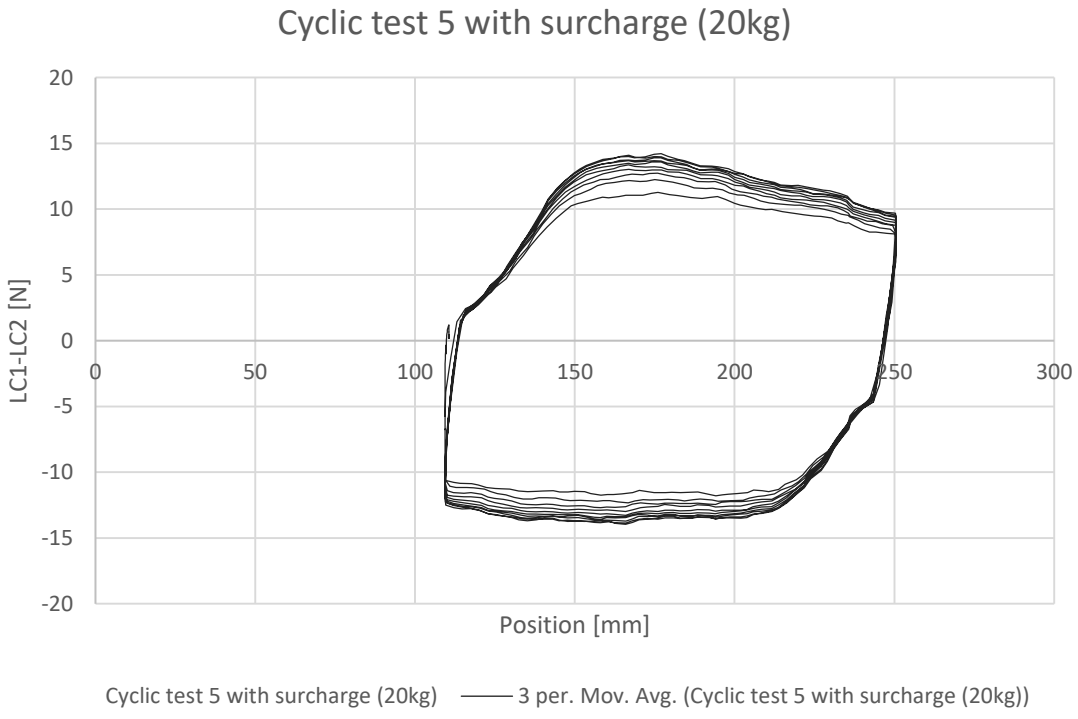

Figure A. 20 - Cyclic Test 5 with surcharge (20kg)

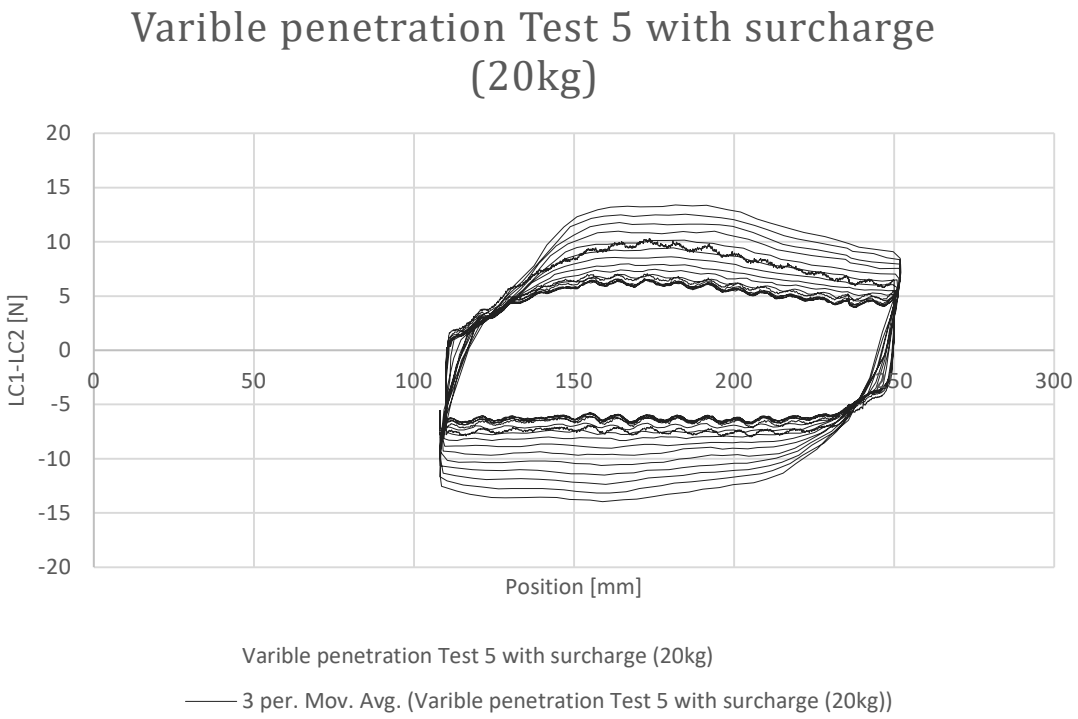

Figure A. 21 - Variable penetration rate Test 5 with surcharge (20kg)

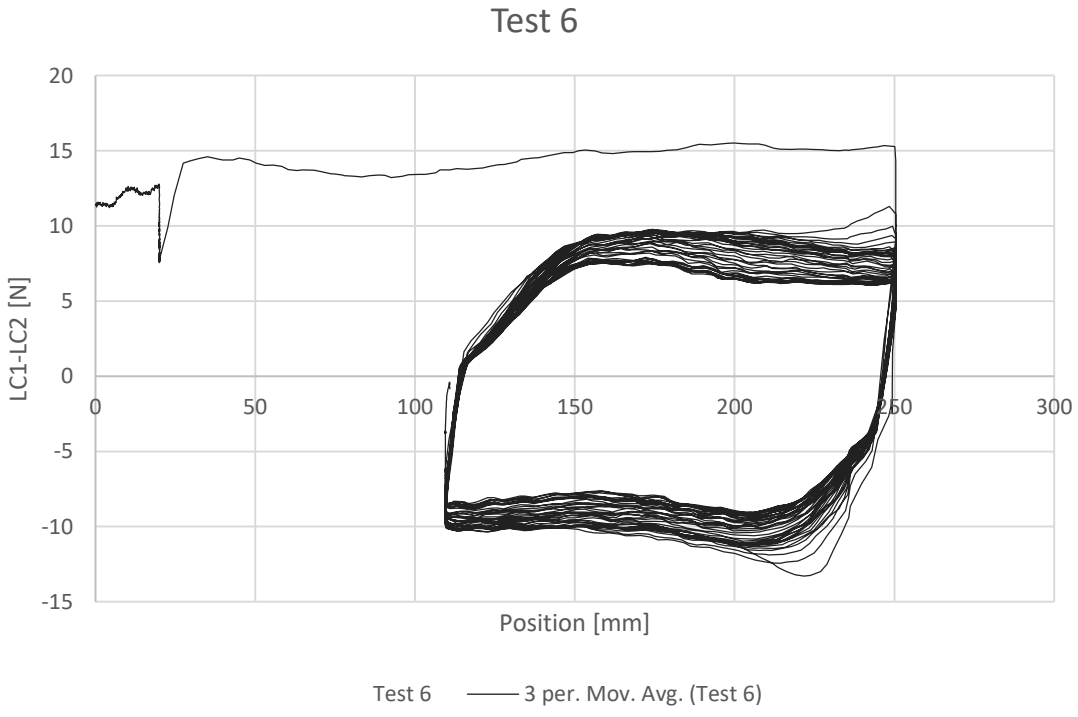

Figure A. 22 - Cyclic Test 6 (30mm ball)

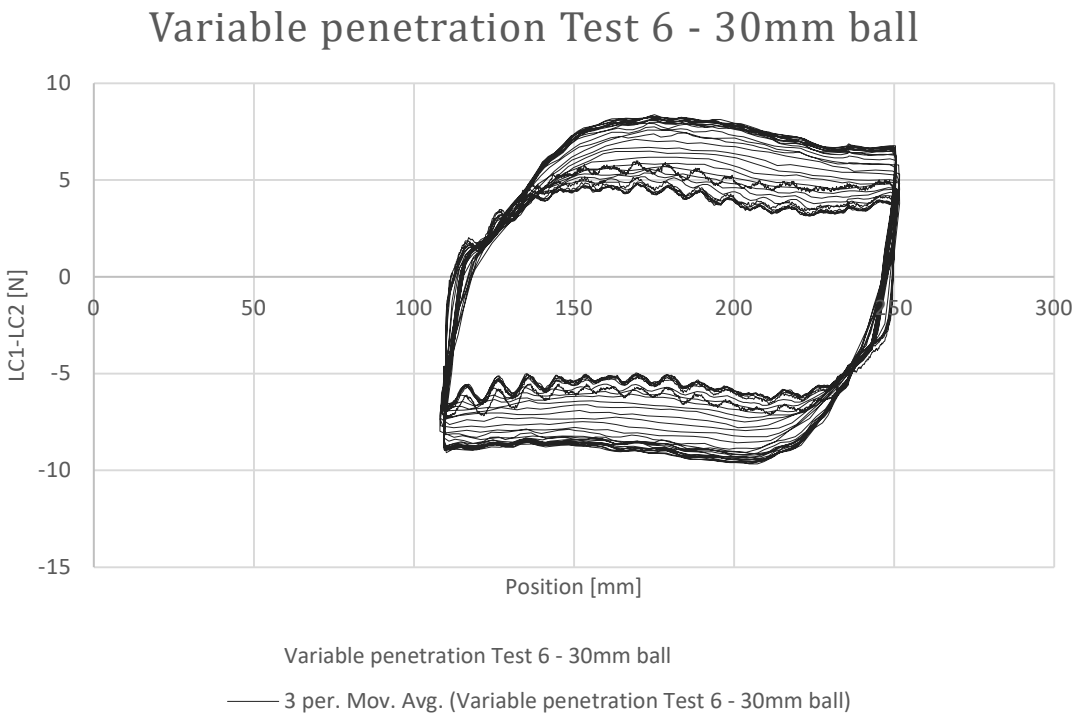

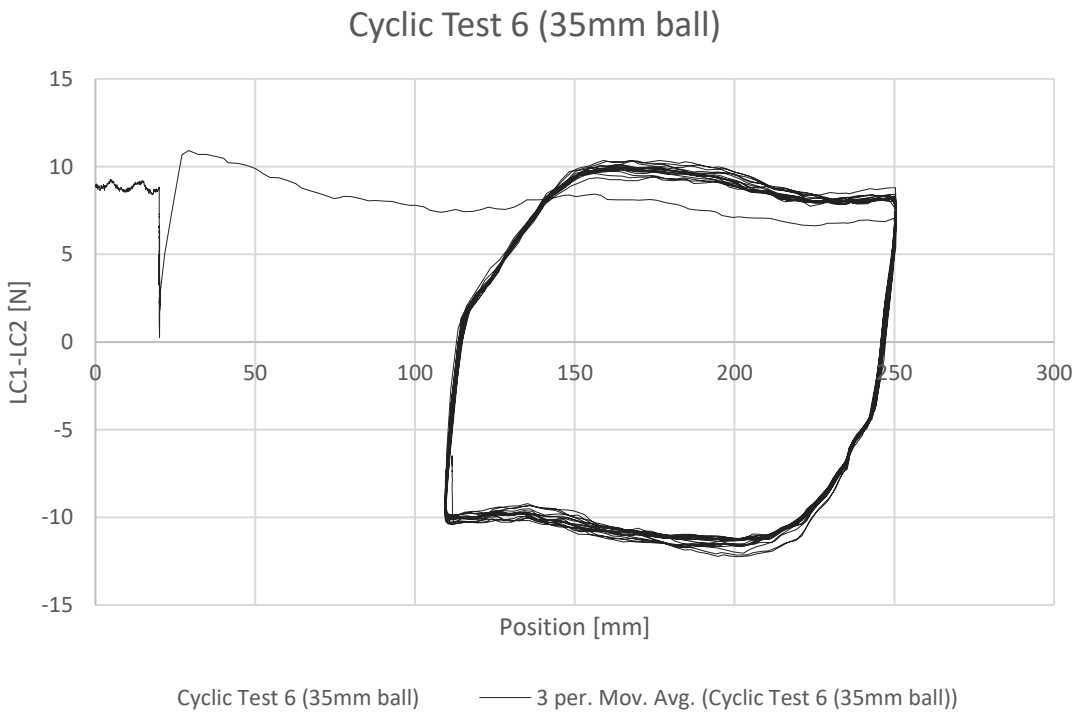

Figure A. 23 - Cyclic Test 5 (35mm ball)

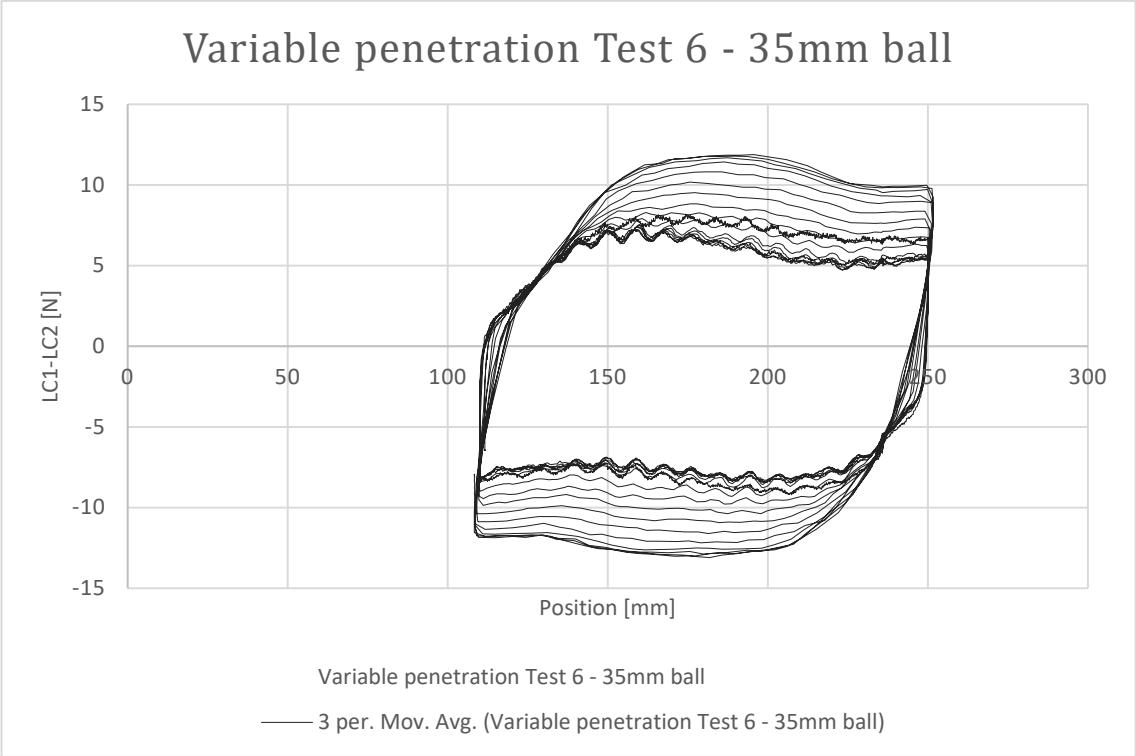

Figure A. 24 - Variable penetration rate Test 6 (35mm ball)

C. DEGRADATION CURVES (CYCLIC TESTS)

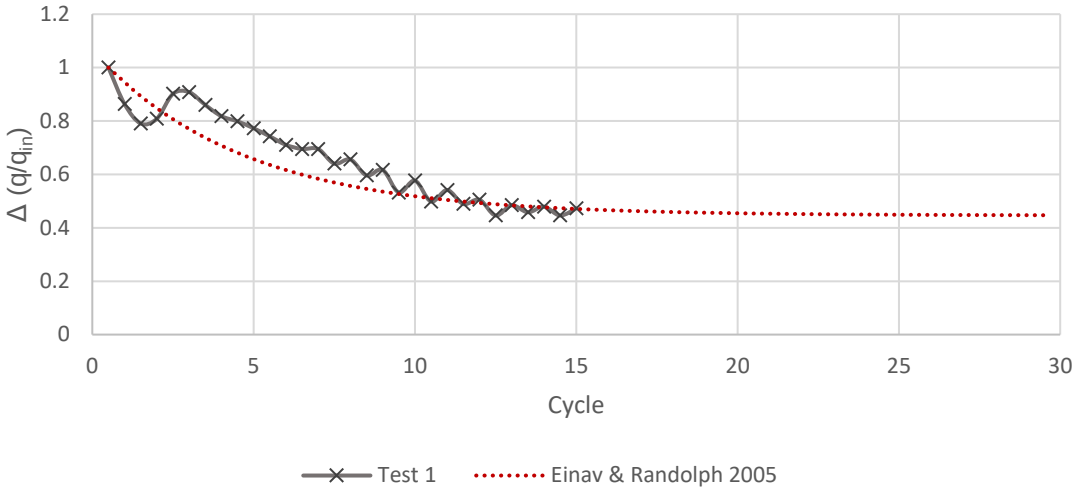

Figure A. 25 - Degradation curve Test 1

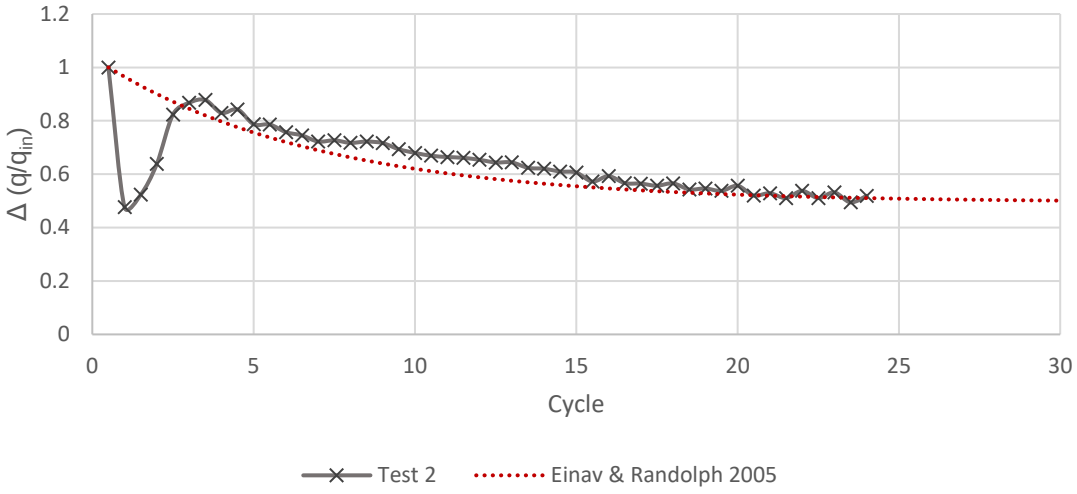

Figure A. 26 - Degradation curve Test 2

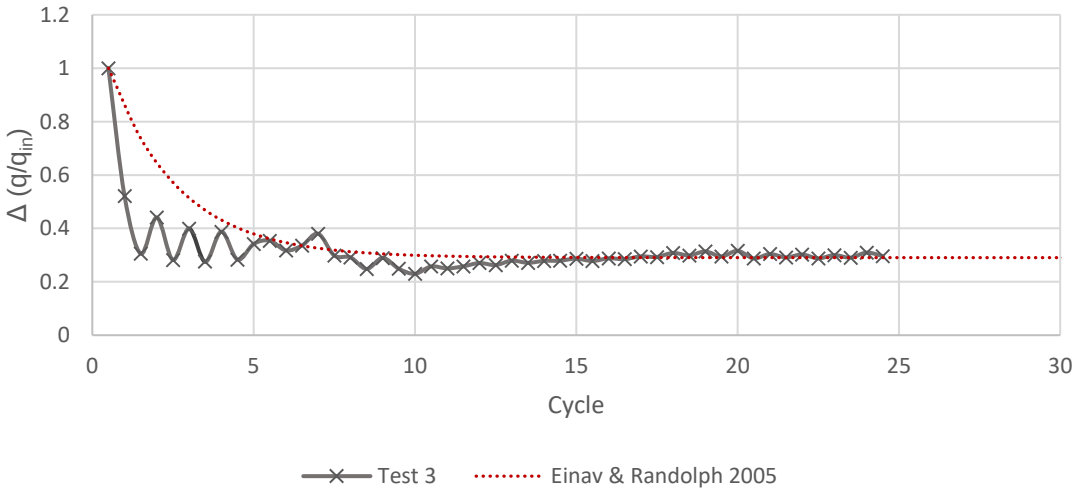

Figure A. 27 - Degradation curve Test 3

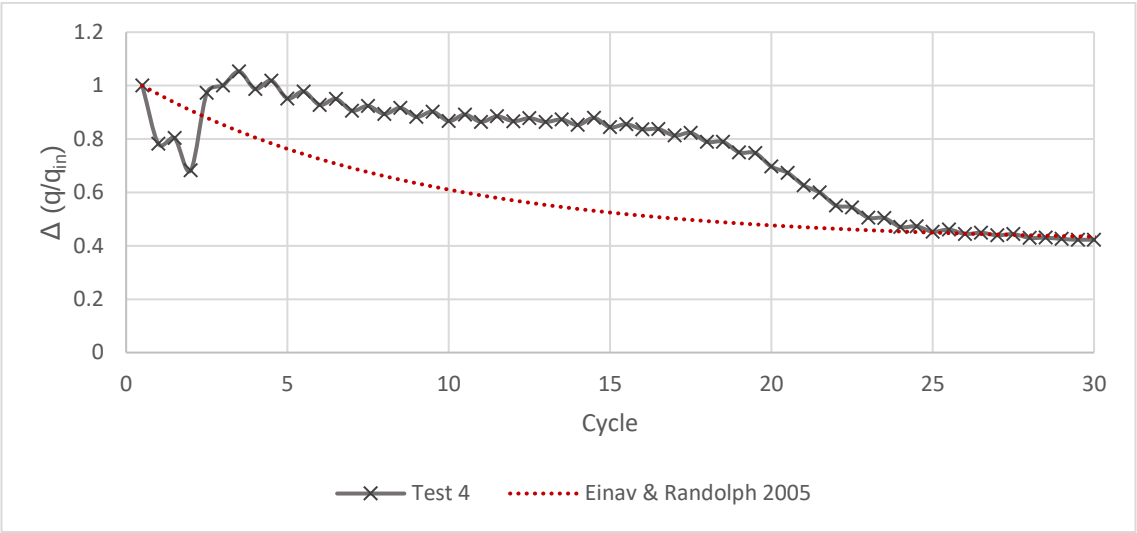

Figure A. 28 - Degradation curve Test 4

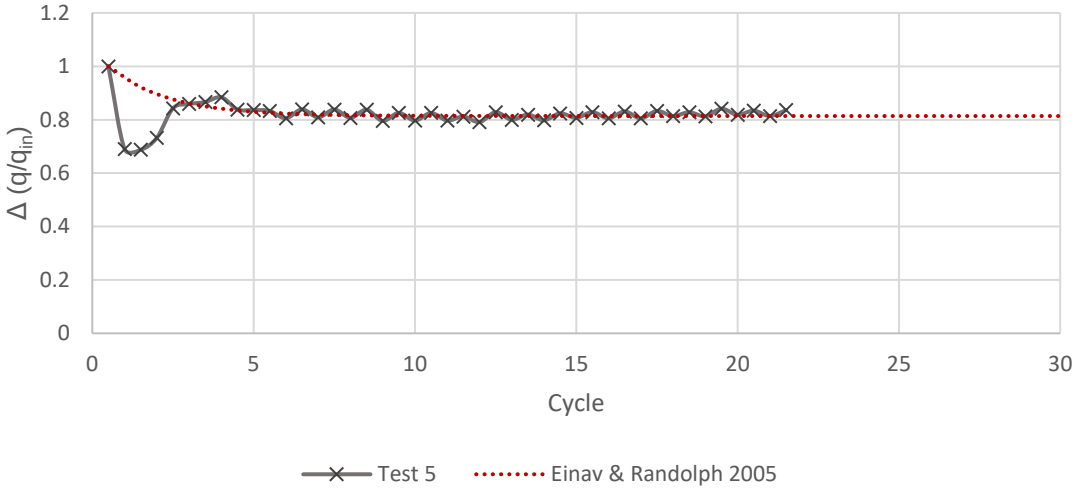

Figure A. 29 - Degradation curve Test 5

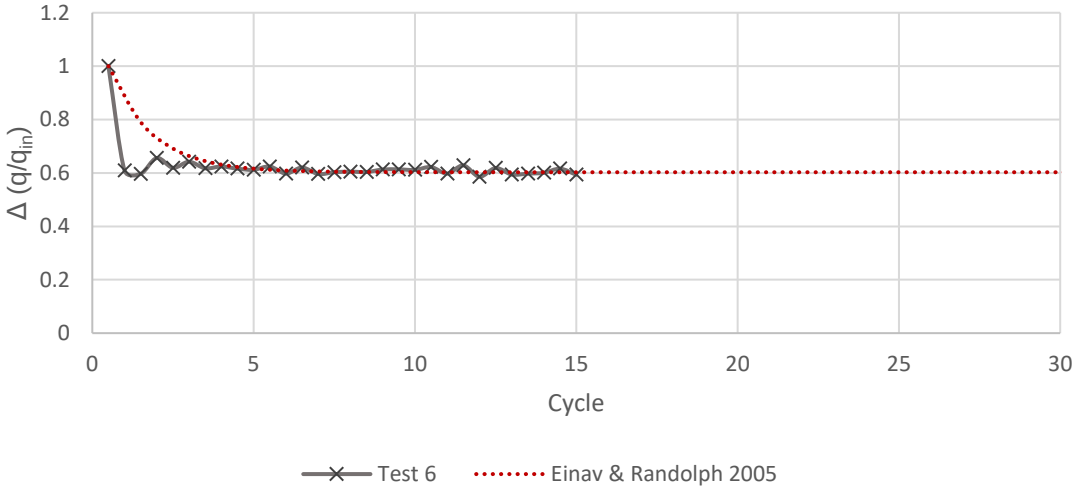

Figure A. 30 – Degradation curve Test 6

D. HYPERBOLIC SINE CURVES (VARIABLE PENETRATION RATE TESTS)

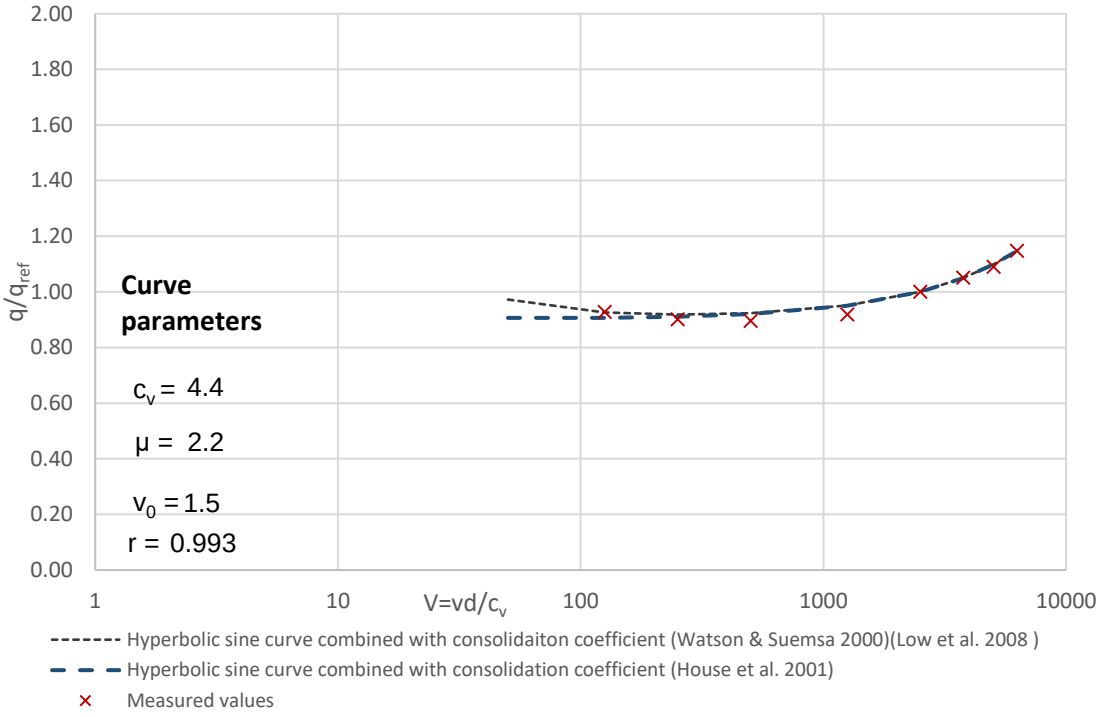

Figure A. 31- Hyperbolic sine curve combined with consolidation coefficient Test 1

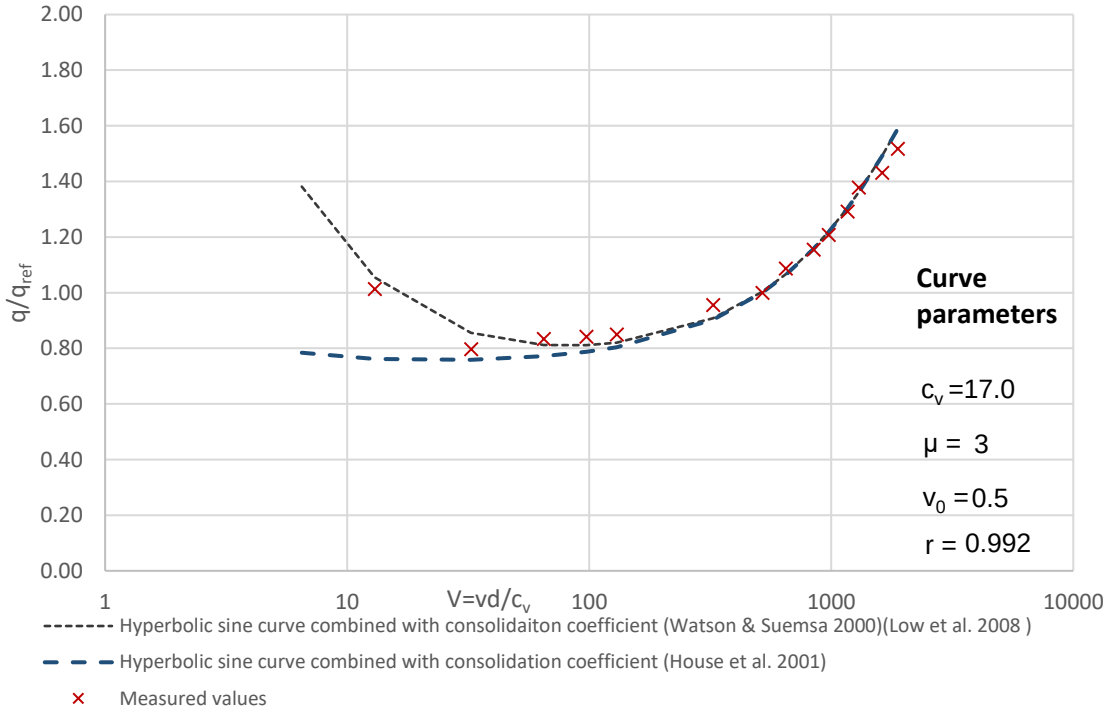

Figure A. 32 - Hyperbolic sine curve combined with consolidation coefficient Test 2

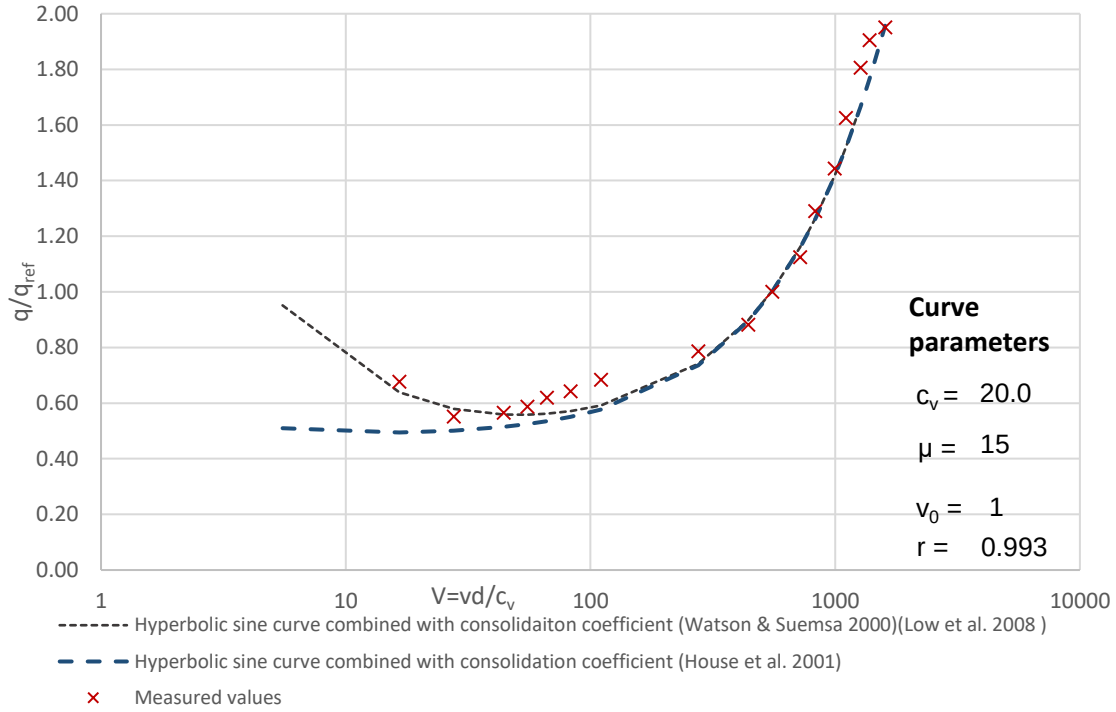

Figure A. 33 - Hyperbolic sine curve combined with consolidation coefficient Test 4

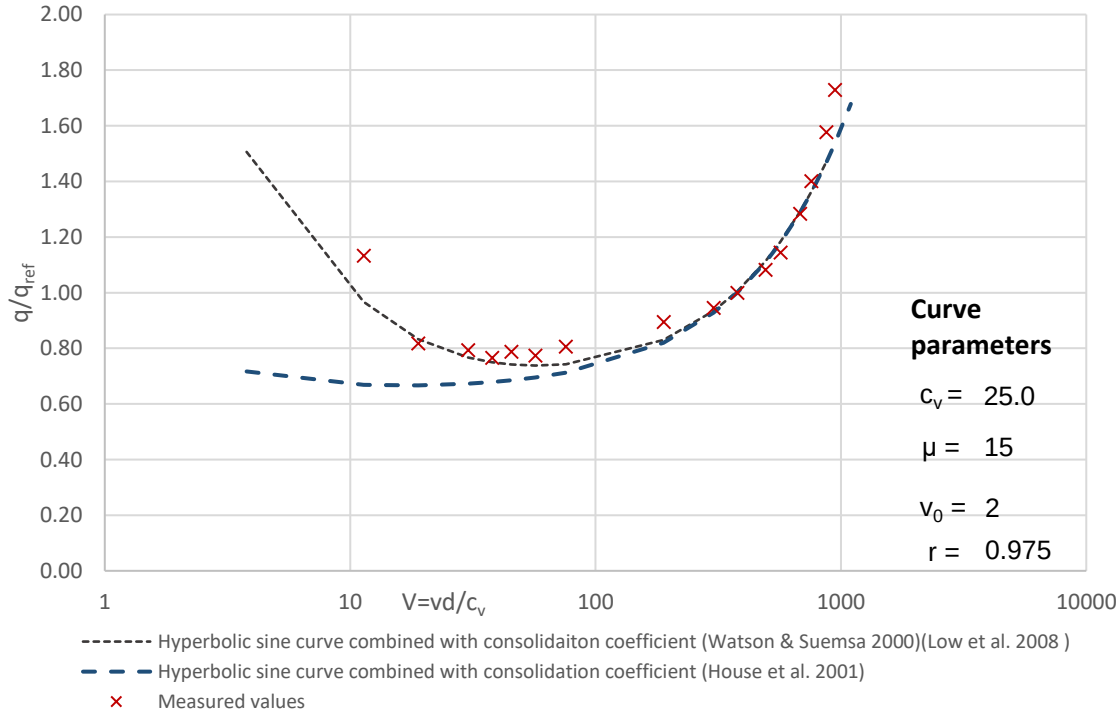

Figure A. 34 - Hyperbolic sine curve combined with consolidation coefficient Test 5

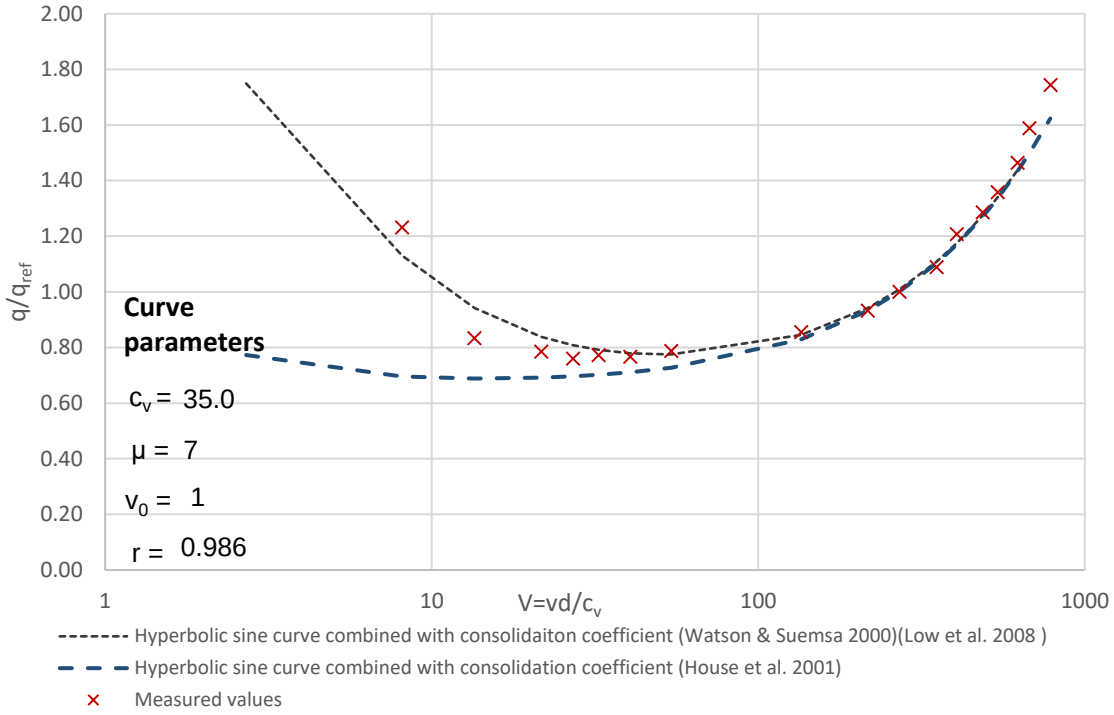

Figure A. 35 - Hyperbolic sine curve combined with consolidation coefficient Test 5 (with 20kg surcharge)

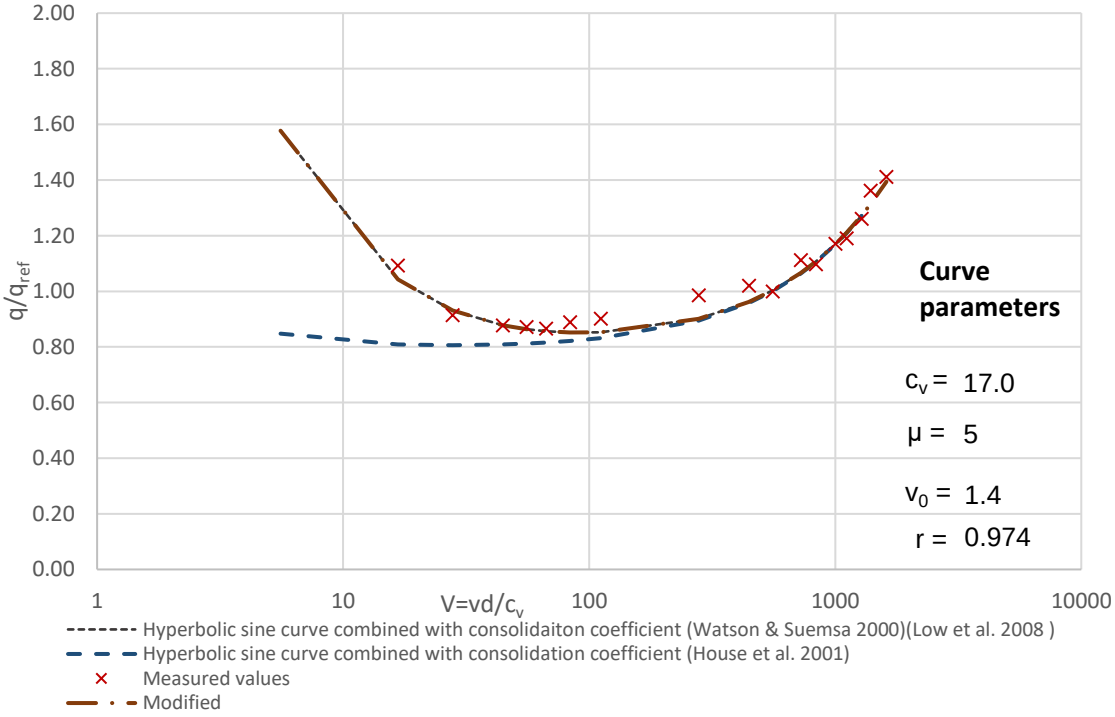

Figure A. 36 - Hyperbolic sine curve combined with consolidation coefficient Test 6

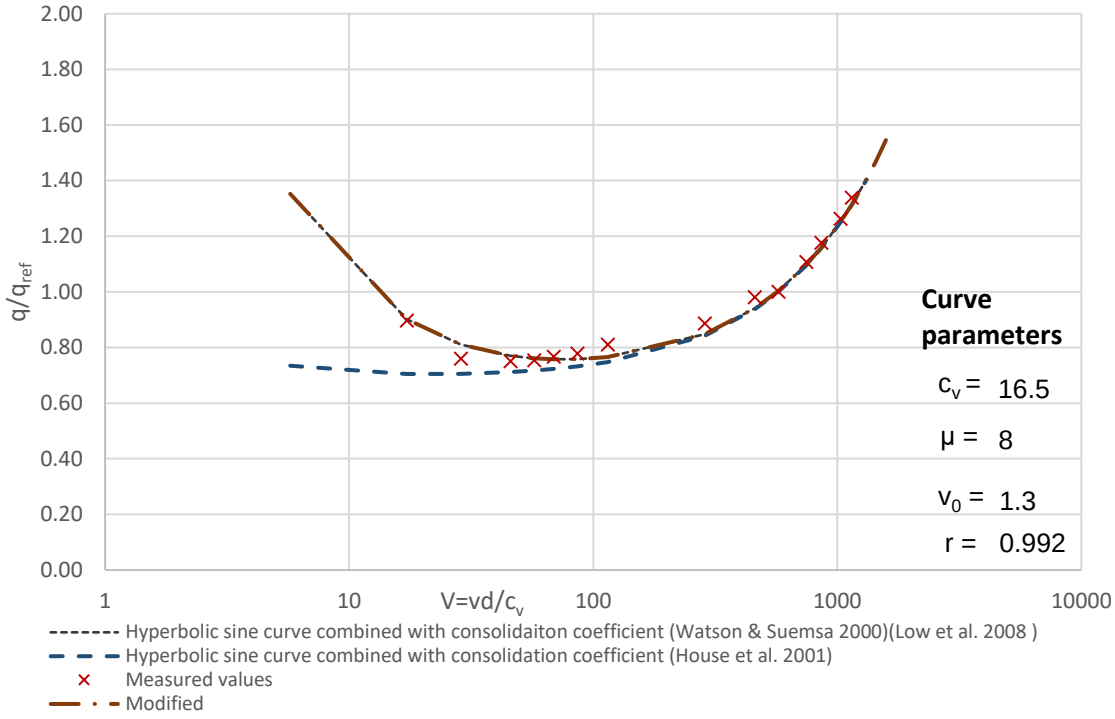

Figure A. 37 - Hyperbolic sine curve combined with consolidation coefficient Test 6 (35mm ball)

E. LABORATORY CLASSIFICATION TESTS RESULTS

Laboratory classification test results

Test 1

x coordinate	y coordinate	Test depth	w	Unit weight	Fall cone	Laboratory vane		
					s_u	s_u	$s_{u,rem}$	Sensitivity
[mm]	[mm]	[mm]	[%]	[kN/m^3]	[kPa]	[kPa]	[kPa]	[-]
170	85	112				1.29	0.67	1.92
250	85	92				1.56	0.70	2.23
250	140	112				1.46	0.67	2.16
350	85	112				1.48	0.67	2.20
170	160	65	60.29	16				
350	85	100	56.25	16.3				
170	85	100	65.22	15.7				
350	85	130	54.55	16.4				
350	85	160	51.32	16.7				
50	85	160	51.23	16.7				
113	110	70			0.40			
70	140	70			0.52			
380	140	60			0.61			
280	40	60			0.41			
170	60	60			0.23			
170	10	100			0.48			
120	130	100			0.82			
240	130	100			0.55			
350	130	100			0.76			
360	85	100			0.84			
360	60	100			1.12			
360	40	100			1.29			
340	40	100			0.83			
300	40	100			0.96			
250	40	100			0.83			
200	40	100			0.58			
150	40	100			0.50			
100	40	100			0.62			
50	40	100			0.87			
60	85	100			0.35			
60	130	100			1.41			
50	130	150			1.15			
100	130	150			1.26			
150	130	150			1.54			
200	130	150			1.17			
250	130	150			1.62			
300	130	150			1.91			
350	130	150			2.62			
380	140	150			2.60			
380	85	150			2.70			
380	40	150			2.05			
350	40	150			1.79			
300	40	150			1.96			
250	40	150			1.28			
200	40	150			1.55			
100	40	150			1.18			

Laboratory classification test results

Test 1

x coordinate	y coordinate	Test depth	w	Unit weight	Fall cone	Laboratory vane		
					s_u	s_u	$s_{u,rem}$	Sensitivity
[mm]	[mm]	[mm]	[%]	[kN/m^3]	[kPa]	[kPa]	[kPa]	[-]
50	40	150			0.80			
50	85	150			1.38			
50	100	150			0.90			

Laboratory classification test results

Test 2

x coordinate	y coordinate	Test depth	w	Unit weight	Fall cone	Laboratory vane		
					s_u	s_u	$s_{u,rem}$	Sensitivity
[mm]	[mm]	[mm]	[%]	[kN/m^3]	[kPa]	[kPa]	[kPa]	[-]
270	140	117				2.54	0.81	3.13
200	140	112				2.16	0.94	2.29
130	140	112				1.5	0.81	1.83
270	30	112				2.5	1.05	2.36
200	30	112				1.7	0.86	2.00
130	30	112				1.6	0.86	1.84
370	140	92				1.3	0.67	1.88
370	85	112				1.6	0.78	2.07
370	140	40	68.06	15.6				
350	85	60	61.7	15.6				
200	85	60	70	15.5				
50	85	60	64.91	15.8				
350	85	90	56.41	16.3				
200	85	90	57.14	16.2				
50	85	90	55.26	16.4				
350	85	110	53.88	16.5				
200	85	110	56.65	16.3				
50	85	110	67.52	15.6				
350	85	160	46.97	17				
200	85	160	46.38	17.1				
50	85	160	55.74	16.3				
50	140	50			0.27			
100	140	50			0.27			
150	140	50			0.25			
200	140	50			0.28			
250	140	50			0.30			
300	140	50			0.65			
350	140	50			0.54			
380	85	50			0.54			
350	85	50			0.49			
380	30	50			0.65			
350	30	50			0.55			
350	60	50			0.46			
300	30	50			0.81			
300	60	50			0.55			
250	30	50			0.33			

Laboratory classification test results

Test 2

x coordinate	y coordinate	Test depth	w	Unit weight	Fall cone	Laboratory vane		
					s_u	s_u	$s_{u,rem}$	Sensitivity
[mm]	[mm]	[mm]	[%]	[kN/m^3]	[kPa]	[kPa]	[kPa]	[-]
250	60	50			0.54			
200	30	50			0.31			
200	60	50			0.35			
150	30	50			0.34			
150	60	50			0.13			
100	30	50			0.35			
100	60	50			0.77			
50	30	50			0.33			
50	60	50			0.80			
50	85	50			0.78			
50	85	50			0.44			
50	140	80			0.88			
50	110	80			0.79			
150	140	80			0.49			
150	110	80			0.64			
200	140	80			0.50			
200	110	80			0.52			
250	140	80			0.71			
250	110	80			0.68			
350	140	80			0.75			
350	110	80			0.53			
380	85	80			0.67			
350	85	80			0.75			
350	30	80			0.76			
350	60	80			0.54			
250	30	80			0.83			
250	60	80			0.84			
200	30	80			0.50			
200	60	80			0.45			
150	30	80			0.79			
150	60	80			0.55			
50	30	80			0.65			
50	60	80			0.69			
50	85	80			0.63			
50	85	80			0.51			
50	140	110			0.81			
50	110	110			1.38			
150	140	110			1.42			
150	110	110			0.78			
200	140	110			1.13			
200	110	110			1.41			
250	140	110			1.95			
250	110	110			1.13			
350	140	110			0.87			
350	110	110			1.30			
380	85	110			1.41			
350	85	110			1.51			

Laboratory classification test results

Test 2

x coordinate	y coordinate	Test depth	w	Unit weight	Fall cone	Laboratory vane		
					s_u	s_u	$s_{u,rem}$	Sensitivity
[mm]	[mm]	[mm]	[%]	[kN/m^3]	[kPa]	[kPa]	[kPa]	[-]
350	30	110			0.81			
350	60	110			0.88			
250	30	110			2.37			
250	60	110			1.48			
200	30	110			1.30			
200	60	110			1.48			
150	30	110			1.57			
150	60	110			0.83			
50	30	110			2.08			
50	60	110			1.53			
50	85	110			0.75			
50	85	110			0.35			
200	85	110			0.46			
150	85	110			0.45			
50	110	160			1.43			
150	110	160			1.62			
200	110	160			2.35			
250	110	160			2.57			
350	110	160			1.77			
350	60	160			2.22			
250	60	160			2.27			
200	60	160			2.06			
150	60	160			2.53			
50	60	160			2.00			
50	85	160			1.46			

Laboratory classification test results

Test 3

x coordinate	y coordinate	Test depth	w	Unit weight	Fall cone	Laboratory vane		
					s_u	s_u	$s_{u,rem}$	Sensitivity
[mm]	[mm]	[mm]	[%]	[kN/m^3]	[kPa]	[kPa]	[kPa]	[-]
300	85	110				1.92	0.92	2.09
300	140	110				2.24	0.65	3.46
100	140	110				2.13	1.08	1.98
300	30	80				1.8	0.67	2.60
360	85	110				2.2	0.92	2.35
50	85	40	67.31	15.6				
200	85	40	69.81	15.4				
350	85	40	65.52	15.7				
50	85	90	51.92	16.6				
200	85	90	51.06	16.7				
350	85	90	51.72	16.6				
350	85	110	50	16.8				
200	85	110	55.81	16.3				
50	85	110	60	16.1				

Laboratory classification test results

Test 3

x coordinate	y coordinate	Test depth	w	Unit weight	Fall cone	Laboratory vane		
					s_u	s_u	$s_{u,rem}$	Sensitivity
[mm]	[mm]	[mm]	[%]	[kN/m^3]	[kPa]	[kPa]	[kPa]	[-]
50	85	130	44.83	17.2				
200	85	130	47.06	17				
350	85	130	47.83	16.9				
50	85	160	45.65	17.1				
200	85	160	42.11	17.5				
350	85	160	43.55	17.5				
350	30	40			0.49			
350	60	40			0.33			
250	30	40			0.52			
250	60	40			0.26			
200	30	40			0.34			
200	60	40			0.25			
150	30	40			0.34			
150	60	40			0.26			
50	30	40			0.32			
50	60	40			0.32			
50	85	40			0.29			
50	140	40			0.33			
50	110	40			0.27			
150	140	40			0.38			
150	110	40			0.24			
200	110	40			0.23			
250	140	40			0.34			
250	110	40			0.28			
350	140	40			0.68			
350	110	40			0.39			
350	140	90			1.30			
350	110	90			1.45			
250	140	90			0.83			
250	110	90			0.63			
200	140	90			1.42			
200	110	90			0.82			
150	140	90			1.50			
150	110	90			0.82			
50	140	90			1.40			
50	110	90			1.58			
50	85	90			0.67			
50	30	90			1.12			
50	60	90			0.93			
150	30	90			1.50			
150	60	90			0.78			
200	30	90			0.39			
200	60	90			0.64			
250	30	90			1.37			
250	60	90			0.78			
350	30	90			1.53			
350	60	90			1.27			

Laboratory classification test results

Test 3

x coordinate	y coordinate	Test depth	w	Unit weight	Fall cone	Laboratory vane		
					s_u	s_u	$s_{u,rem}$	Sensitivity
[mm]	[mm]	[mm]	[%]	[kN/m^3]	[kPa]	[kPa]	[kPa]	[-]
150	85	90			0.32			
200	85	90			0.54			
250	85	90			0.45			
350	85	90			1.24			
50	85	90			0.00			
350	30	110			1.79			
350	60	110			1.58			
250	30	110			1.78			
250	60	110			1.36			
200	30	110			1.77			
200	60	110			1.47			
150	30	110			1.60			
150	60	110			1.22			
50	30	110			1.83			
50	60	110			1.61			
50	85	110			0.71			
50	140	110			2.46			
50	110	110			2.05			
150	140	110			1.40			
150	110	110			1.14			
200	140	110			1.37			
200	110	110			1.39			
250	140	110			1.78			
250	110	110			1.49			
350	140	110			1.34			
350	110	110			1.61			
350	85	110			1.53			
250	85	110			0.77			
200	85	110			0.75			
150	85	110			0.76			
50	140	130			2.00			
100	140	130			2.66			
150	140	130			1.95			
200	140	130			1.78			
250	140	130			1.76			
300	140	130			1.52			
350	140	130			1.84			
50	110	130			1.90			
100	110	130			1.94			
150	110	130			1.53			
200	110	130			2.62			
250	110	130			2.92			
300	110	130			2.26			
350	110	130			1.95			
50	30	130			1.82			
100	30	130			2.26			
150	30	130			2.26			

Laboratory classification test results

Test 3

x coordinate	y coordinate	Test depth	w	Unit weight	Fall cone	Laboratory vane		
					s_u	s_u	$s_{u,rem}$	Sensitivity
[mm]	[mm]	[mm]	[%]	[kN/m^3]	[kPa]	[kPa]	[kPa]	[-]
200	30	130			2.22			
250	30	130			1.82			
300	30	130			1.45			
350	30	130			2.03			
50	60	130			2.34			
100	60	130			2.94			
150	60	130			2.24			
200	60	130			1.93			
250	60	130			2.47			
300	60	130			1.45			
350	60	130			1.50			
50	85	130			1.97			
350	85	130			1.42			
50	140	160			3.42			
100	140	160			3.30			
150	140	160			3.24			
200	140	160			6.35			
250	140	160			4.59			
300	140	160			3.96			
350	140	160			3.99			
50	110	160			4.40			
100	110	160			4.87			
150	110	160			9.87			
200	110	160			5.29			
250	110	160			4.69			
300	110	160			4.79			
350	110	160			2.54			
50	30	160			4.69			
100	30	160			8.31			
150	30	160			5.17			
200	30	160			6.33			
250	30	160			3.70			
300	30	160			3.19			
350	30	160			3.35			
50	60	160			4.65			
100	60	160			6.95			
150	60	160			7.84			
200	60	160			3.45			
250	60	160			4.00			
300	60	160			3.41			
350	60	160			4.25			

Laboratory classification test results

Test 4

x coordinate	y coordinate	Test depth	w	Unit weight	Fall cone	Laboratory vane		
					s_u	s_u	$s_{u,rem}$	Sensitivity
[mm]	[mm]	[mm]	[%]	[kN/m^3]	[kPa]	[kPa]	[kPa]	[-]
200	140	110				2.08	1.21	1.71
300	140	110				2.43	1.21	2.00
370	85	110				3.59	1.13	3.17
200	30	110				2.56	1.32	1.94
300	30	110				2.78	1.21	2.29
50	85	50	55.17	16.4				
200	85	50	59.26	16.1				
350	85	50	57.14	16.2				
50	85	80	52.94	16.5				
200	85	80	56.6	16.3				
350	85	80	56.76	16.3				
50	85	110	51.92	16.6				
200	85	110	55.56	16.4				
350	85	110	53.66	16.5				
50	85	160	38.99	17.8				
200	85	160	42.37	17.4				
50	140	50			0.87			
150	140	50			0.77			
200	140	50			0.80			
250	140	50			0.78			
350	140	50			0.87			
50	110	50			0.72			
150	110	50			0.55			
200	110	50			0.81			
250	110	50			0.68			
350	110	50			0.71			
350	85	50			0.78			
50	30	50			1.37			
150	30	50			0.82			
200	30	50			0.79			
250	30	50			1.51			
350	30	50			0.66			
50	60	50			1.57			
150	60	50			0.78			
200	60	50			0.78			
250	60	50			0.83			
350	60	50			0.72			
50	85	50			0.78			
150	85	50			0.77			
200	85	50			0.83			
250	85	50			0.77			
50	140	80			1.43			
150	140	80			0.88			
200	140	80			0.83			
250	140	80			0.84			
350	140	80			0.92			
50	110	80			0.89			

Laboratory classification test results

Test 4

x coordinate	y coordinate	Test depth	w	Unit weight	Fall cone	Laboratory vane		
					s_u	s_u	$s_{u,rem}$	Sensitivity
[mm]	[mm]	[mm]	[%]	[kN/m^3]	[kPa]	[kPa]	[kPa]	[-]
150	110	80			0.50			
200	110	80			0.48			
250	110	80			0.54			
350	110	80			1.48			
350	30	80			1.77			
250	30	80			1.12			
200	30	80			0.82			
150	30	80			1.11			
50	30	80			1.57			
350	60	80			1.67			
250	60	80			0.79			
200	60	80			0.72			
150	60	80			0.82			
50	60	80			1.19			
50	85	80			0.86			
150	85	80			0.75			
200	85	80			0.62			
250	85	80			0.88			
350	85	80			1.54			
50	140	110			1.42			
150	140	110			1.43			
200	140	110			2.46			
250	140	110			1.51			
350	140	110			2.39			
50	110	110			0.88			
150	110	110			1.49			
200	110	110			1.91			
250	110	110			1.47			
350	110	110			2.78			
50	30	110			1.96			
150	30	110			1.77			
200	30	110			1.37			
250	30	110			1.48			
350	30	110			1.99			
50	60	110			1.20			
150	60	110			0.79			
200	60	110			1.24			
250	60	110			0.87			
350	60	110			2.24			
50	85	110			1.50			
150	85	110			0.78			
200	85	110			1.30			
250	85	110			0.67			
350	85	110			1.90			
50	140	140			2.07			
150	140	140			1.93			
200	140	140			1.79			

Laboratory classification test results

Test 4

x coordinate	y coordinate	Test depth	w	Unit weight	Fall cone	Laboratory vane		
					s_u	s_u	$s_{u,rem}$	Sensitivity
[mm]	[mm]	[mm]	[%]	[kN/m^3]	[kPa]	[kPa]	[kPa]	[-]
250	140	140			3.19			
350	140	140			2.00			
50	110	140			2.85			
150	110	140			1.96			
200	110	140			1.65			
250	110	140			2.17			
350	110	140			2.17			
50	30	140			2.60			
150	30	140			3.31			
200	30	140			3.96			
250	30	140			5.10			
350	30	140			2.55			
50	60	140			2.48			
150	60	140			2.89			
200	60	140			2.28			
250	60	140			3.90			
350	60	140			4.44			
50	85	140			2.60			
350	85	140			0.00			
50	140	160			4.25			
150	140	160			6.08			
200	140	160			8.47			
250	140	160			5.23			
350	140	160			4.35			
50	110	160			4.65			
150	110	160			8.31			
200	110	160			7.31			
250	110	160			7.41			
350	110	160			9.35			
50	30	160			7.87			
150	30	160			8.51			
200	30	160			8.55			
250	30	160			9.92			
350	30	160			8.39			
350	85	160			8.09			
50	60	160			4.50			
150	60	160			6.13			
200	60	160			8.59			
250	60	160			9.82			
350	60	160			5.65			

Laboratory classification test results

Test 5

x coordinate	y coordinate	Test depth	w	Unit weight	Fall cone	Laboratory vane		
					s_u	s_u	$s_{u,rem}$	Sensitivity
[mm]	[mm]	[mm]	[%]	[kN/m^3]	[kPa]	[kPa]	[kPa]	[-]
200	140	110				1.70	1.16	1.47
300	140	110				2.75	0.94	2.91
370	140	110				1.6	0.81	2.00
370	85	110				1.9	0.81	2.33
370	30	110				1.6	0.94	1.71
300	30	110				3.0	1.19	2.55
200	30	110				1.6	0.94	1.66
100	30	110				1.2	1.08	1.15
50	85	60	50					
200	85	60	52					
350	85	60	55					
50	85	80	54.29					
200	85	80	58.33					
350	85	80	53.13					
50	140	60			1.52			
150	140	60			1.22			
200	140	60			1.92			
250	140	60			1.51			
350	140	60			0.68			
50	110	60			0.88			
150	110	60			1.42			
200	110	60			1.18			
250	110	60			1.53			
350	110	60			0.79			
50	30	60			1.49			
150	30	60			2.27			
200	30	60			1.42			
250	30	60			1.55			
350	30	60			0.80			
50	60	60			0.73			
150	60	60			1.99			
200	60	60			1.36			
250	60	60			1.10			
350	60	60			0.82			
50	85	60			0.47			
150	85	60			1.23			
200	85	60			0.66			
250	85	60			0.70			
350	85	60			0.63			
50	140	80			0.82			
150	140	80			0.81			
200	140	80			1.28			
250	140	80			0.89			
350	140	80			1.51			
50	110	80			0.70			
150	110	80			0.80			
200	110	80			0.87			

Laboratory classification test results

Test 5

x coordinate	y coordinate	Test depth	w	Unit weight	Fall cone	Laboratory vane		
					s_u	s_u	$s_{u,rem}$	Sensitivity
[mm]	[mm]	[mm]	[%]	[kN/m^3]	[kPa]	[kPa]	[kPa]	[-]
250	110	80			0.83			
350	110	80			1.44			
50	30	80			1.50			
150	30	80			1.79			
200	30	80			1.20			
250	30	80			1.79			
350	30	80			0.70			
50	60	80			0.63			
150	60	80			1.47			
200	60	80			0.71			
250	60	80			0.78			
350	60	80			1.12			
50	85	80			0.52			
150	85	80			0.67			
200	85	80			0.88			
250	85	80			0.64			
350	85	80			0.77			

Laboratory classification test results

Test 6

x coordinate	y coordinate	Test depth	w	Unit weight	Fall cone	Laboratory vane		
					s_u	s_u	$s_{u,rem}$	Sensitivity
[mm]	[mm]	[mm]	[%]	[kN/m^3]	[kPa]	[kPa]	[kPa]	[-]
250	140	110				1.8	0.94	1.86
50	140	110				1.62	0.81	2.00
50	30	110				1.62	0.81	2.00
250	30	110				1.59	0.97	1.64
350	85	80	56.08	16.3				
350	85	120	54.25	16.5				